NTNU
Norwegian University of
Science and Technology

A global assessment of a floating bridges ability to withstand a ship collision

Kristin Victoria Jansen

Master Thesis, Spring 2016

for

Stud. Techn. Kristin Victoria Jansen

A global assessment of a floating bridges ability to withstand a ship collision

En global vurdering av en flytebro sin evne til å motstå en skipskollisjon

With floating bridges becoming more used for fjord crossings along the Norwegian fjords, it is important to know how a bridge will respond to a ship collision. The objective of this thesis is therefore to assess the resistance of the pontoons in the bridge if an impact occurs. This means that the energy absorption and deformations of the bridge must be analyzed. In general, nonlinear finite element analysis is required, together with procedures to estimate the energy that will be absorbed.

The candidate shall address the following topics:

1. An overview of existing floating bridges. Similarities and differences are to be highlighted. Projects related to the structures should also be covered.
2. Relevant theory of impact loading shall be reviewed. In particular, formulations which are implemented in relevant standards are to be considered. Also, studies on ship collision risk studies are to be described.
3. Methods for assessment of impact energy and associated structural response shall be reviewed. A sensitivity study concerning mesh refinement shall be included for a particular ship and bridge concept. Some background to the numerical algorithms which are implemented in relevant computer software which is to be applied for the different types of calculation should be given. The analysis is to be carried out using the computer program ABAQUS.
4. Parametric studies concerning the modeling of the bridge and its resistance should be performed. The effect of changing the thickness of the material, as well as the number of bulkheads should be conducted.

The work scope may prove to be larger than initially anticipated. Subject to approval from the supervisor, topics may be deleted from the list above or reduced in extent. In the thesis the

candidate shall present his personal contribution to the resolution of problems within the scope of the thesis work. Theories and conclusions should be based on mathematical derivations and/or logic reasoning identifying the various steps in the deduction.

The candidate should utilize the existing possibilities for obtaining relevant literature.

The thesis should be organized in a rational manner to give a clear exposition of results, assessments, and conclusions. The text should be brief and to the point, with a clear language. Telegraphic language should be avoided.

The thesis shall contain the following elements: A text defining the scope, preface, list of contents, summary, main body of thesis, conclusions with recommendations for further work, list of symbols and acronyms, references and (optional) appendices. All figures, tables and equations shall be numbered.

The supervisor may require that the candidate, in an early stage of the work, presents a written plan for the completion of the work.

The original contribution of the candidate and material taken from other sources shall be clearly defined. Work from other sources shall be properly referenced using an acknowledged referencing system.

The thesis shall be submitted in electronic form:

- Signed by the candidate

- The text defining the scope included

- In bound volume(s)

- Drawings and/or computer prints which cannot be bound should be organized in a separate   folder.

Trondheim, February 4,2016

Bernt J. Leira

Preface

This master thesis is written as the final task of my education in Marine Technology at the Norwegian University of Science and Technology. The master make up 30 credit point, and is the only project/course during the spring semester. The work in this thesis was conducted at the Marinteknisk senter in Trondheim.

The scope of work was suggested to my by my supervisor Bernt Johan Leira in the fall of 2015, when I wrote my project thesis on the same topic. The project thesis was focusing on a local analysis of the bridge, and is here extended into a global analysis. I would like to thank my supervisor for the good help I have received when I have been stuck or have had questions.

Trondheim, June 28th, 2016

Kristin Victoria Jansen

Summary

It is planned to exchange the ferry connections along the western coast of Norway with fixed road connections. To be able to do this, new concepts for fjord crossings have to be used. One of these alternatives is a floating bridge, that stands on pontoons to keep it afloat. This is a reason that it will be a good concept as a solution to cross the wide and deep fjords. A bridge of this type will therefore be in the risk of a ship collision.

In this thesis an assessment of the resistance of the pontoons during an impact has been conducted. To do this, the energy absorption and deformations in the bridge was analyzed. To do this nonlinear finite element analysis is required, together with procedures to estimate the energy that will be absorbed.

The first part of the thesis is based on theory. It starts out with describing the concept of floating bridges by going through those that has already been built, before it describes the project "Ferjefri E39" and the basic concepts of a bridge of this type. A closer look is taken at ship collisions, and the standards that exists for collisions, developed numerical methods and risk studies that have been conducted in the field. The last parts of the theory is mainly connected to the finite element method for both a linear and nonlinear approach, with a closer look at the theory for shell and beam elements. In the end of the theory section, the procedure behind an explicit dynamic analysis is described.

The second part of the thesis describes what has been done in the finite element analysis program ABAQUS. This program was selected to conduct the necessary analyses for the thesis. A model of a floating bridge was designed, and properties were assigned to the model. This model was then used to perform a mesh refinement study on the bridge. A parameter study on the shell thickness and number of bulkheads was also conducted.

The results that are presented are mainly of the structural forces, stresses, moments and energies. These are presented in plots, and are later discussed. The most important results are those connected to the structural integrity of the bridge, and if it will be able to keep afloat without sinking. From the results it could be seen that the shell thickness in the pontoon was a large factor in the deformation process. A thin walled shell with a thickness of 1 cm would buckle completely, while the pontoon with a shell thickness of 4 cm not would reach yield stress at all. For the study related to the amount of bulkheads, also this had great significance on the results. The difference in maximum stress was large with over a 100 MPa difference. While the model without bulkheads would go into total collapse, the pontoon with many bulkheads kept its integrity. By having very few or no bulkheads at all will not give the pontoon enough stiffness to prevent the vessel from penetrating it. Further, bulkheads have the important role of keeping the entire pontoon from flooding if it gets penetrated. It kan therefore be seen as an important structural element.

Sammendrag

Det er planlegt å bytte ut ferjeforbindelsene langs den vestlige kysten av Norge med faste veiforbindelser. For å kunne gjennomføre dette er det nødvendig å ta i bruk ny teknologi for fjordkrysninger. Et av alternativene for fjordkrysningen er å bygge en flytebro, som står på pontinger i vannet for å holde den flytende. På grunn av disse egenskapene er en flytebro en velegnet løsning for å kunne krysse dype og vide fjorder. En bro av denne typen vil derfor stå i fare for å bli utsatt for en skipskollisjon.

I denne oppgaven har det blitt utført en vurdering av pontongenes motstand under et sammenstøt. For å gjøre dette måtte energiopptaket og deformasjonene i broen analyseres. For å kunne gjøre dette trenger man ikke lineær elementmetode, sammen med fremgangsmetoder for å estimere energien som absorberes.

Den første delen av oppgaven behandler teori. Den starter med å beskrive konseptet flytebroer ved å få gjennom broer som allerede er bygget, før den beskriver prosjektet Ferjefri E39 og de grunnleggende konseptene for broer av denne typen. Videre tar den et dypere blikk på teorien bak skipskollisjoner og standardene som finnes for kollisjoner, de eksisterende numeriske metoder og risikostudier som har blitt gjennomført. Den siste delen av teorien er for det meste satt i sammenheng med elementmetoden for både lineære og ikke lineære tilfeller. Teorien for skall elementer og bjelker blir sett ekstra nøye på. Helt i slutten av teoridelen beskrives teorien bak dynamisk eksplisitt analyse.

Den siste delen omhandler analysen som er gjort i elementmetode programmet ABAQUS. Prgrammet ble valgt for å utføre de nødvendige analysene for oppgaven. En modell av en flytebro ble designet i programmet, og gitt egenskaper. Denne modellen ble så benyttet til å gjennomføre en undersøkelse med forfining av mesh størrelsen. Videre har det også blitt utført en parameterstudie av skalltykkelsen of antall skott i pontongen.

De resultatene som presenteres er stort sett av strukturelle krefter, spenninger, momenter og energinivåer. Disse er presentert i grafer, og blir senere diskutert. De viktigste resultatene er de som er relatert til den strukturelle integriteten til broen, og om den evner å holde seg flytende uten å synke. Fra resulatene kan man se at skalltykkelsen i pontongen var en viktig faktor under deformasjonsprosessen. Et tynnvegget skall med en tykkelse på 1 cm hadde fullstendig knukket sammen, mens det tykkveggede skallet på 4 cm ikke engang nådde flyt-grensen for materialet.I studien relatert til antall skott i pontongen viste det seg at også denne hadde stor innflytelse på resultatene. Forskjellen i maksimalt spenningsnivå var på over 100 MPa for de to tilfellene. Mens modellen uten skott gikk inn i total kollaps, klarte pontongen med mange skott å holde på integriteten sin. Ved å ha veldig få eller ingen skott, ville ikke pontongen ha nok stivhet til å kunne hindre skipet i å penetrere den. Videre, har skott den viktige rollen å hindre hele pontongen fra å fylles med vann ved penetrering. De kan derfor sees på som viktige strukturelle komponenter.

Contents

List of Figures

List of Tables

Abbreviation

NTP	National Transport Plan
NPRA	Norwegian Public Roads Administration
ALS	Accidental Limit State
SLS	Serviceability Limit State
ULS	Ultimate Limit State
FLS	Fatigue Limit State
DNV	Det Norske Veritas
NORSOK	Norsk sokkels konkurranseposisjon
AIS	Automatic Identification System
FEM	Finite Element Method
FEA	Finite Element Analysis
MPa	Mega Pascal
GPa	Giga Pascal
MN	Mega Newton
MNm	Mega Newton Meter
S4R	4-noded shell element with reduced integration and hourglass control
S3R	3-noded shell element with reduced integration and hourglass control
d.o.f.	Degrees of freedom
AIS	Automatic System Identification
HSC	High Speed Passenger crafts
GT	Gross Tonnage

Nomenclature

E_k	Kinetic energy
E_s	Strain energy
$E_{s,s}$	Strain energy absorbed in ship
$E_{s,i}$	Strain energy absorbed in installation
m	Mass
a	Added mass
v	Velocity
v_c	Common velocity at end of impact
v_s	Velocity of ship
v_i	Velocity of installation
a_s	Added mass of ship
a_i	Added mass of installation
m_s	Mass of ship
m_i	Mass of installation
ΔE	Change in kinetic energy
β	Factor of dissipated kinetic energy absorbed as strain energy
A_i	Area under the load-deformation curve for the installation
A_s	Area under the load-deformation curve for the ship
σ_0	Compressive flow stress including strain rate effects
σ_0	Flow stress based on the mean value of the yield and ultimate strength of the material
σ_{0s}	Static strength of steel material
β_g	Coefficient dependent on edge restraints
m	Coefficient dependent on edge restraints
t	Average thickness for the cross-section under consideration
n	Sum of cuts and flanges for the cross-section under consideration
$\dot{\varepsilon}$	Strain rate
v_x	Velocity in longitudinal direction during impact
s	Frame spacing
A	Cross-sectional area of deformed steel material
n_c	Number of cruciforms in a cross-section under consideration

n_T	Number of T-sections in a cross-section under consideration
n_{AT}	Number of angle and T-sections in a cross-section under consideration
n_f	Number of flanges, angles, T-section and cruciforms in a cross-section under consideration
P_c	Total crushing force
P_m	Mean crushing force
b_i	Width of i'th plate flange
t_i	Thickness of i'th plate flange
H	Folding length of the distorted plate flanges
R_s	Load on ship during deformation
R_i	Load on installation during deformation
J	Mass moment of inertia of installation (including added mass) with respect to effective pivot point
z	Distance from pivot point to point of contact
β	Factor of dissipated kinetic energy
$\boldsymbol{S}$	Generalized nodal point forces
$\boldsymbol{k}$	Element stiffness matrix
$\boldsymbol{v}$	Element nodal point displacements
$\boldsymbol{S}^0$	Nodal point forces for external loads
$\boldsymbol{a}$	Nodal displacement vector
$\boldsymbol{R}$	Structure nodal point forces due to external loads
$\boldsymbol{r}$	Structure nodal point displacements
$\boldsymbol{R}^0$	Nodal point forces due to external loads
$\boldsymbol{f}$	Element force vector
$\boldsymbol{f}_b$	Element boundary vector
$\boldsymbol{f}_l$	Element load vector
$\boldsymbol{D}$	Hooke's law on matrix form
$\boldsymbol{K}$	Global stiffness matrix
$\boldsymbol{K}_M$	Global material stiffness matrix
$\boldsymbol{K}_G$	Global geometrical stiffness matrix
$\boldsymbol{\sigma}$	Stress vector
$\boldsymbol{\varepsilon}$	Strain vector

E	Young's modulus
G	Shear modulus
ν	Poisson's ratio
γ	Shear strains
τ	Shear stress
M	Moment
V	Shear force
N	Normal force
A	Cross-sectional area
$\boldsymbol{u}$	Displacement vector
$\boldsymbol{A}$	Effective cross-sectional area on matrix form
$\boldsymbol{W}$	Weighting matrix
K'	Plastic tangent modulus
ϵ	Strain on nominal form
$\dot{\epsilon}$	Strain rate on nominal form
$\dot{\varepsilon}$	Strain rate on true form
$\bar{\sigma}$	Effective stress
$\bar{\varepsilon}$	Effective strain
$\dot{\bar{\varepsilon}}$	Effective strain rate
f	loading function
W^p	Plastic work
ε	Mechanical strain
α	Yield "offset"
W	Work
V	Volume
U	Energy dissipation
$\boldsymbol{M}$	Nodal mass matrix
$\ddot{\boldsymbol{u}}$	Nodal accelerations
$\dot{\boldsymbol{u}}$	Nodal velocities
$\boldsymbol{u}$	Nodal displacements
t	time
ρ	Material density
r	radius

I_p	Polar moment of inertia
J	Torsional constant
I_{xy}	Product moment of inertia
I_x	Second moment of area about the x-axis
I_y	Second moment of area about the y-axis
∇	Displaced volume
Δ	Mass
T	Draft
A_{wl}	Waterline area
y_c	Distance to center of area
a	Distance from axis of rotation
b	Width
h	Height
A	Area
BM_T	Distance between metacenter and center of buoyancy in the transverse direction
BM_L	Distance between metacenter and center of buoyancy in the longitudinal direction
KB	Distance from keel to center of buoyancy
KG	Distance from center of gravity to keel
GM	Distance from center of gravity to metacenter
D	Depth of structure
g	constant for gravitational acceleration
C_{44}	Spring stiffness for roll motion
C_{55}	Spring stiffness for pitch motion
$\boldsymbol{F}$	External applied forces matrix
$\boldsymbol{I}$	Internal element forces matrix
q	Distributed loading
L	Length of beam element
I	Second moment of area
σ	Stress
$d\sigma$	Incremental stress

σ_x Stress in x-direction

σ_y Stress in y-direction

σ_y yield stress

σ_z Stress in z-direction

σ_m Hydrostatic stress

σ_d Deviatoric stress

$\bar{\sigma}$ Effective stress

t Thickness of element

1 Introduction

1.1 Scope of work

Because the Norwegian Public Roads Administration want to replace the ferries along the Norwegian coast with floating bridges, it is of importance to know how the bridge will respond to a ship collision. Such an event may lead to fatal events and loss of human lives. The objective of the thesis is therefore to assess the resistance of the pontoons in the bridge if such an event should occur. To do this, the energy absorption and deformations of the bridge must be analyzed. In general, nonlinear finite element analysis is required together with procedures that estimates the energy that must be absorbed.

The following topics will be covered:

1. An overview of existing floating bridges. Similarities and differences are to be highlighted. Projects related to the structures should also be covered.

2. Relevant theory of impact loading shall be reviewed. In particular, formulations which are implemented in relevant standards are to be considered. Also, studies on ship collision risk studies are to be described

3. Methods for assessment of impact energy and associated structural response shall be reviewed. A sensitivity study concerning mesh refinement shall be included for a particular ship and bridge concept. Some background to the numerical algorithms which are implemented in relevant computer software which is to be applied for the different types of calculation should be given. The analysis is to be carried out using the computer program ABAQUS.

4. Parametric studies concerning the modeling of the bridge and its resistance should be performed. The effect of changing the thickness of the material, as well as the number of bulkheads should be conducted.

1.2 General

In this thesis there is first a part that consists of theory. The theory will cover floating bridges, ship collisions, the finite element method both for linear and nonlinear applications as well as a chapter on dynamic explicit analysis. In the chapter on floating bridges the background information is discussed together with a presentation of existing bridges and the project "Ferjefri E39". The part on ship collisions covers the general collision mechanics, numerical methods developed for collisions, the standards and collision risk studies. The finite element chapter take a general approach before it describes shell and beam theory, since these elements have been used in the analysis. The next part is mainly an description of the approach that was used to make the ABAQUS model, before results are presented and discussed.

Floating bridges are very useful for crossing water stretches that are either very deep or wide. This make them nearly impossible to cross with a regular suspension bridge or a tunnel. The bridge floats on pontoons in the water, and is therefore independent of a gravity based foundation. Along the Norwegian western coast there are a lot of ferry connection because of the wide and deep fjords that are scattered along the coast. These connection leads to a long travel time between the cities of Kristiansand, Stavanger, Bergen, Ålesund, Molde and Trondheim among others. These are many of the largest cities that can be found in Norway, and it is important to make a connection between them that will reduce the travel time and lead to a better infrastructure. This is thought to give socioeconomic gain.

Most failures of marine structures are due to accidental actions such as fires, explosions or ship collisions and not environmental loads. Because of this it is important to know how a ship collision will affect a structure (Jansen, 2015). There are several design criteria that has to be fulfilled through a structural design. In the book from Torgeir Moan, we have the following statement of what a structure should be: *Structures are designed to fulfill serviceability and safety criteria in an optimal manner. A structure is safe if it will not fail under foreseeable actions, leading to loss of lives, injury, pollution or economic loss...* (Moan, 2000). An accidental action occurs when there is a technical or human error. An error of this size may lead to a fatal accident and loss of human lives.

2   Floating bridges

This chapter is mainly taken from my project thesis (Jansen, 2015). As mentioned in the introduction, a floating bridge stand on pontoons and float in the water. These types of bridges will provide the a larger span length compared to other bridges. Throughout history, several bridges of this type has been built. They can be dated as far back as to 2000 BC, and has both then and now typically been used for military transport (Watanabe and Utsunomiya, 2003). In the beginning they were just boats connected together, but has with the technological development throughout the centuries become very complicated structures. There has been built several types of floating bridges around the world, and two of them has been built in Norway. This is the Bergsøysund bridge and the Nordhordaland bridge. As Norway is a country with a very long coastline and a lot of deep fjords, there is a lot of ferry traffic along the western coast. The ferry traffic makes driving along the coast time consuming, and it is therefore desirable to develop a concept where the fjords can be crossed through a tunnel or over a bridge. This is now a project under development of the Norwegian Public Roads Administration, and this is called "Ferjefri E39" (Statens Vegvesen). To this day, it is the easier fjord crossings that has been crossed with bridges and the most extreme cases still has ferries. The fjords to be crossed are very deep and broad. In addition, there are a lot of vessel traffic in the fjords. It is becoming more and more cruise ships along the coast that travel inside the fjords, which a need for a ship passage in the bridge. The fjord that is expected to be the toughest to cross is Sognefjorden, which is Norway's longest fjord.

It is assumed by (Watanabe and Utsunomiya, 2003) that a suspension bridge has a span limit of 3000 meters. This is related to the material properties of steel, which are used to build such bridges. Tunnels have limitations as well because of the water depth. If the waters get too deep, it is not possible to place a tunnel either on or below the seabed. But through the oil production on the Norwegian continental shelf, it has been developed a lot of knowledge on the area of offshore structures. This knowledge has been applied to the two bridges that has been built in the country, and has made them innovative compared to other bridges that has been built around the world.

In the Norwegian fjords most of the ship traffic consists of smaller vessels that carry cargo. The large cruise ships have not yet traveled into the fjords, even though they are expected to

do that in the future. A cruise ship will have a much larger mass than a regular cargo vessel, and in that case the bridge should have larger dimensions. This is both with respect to the bridge opening for the ships to pass, but also with respect to the extra kinetic energy from the larger vessels that has to be absorbed. Because of the ship traffic, most bridges need an opening for ship traffic to pass through. This passage should be so wide that a ship can pass through without any trouble. But accidents do happen, and it has to be assumed that an impact may occur. In (Frandsen et al., 1991)it was stated that the bridge opening has to be high and wide enough for a ship to pass, where the only risk of collisions are a navigational error or technical failure on board the vessel. The opening must be so large that a ship do not get increased navigational difficulties that may lead to an impact. This means that the opening should be quite wide, and adapted to the ship traffic that is normal in the area.

2.1   Concepts for crossing fjords

There are several concepts that has been developed for crossing large water stretches, and these are described in table 1 shown below. There are suspension bridges, submerged tunnels, and floating bridges, but also different designs within the solutions. The Norwegian Public Roads Administration is currently working on developing a concept for crossing Bjørnafjorden, right north of Bergen along the Norwegian western coast (Veg). There has not yet been established if it will be built as a floating bridge or as submerged tunnel, but when finished it will become the world's longest bridge or tunnel of its kind (Teknisk ukeblad).

As can be seen from the illustrations, there are very many concepts that can be used for crossing water stretches. There are gravity based bridges, which is suited for relatively shallow waters that does not have a soft soil. Then you have the bridges that are floating, and also here we can see deviations. There are bridges with continuous pontoons and single pontoons, as the two Norwegian bridges have. There are also differences in the anchoring systems, some are built with dolphins, but most of them have anchors. This is different from Nordhordaland and Bergsøysund bridge, as these has not been anchored, but are built in a way, that anchors aren't needed for the stability of the bridges. At last I will take a look at the different concepts that has been developed for tunnels.

Table 1: Classification of floating bridges and tunnels (Watanabe and Utsunomiya, 2003, p. 128)

	Types and spatial position	**Description**
1	Deeper than seabed	Underwater tunnel (see fig. 2.(4))
2	Just beneath seabed	Immersed tunnel (see fig. 2.(3))
3	Structure completely immersed in water	Submerged floating bridge or tunnel (see fig. 2.(2))
4	Foundation completely submerged	
	Foundation(s) resting on seabed	Bridges with gravity foundation(s) (see fig. 1d)
	Continuous foundation	Floating bridge with continuous submerged foundation
	Separated foundation	Floating bridge with separated foundations
5	Semi-submerged foundations	Floating bridge with semi-submerged foundations (see fig. 1c)
6	Pontoon foundations	Floating bridge with pontoon foundations (see fig. 1b)
7	Pontoon girders	Continuous pontoon bridge (see fig. 1a)
8	Trains running in water without shield	Amphibious train
9	Foundations secured at seabed	Conventional (land-based) design

As we can see from figure 2, there are mainly three different kinds of tunnels. There is the type that goes under the seabed, the one that lies on the seabed, and the new kind that hasn't been built anywhere in the world yet, the submerged floating tunnel. It is this last kind that is relevant for the "Ferjefri E39" project. Several companies are trying to evolve a tunnel that floats in the fjord, either through natural buoyancy or connected to floating pontoons. It is this concept that are in "competition" with the floating bridges for crossing the fjords along E39. The two other types of tunnel are quite normal, and has been built all around the world.
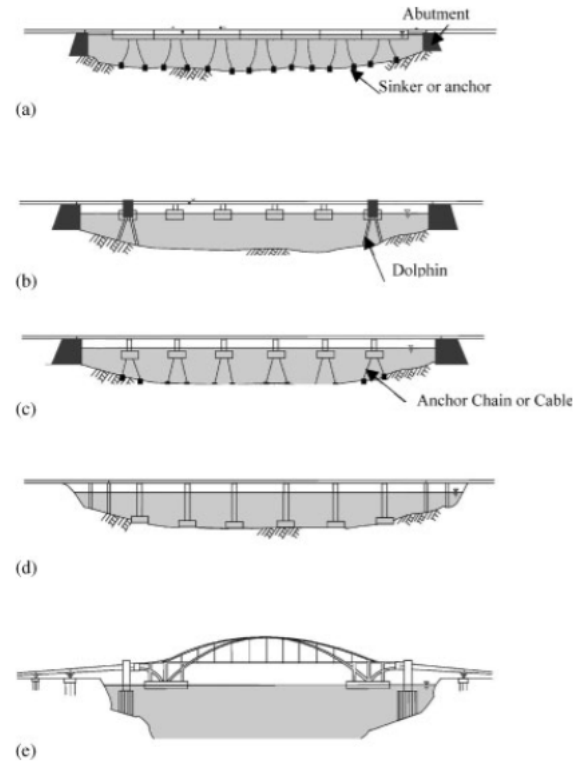
Figure 1: Floating bridge: (a) continuous pontoon bridge; (b) separated pontoon bridge; (c) semi-submerged foundation; (d) bridges with gravity foundation; (e) long-spanned separated foundation, (Watanabe and Utsunomiya, 2003, p. 128)
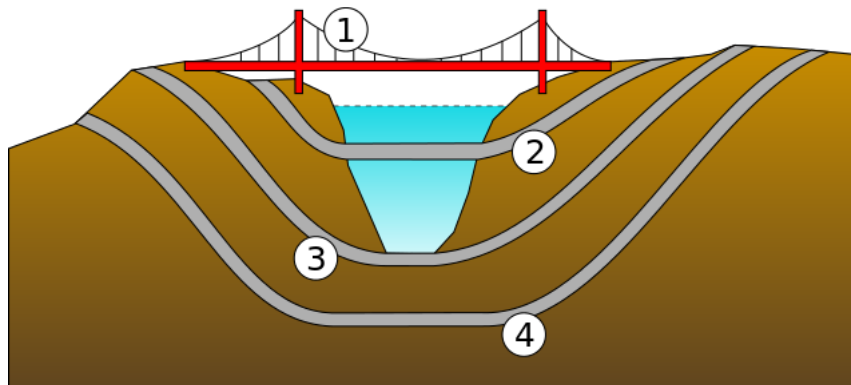
Figure 2: Types of water-spanning structures: (1) Suspension bridge; (2) Submerged floating tunnel; (3) Immersed tunnel; (4) Underwater tunnel (Wikipedia, a)

2.2 Floating bridges in Norway

2.2.1 Bergsøysund bridge

The bridge was opened in 1992, and is a part of the road connection between the islands surrounding Kristiansund and the mainland. The bridge is designed based on American tech-

nology developed for floating bridges that was combined with the knowledge gained from the Norwegian offshore technology. The bridge has a length of 931 meters and 13 spans, where the longest is 106 meters. It stands on seven concrete pontoons, and has a super-structure consisting of steel truss work. The bridge has a horizontal curvature with a radius of 1300 meters.

Figure 3: The Bergsøysundet bridge (Wikipedia, b)

Building the bridge this way resulted in a large increase in the bridges ability to withstand rolling motion, as well as not hindering the waves and current at the location. By using steel elements in the superstructure it will act as as an arch rib when the current is coming from the convex side, and as a catenary cable when the current comes from the other side. These abilities effectively transforms the hydraulic loads into axial member forces in the superstructure and reaction forces at the ends of the bridge. The ends are only con-nected through flexible rods, and excavation of the seabed can be avoided (Watanabe and Utsunomiya, 2003).

2.2.2   Nordhordland bridge

This is the second bridge that was built in Norway, and was opened in 1994. The bridge is located north of Bergen, and it connects Flatøy in Meland municipality with the mainland

straight north of Bergen. The bridge make it easier for the inhabitants on the island to travel to Bergen as it replaced an old ferry connection. The bridge is a combination of a cable-stayed bridge and a floating bridge, where the floating part is built after the same principles used for Bergsøysund bridge. Around the ship opening at the end, it has a tower, from where the cables support the weight of the bridge. The rest of the bridge is a floating bridge of 1243 meters. This part rests on ten concrete pontoons with a span of 113.25 meters between them. With its 1614 meters, it is the second longest bridge in Norway, and the worlds longest free floating bridge (Watanabe and Utsunomiya, 2003). The ten pontoons of the bridge is designed with 9 compartments, where two of them can be flooded without risking a danger to the bridge sinking.

Figure 4: Nordhordaland bridge (NrK)

The Norwegian Public Roads Administration could after the opening observe patterns in the development of traffic. The first year after the opening of the bridge, they experienced a 40 % increase in traffic. The following years it was a stable growth of 4.2 % each year, until 2006 when the toll money was removed. This year there was 25 % more vehicles that crossed the bridge. In the later years there has been a stable increase of 4.3 % every year.

2.3 Floating bridges around the world

2.3.1 Yumemai bridge

The Yumemai bridge is 410 meters long, and has a main span of 280 meters (Watanabe and Utsunomiya, 2003). It is a floating swing arch bridge, and was made to connect two smaller islands to the regional road network in Japan. The design of the bridge emphasized the considerations of waves, wind and earthquakes, swinging mechanism and durability. It stands on 2 pontoons made of steel, and is anchored through dolphins.

Figure 5: Yumemai bridge (Wikipedia, c)

2.3.2 Lacey V. Murrow bridge and 3rd Lake Washington bridge

The Lacey V. Murrow bridge, or the 1st Lake Washington bridge was built in 1940, and is 2018 meters long (Watanabe and Utsunomiya, 2003). The bridge has a total of 23 pontoons made of precast concrete. It is held in place through a cable anchor and crosses the lake in a straight line. Parallel to this bridge goes the 3rd Lake Washington bridge. This bridge was built much later, in 1989, and is only 1771 meters long. It has 18 pontoons, but are otherwise equal to Lacey V. Murray with respect to pontoon material and the anchorage system. These two bridge crosses Lake Washington in the state of Washington in the USA.

Figure 6: Lacey V. Murrow bridge (left) and 3rd Lake Washington bridge (right) (Wikipedia, c)

2.3.3   Hood canal bridge

The Hood Canal bridge was the second floating bridge to be built in the USA. Similarly to the two other bridges just described, it has pontoons made of precast concrete and cable anchoring. The total length of the bridge is 1988 meters, it has a total of 25 pontoons and crosses the water in a straight line. The bridge sunk during a restoration of it in 1990, but was later rebuilt in 1993.

Figure 7: Hood Canal bridge (Chuck Pefley)

From this it can be seen that all of the American bridges are built in a very similar manner. They do all have precast concrete pontoons, a cable anchoring system. and cross the water in a straight line. The only difference between them is their length, and therefore also the number of pontoons. The Yumemai bridge in Japan is the only one that is anchored through dolphins, while the two Norwegian bridges does not have an anchorage system at all. The amount of pontoons is clearly dependent on the length of the bridge, where Yumemai is the shortest with two pontoons, and Lacey V. Murrows is the longest. The bridge has 23 pontoons, but it does not have the largest amount of pontoons. The Hood Canal bridge has the largest amount of pontoons with 25. The Hood Canal bridge is only only 30 meters shorter than the Lacey V. Murrow bridge, so the difference in pontoons can be explained through building year among other reasons.

2.4 Ferjefri E39

As mentioned earlier, the Norwegian Public Roads Administration (NPRA) is investigating how to make a fixed road connection between Kristiansand and Trondheim in Norway (Statens Vegvesen). The project was first presented in the summer of 2010 by the Minister of Transport and Communication. As the road can be considered as the main road along the western coast of Norway, it is of importance to diminish the travel time. The NPRA was asked to give an account of the socioeconomic consequences of the project, as well as the technological possibilities for the fjord crossings. In the summer of 2013 it was up for treatment in the Norwegian parliament. There a resolution was made for the Norwegian National Transport Plan (NTP) 2014-2023. The governments ambition was that the project should be finished, with an improvement of the roads within a 20 year period. When it was taken into the NTP it went from being a possibility study to being a project of the NPRA to collect research and development. Now, they shall contribute with new knowledge into the building projects along the Norwegian western coast. The project in itself is divided into four different parts; the technical development of fjord crossing concepts, an explanation of the social consequences, to find possible solutions for renewable energy and find implementation strategies and contract forms.

The travel time from Kristiansand to Trondheim is estimated to be 21 hours. It is assumed that a new road without ferries will reduce the traveling time by 7-8 hours. This corresponds to a 40 % decrease in travel time. Along the road there are 7 fjords that needs to be crossed. They vary in depth and width, where Sognefjorden is the deepest with a depth over 1250 meters and Bjørnafjorden the widest with a 6 kilometer width. The roads along the Norwegian western coast has a total of 8 ferry connections along the road. It is therefore desirable to build fixed road connections in the form of submerged tunnels or floating bridges, because the fjords are much too deep and wide for regular tunnels and bridges. The distance along the road today is 1068 kilometers, and is presumed to be 47 kilometers shorter when the project is finished. It is only the crossing of Sognefjorden that has been studied to this date. This is because this crossing will become the most extreme fjord crossing that has ever been completed, and if this can be crossed, the other smaller fjords can be as well. Because new technology must be found before the project can be realized, It is interesting to look to the technology that Norway already holds from offshore activity.

For the project, three different kind of main crossing methods has been recommended, together with different types of these. They are a floating bridge, a submerged floating tunnel (SFT) and a fixed bridge. Here they are given in the prioritized order:

Table 2: Recommended solutions for crossing Sognefjorden (Veg)

Type of bridge	Solution
Floating bridge	Anchored in the ends with a cable-stayed bridge on pontoons mid-fjord
Floating bridge	Anchored in the ends with a cable-stayed bridge over a shipping lane in the shoreline
Floating bridge	Combined with a SFT under the shipping lane
SFT	Two parallel, curved tubes connected to pontoons at the water surface
SFT	SFT en a horizantal curve with pontoons and anchorage with horizontal braces to the shore
Suspension bridge	With one main span crossing the entire width of the fjord
Suspension bridge	With towers fundamented on floating pontoons

3   Ship impact

Large parts of the theory presented in this chapter is taken from my project thesis (Jansen, 2015). A ship impact is assumed to be one of the major hazards for marine structures. The damage from the impact may lead to flooding and loss of buoyancy for floating structures. If the impact leads to a large deformation, the structural strength of the bridge may also be of concern. Unfortunately, it is difficult to know the exact forces that will occur in an impact without extensive knowledge on the different aspects of the collision. Theses varies greatly from time to time, as the hull shapes are different, and so are the vessel speed and masses (Moan, 2000).

Structural design is carried out by taking different limit states into account. The first three is serviceability limit state (SLS) , ultimate limit state (ULS) and fatigue limit state (FLS). These only concern the design checks of components under functional and environmental actions. The one I will be looking into here, is the accidental limit state (ALS), which is a survival check of a structural system that has been damaged by an accidental action, such as an impact.

The design of a structure that is in risk of experiencing a collision is designed according to the limit state of accidental actions (ALS) (Amdahl, 2015). These events should not have an annual exceedance level higher than 10^{-4}, and the accidental actions or damage conditions should be established by using risk analysis. This means that you allow local failures in form of denting, plasticity and buckling to occur, but the total integrity of the structures should be secure. When the structure is damaged, it should be able to withstand environmental forces that has an annual return period of 10^{-2}. This is known as an ULS check, and the structure must not be in risk of a total collapse.

The event of a collision can be described by the probability of an impact occurring multiplied with the consequences of that action. The two factors must be related in a way that a major impact that endangers human lives, structures and environment must have a low occurrence rate, and vice versa; an impact that only occurs frequently must result in small consequences (Amdahl and Søreide, 1983).

From this, it can be seen that it is important to find the load that is assumed to have a return period of 10 000 years. At the same time it thee structure must be ensured against minor impacts.

Collisions can be divided into two categories: (Moan, 2000).

- Powered collisions: Collisions where the vessel is steaming towards the installation

- Drifting collisions: Collisions where the vessel is drifting towards the installation

Where a powered collision probably will lead to a larger damage on the structure.

The ship collision load is characterized by a kinetic energy, governed by the mass of the ship, including hydrodynamic added mass and the speed of the ship at the instant of impact. (Veritas, 2010, p. 10)

There are several theories that can be used for calculating the forces that occur during an impact. Most of the developed theories are for ship-to-ship or ship-to-structure collisions, and parts of them are still applicable to bridges. The forces in this type of collision is normally very large and only lasts for a short amount of time. The different methods used to calculate these types of problems are based on energy dissipation methods. This means that the kinetic energy in the impact has to be absorbed by the ship and the structure as strain energy. Small amounts of the kinetic energy may remain as kinetic energy after the collision depending on the impact conditions. The kinetic energy is given by (Amdahl, 2015):

$$E_k = \frac{1}{2}(m+a)v^2 \tag{3.1}$$

And is the basis for most calculations related to ship impacts. DNV rules use a minimum size of 5000 tons and a speed of a least $2\,\frac{m}{s}$ as the requirement for accidental limit states. The added mass is set to be 0.1 for a sideways collision, and 0.1 for a collision in the longitudinal direction. To be able to derive a mathematical problem for an impact there are two criteria that must be fulfilled for the external collision mechanics:

- Conservation of momentum

- Conservation of energy

In ship collision scenarios it is normal to distinguish between the external and internal dynamics. The external dynamics covers the rigid body motions and the given amount of energy that has to be dissipated. The internal dynamics determine how the energy is dissipated throughout the structure and it is related to the local processes of the structural deformation and damage (de Jonge and Laukeland, 2013). The damage caused in a collision can be calculated in two steps. this holds if the duration of the impact is short compared to the period that governs the motion. The first step is to find the external mechanics of the collision, and from these results calculate the kinetic energy that has to be dissipated as strain energy.

The conservation of momentum is based on the following principle. For two colliding bodies without any external effects, the only force that will have an impact on the system is the collision force. This force will be equal, and directed in two opposite directions. By integration of Newton's second law of motion, $F = ma$, over time, we get that the sum of the masses and velocities must be equal before and after the collision. The time domain used in the integration is the time that the impact lasts. The momentum can then be found from the equation (Skanska):

$$m_{s1} v_{s1} + m_{i1} v_{i1} = m_{s2} v_{s2} + m_{i2} v_{i2} \tag{3.2}$$

Where the left hand side of the equation is the momentum before the collision, and the right hand side is after the collision. In an impact which is completely plastic, the colliding bodies will either propagate with a new common velocity or stop and stand still. If the two velocities after the collision is added together and set as a new coefficient, we can now rewrite the equation as:

$$v_c = \frac{m_s v_s + m_i v_i}{m_s + m_i} \tag{3.3}$$

In this equation, v_c is the common velocity at the end of the impact, and the mass and speed of the ship is denoted by s and the components for the bridge is denoted by i. The conservation of energy also has to be found. It is given by:

$$\frac{1}{2} m_s v_s{}^2 + \frac{1}{2} m_i v_i{}^2 = \frac{1}{2}(m_s + m_i) v_c{}^2 + E_{s,s} + E_{s,i} \tag{3.4}$$

And we get the total energy that has to be dissipated as strain energy by the ship and the

bridge expressed as (Amdahl and Søreide, 1983):

$$E_{s,s} + E_{s,i} = \frac{1}{2} m_s v_s^2 \frac{(1 - \frac{v_i}{v_s})^2}{1 + \frac{m_s}{m_i}} \tag{3.5}$$

Where $E_{s,s}$ is the energy that is absorbed by the ship, and $E_{s,i}$ is the energy absorbed by the platform. From this equation, we can see that if the installation has a velocity as well, and this is directed in the opposite direction of the vessel speed, the amount of kinetic energy that has to be absorbed in the impact may exceed the kinetic energy of the vessel. If the impact on the other hand is between a ship and a fixed installation, the value for m_i is set equal to ∞ and v_i equal to 0. Because there often is not enough reliable data available to calculate the energy absorption, E_s, in the ship, this parameter is often neglected, which will give a more conservative calculation for the installation.

As the added mass must be included for buoyant structures, this term has to be added to the mass terms. This is done for the added mass of the ship and the bridge, respectively. It is also of interest to look at the energy that is lost during the process of the collision, mainly through plastic deformations. This will be the difference in the kinetic energy that is lost during the impact. If the installation is assumed to not have a velocity before the collision, this can be expressed as:

$$\Delta E = \frac{1}{2} m_s v_s^2 - \frac{1}{2}(m_s + m_i) v_c^2 \tag{3.6}$$

Where the common velocity can be expressed as in equation (3.7) if the installation stands still, and does not have a momentum before the collision.

$$v_c = \frac{m_s}{(m_s + m_i)} v_s \tag{3.7}$$

By substituting this equation into equation (3.6), we obtain the following expression:

$$\Delta E = \frac{1}{2} m_s v_s^2 \left(1 - \frac{m_s}{(m_s + m_i)}\right) \tag{3.8}$$

If the mass of the installation is large compared to the mass of the vessel, this can then be written as:

$$\Delta E = \frac{1}{2} m_s v_s^2 \left(1 - \frac{m_s}{m_i} \right) \tag{3.9}$$

The next step is to look at the internal collision mechanics and find the distribution of strain energy in the ship and the installation. From this, it is possible to find the damage in the installation. It is the external collision mechanics that determine the amount of kinetic energy that is dissipated as strain energy. This can be found from the relationship:

$$E_s = \beta E_k \tag{3.10}$$

Where β is the factor of dissipated kinetic energy that is absorbed to be the strain energy. The factor is normally is smaller than 1 and can be expressed as:

$$\beta = \frac{1}{1 + \frac{m_s}{m_i}} \tag{3.11}$$

If the relationship between the load and the deformation of an impact is known, they can be plotted against each other, with the load as as a function of the deformation (Furnes and Amdahl, 1980). These curves will in general be non-linear. An example of this can be seen in figure 12. The area beneath each curve is the amount of energy that is absorbed by the ship and the installation. From these data, it is possible to see the connection between the absorbed energy and the damage that the two bodies will undergo. This relationship can then be expressed on the following form:

$$\frac{1}{2} m_s v_s^2 = A_s + A_i \tag{3.12}$$

Where A_s is the area under the curve for the ship and A_i is the area under the curve for the installation. In the event of any collision, the collision mechanics will work in a certain way. At any instant during the impact it is the weakest element that will deform. If an impact with equally strong structures occur, the collision mechanics start to work when the colliding body penetrates the other one. This will continue to cause deformation until the other structure are able to generate enough membrane forces to start dealing damage to the penetrating body (Storheim and Amdahl, 2014). This effect of the relative strength is often neglected in collision studies, but is an important effect that should be accounted for.

3.1   Bow collisions

Because the bows and bulbs of ships are so individual, it is impossible to derive a model for all the different shapes. Therefore, a model has to be made to each hull shape to make a realistic scenario. This will be very tedious work, and therefore only approximations has been made for several different bow shapes. Some of the different numerical approximations that has been developed will be presented here. It was necessary to pick just a few, because there are so many. The methods presented are based on several model tests, and numerical methods has been applied to find the most fitting equation.

3.2   Minorsky's method

Minorsky developed his method in 1959, making it one of the first proposed methods for calculating ship-crushing loads,. It forms a basis for the methods that has been developed in the later years (Minorsky, 1959). His work is seen as pioneering within the field of ship collisions. He based his method on investigation of what happened in ship-to-ship collisions. From the observations he was able to establish a linear relationship between the volume of steel that was deformed and the energy that was dissipated in the deformation. Through the relationship, it is possible to determine the ship's penetration into the other structure before all of the initial kinetic energy is absorbed. This correlation is shown in figure 8 below.
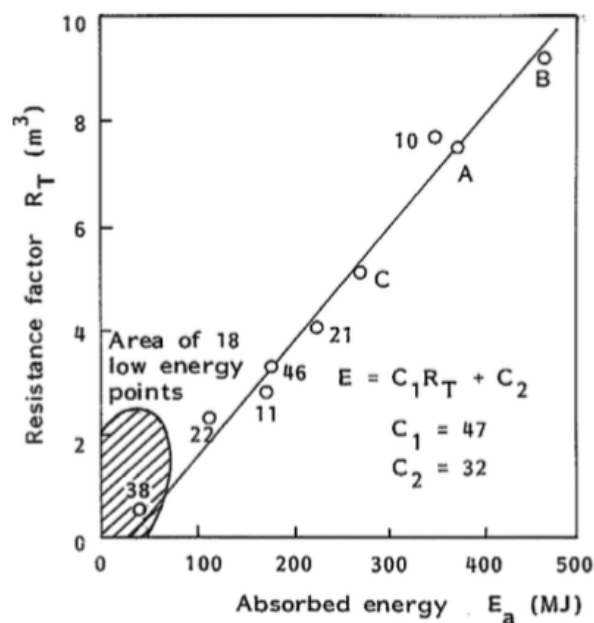

Figure 8: Relationship between the volume of steel deformed and dissipated energy in the deformation (Minorsky, 1959)

In the figure it can be seen that the y-axis is the resistance factor R_T. This factor is found by calculating the volumes that has a depth in the direction of the penetration. And therefore it is dependent on the variations of the stiffeners. Because of this, it is required that you have knowledge on the vessels stiffener spacing and their dimensions. This is done to obtain the volume of the steel that deforms during the impact. If one has this knowledge, Minorsky's method will correlate very well with numerical results. This method does not assess the force development during indentation.

3.2.1 Gerard's method

This method was developed through a series of panel tests that used different stiffener types (Gerard, 1957). These results was then used to find an expression from the correlation between the different parameters. This is the most known method outside of the field of marine structures. The final relationship is given below.

$$\sigma_c = \sigma_0 \beta_g \left[\frac{nt^2}{A} \sqrt{\frac{E}{\sigma_y}} \right]^m \tag{3.13}$$

Where σ_y is the yield stress, σ_0 is the compressive flow stress including the strain rate effects if there is dynamic loading, E is the Young's modulus, β_g and m are coefficients dependent on edge restraints. For a distorted unloaded edge, these values are given as $\beta_g = 0.56$ and $m = 0.85$. n is the sum of cuts and flanges for the cross-section under consideration and the method for finding this is shown in figure 9, t is the average thickness for the cross-section under consideration and A is the cross-sectional area.

The strain rate is given as:

$$\dot{\varepsilon} = \frac{v_x}{s} \tag{3.14}$$

where v_x is the velocity in the longitudinal direction during impact and s is the frame spacing. The method then uses a formula developed by (Marsh and Campbell, 1963) to find the dynamic flow stress σ_0. This relationship is expressed as:

$$\sigma_0(\dot{\varepsilon}) = 1.29 \sigma_{0s} \dot{\varepsilon}^{0.037} \tag{3.15}$$

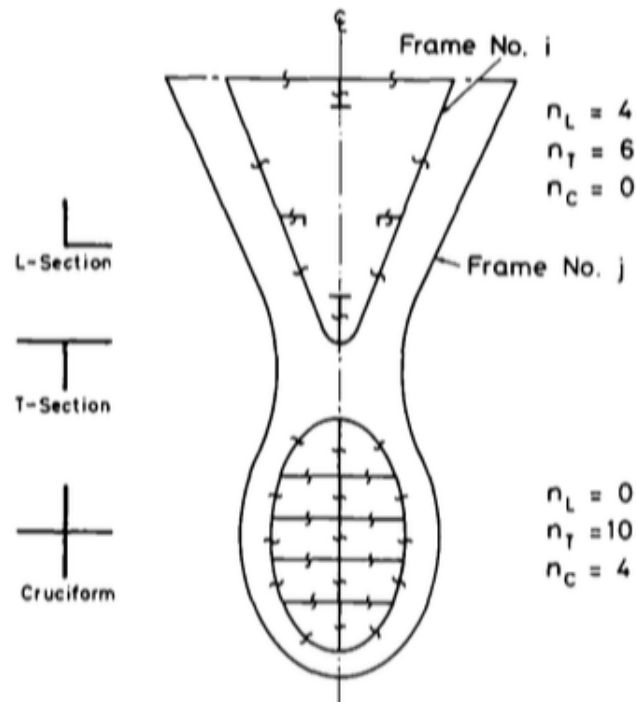where σ_{0s} is the static strength of the steel material.

Figure 9: The method used to cut cross-sections of a bulbous bow to be able to determine the number of basic crushing elements (Terndrup Pedersen et al., 1993)

Gerard's method will predict the maximum crushing load of structures with plates with an error range of ±10% (Terndrup Pedersen et al., 1993). A weakness to this method is that it is based on an experiment where the parameter variation has been limited.

3.2.2 Amdahl's method

The method that Amdahl developed for his dr. ing. thesis was based on theoretical considerations (Amdahl, 1983). This is mainly related to the folding mechanisms of a plate and the theory developed by (Wierzbicki, 1983). This mechanism is shown in figure 10. By looking at the energy dissipated during plastic deformation of basic structural members, an equation that considers several structural elements could be established. The elements that was in the equation included was the angle, the amount of T-sections, and cruciforms.

To be able to find the total crushing force, a specific structure has to be specified. This is done through addition of the contributions from the different basic elements in a specific cross-section. For every element the folding length and crushing load is determined by
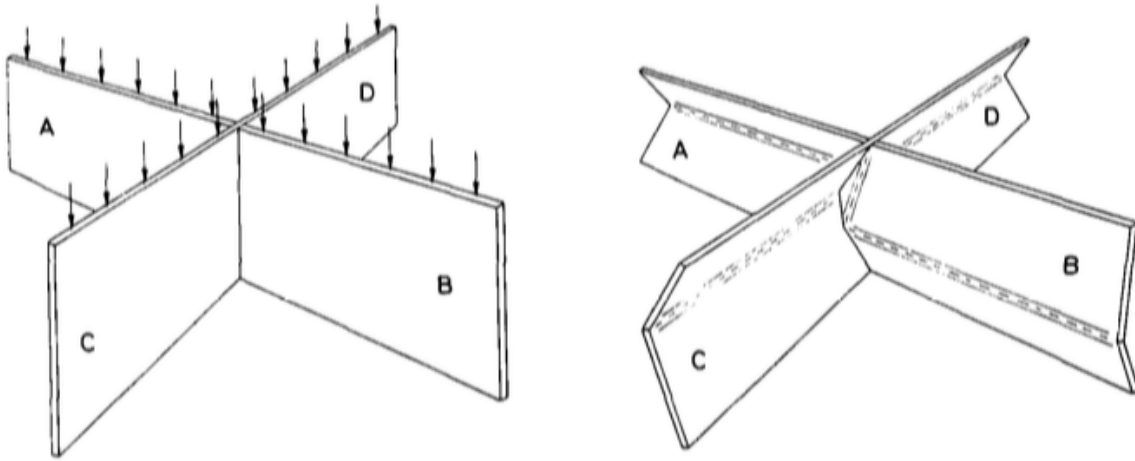
Figure 10: Crushing mechanism for a crucified structural member (Terndrup Pedersen et al., 1993)

minimizing the absorbed energy during the process of the element folding. From this, the following equation for predicting an average crushing strength is found.

$$\sigma_c = 2.42\sigma_0 \left[\frac{n_{AT}\,t^2}{A}\right]^{0.67} \left[0.87 + 1.27\frac{n_c + 0.31 n_T}{n_{AT}}\left(\frac{A}{(n_c + 0.31 n_T)\,t^2}\right)^{0.25}\right]^{0.67} \tag{3.16}$$

Where σ_c is the average crushing strength of the bow, σ_0 is the ultimate strength of the steel used, and are calculated through the equations 3.14 and 3.15, t is the average plate thickness of the cross-section under consideration, A is the cross-sectional area of deformed steel material, n_c is the number of cruciforms in the cross-section that is under consideration, n_T is the number of T-sections in the cross-section and n_{AT} is the number of angle and T-sections in the cross-section. All of the three last parameters can be calculated based on figure 9. The total crushing load is found by multiplying the cross-sectional area with the amount of deformed steel:

$$P_c = \sigma_c A \tag{3.17}$$

3.2.3   Yang and Caldwell's method

This method was developed on the same basis as Amdahl's method was. It has the same assumptions for the deformation and the energy evaluation, as well as it uses the theory of the folding mechanisms in figure 10. One of the differences in Yang and Caldwell from Amdahl is in the assumption of how the energy in the structure is dissipated during the collision. Another difference is that Amdahl uses minimization of the deformation energy during the folding and deformation to determine the folding length and crushing load. Yang and Caldwell on the other hand takes the folding length, H, and sets it equal to the spacing between transverse frames. They also account for the longitudinal stiffeners as an equivalent thickness of the shell. By doing this the plastic bending moment of the equivalent plating is equal to the plastic bending moment of the shell with longitudinal stiffeners (Yang and Caldwell, 1988). The equation then becomes:

$$P_m = \sigma_0 \left[\frac{1.178}{H} \sum^{n_f} b_i t_i^2 + 0.215 \sum^{n_{AT}} t_i + 6.935 \sum^{n_{AT}} t_i^2 + 0.265 H \sum^{n_T} t_i \right.$$
$$\left. + 0.589 \sum^{n_T} t_i^2 + 0.75 H \sum^{n_c} \sum^4 t_i + 0.375 H \sum^{n_c} \sum^4 t_i^2 \right] \quad (3.18)$$

Where P_m is the mean crushing load of structure, σ_0 is the flow stress based on the mean value of the yield and the ultimate strength of the steel, b_i is the width of the i'th plate flange, t_i is the thickness of the i'th plate flange, H is the folding length of the distorted plate flanges, n_c is the number of cruciforms in the cross-section that is under consideration, n_T is the number of T-sections in the cross-section, n_{AT} is the number of angle and T-sections in the cross-section and n_f is the total number of flanges, angles and T-sections and cruciforms.

3.3 Standards

Det Norske Veritas has released a standard for design against accidental loads, DNV-RP-C204 (Veritas, 2010). This standard is similar to the recommendations found in the NORSOK N-004 standard, appendix A (NORSOK, 2004). These standards are developed to make sure that platforms on the Norwegian continent shelf is safe against ship collisions among other things. Even though a bridge is not a platform, it has adapted some of the design from a semi-submersible. Some aspects in the standard can therefore be seen as applicable to a floating bridge. Furthermore, it contains guidelines on simple hand calculations that can be performed to verify results from simulations. I will here look at some of the relevant aspects in the standards.

The structural effects from the collision may be considered in two different ways. One of them is by non-linear dynamic finite element analyses, and the other one is by energy considerations combined with simple elastic-plastic methods. It is often wise to verify an installations integrity by performing some simple hand calculations. The strain energy dissipation should be considered on three different levels:

- Local cross-section

- Component/substructure

- Total system

It should also be looked into the interactions between the three levels. Plastic modes of energy dissipation must be considered for all cross-sections, components and sub-structures. Often elastic strain energy can be disregarded, but the axial flexibility can have a significant effect on the load-deformation relationships on the two lowest levels. The elastic energy on the other hand may have a significant effect on the global model. When looking at the strain dissipation energy, it should be considered at three different levels, all related to how the structure will absorb the strain dissipation energy in the impact:

- Strength design - in this case it is implied that the installation is strong enough to resist the collision force with only minor deformations, and in this way forcing the ship to deform and dissipate the major part of the energy.

- Ductility design - in this case it is implied that it is the installation the undergoes the biggest deformations and has to dissipate the largest amount of the energy.

- Shared-energy design - in this case the strain dissipation is shared between the two structures, and they absorb nearly equal parts of the energy.

In general it should be noted that the difference between ductile and strength is quite small. There is not a very large change in strength that is needed before a structure will deform the other structure instead (Storheim and Amdahl, 2014). A graph of these cases are shown in figure 11.
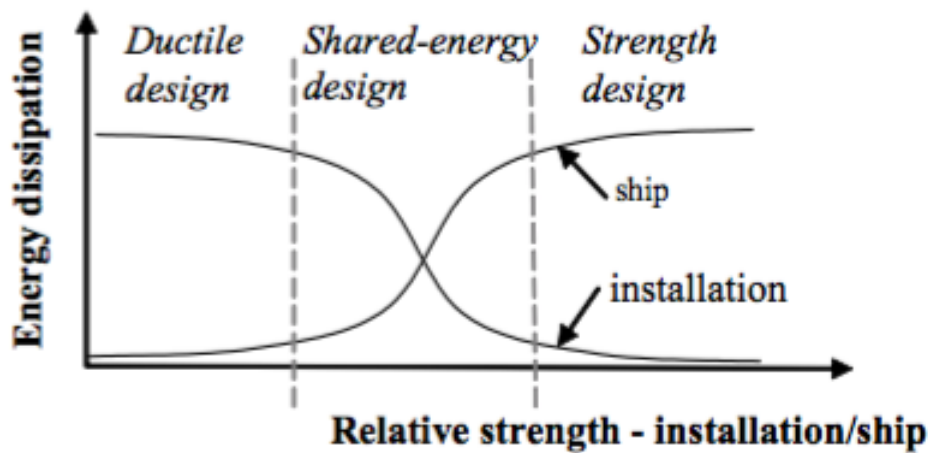

Figure 11: Energy dissipation for strength, ductile and shared-energy design (Veritas, 2010)

As mentioned earlier the kinetic energy in the impact must be dissipated in the installation as strain energy (Veritas, 2010). Depending on the type of installation, the amount of strain energy that must be absorbed can be found from one of the equations given below.

For compliant installations:

$$E_s = \frac{1}{2}(m_s + a_s)v_s{}^2 \frac{(1 - \frac{v_i}{v_s})^2}{1 + \frac{m_s + a_s}{m_i + a_i}} \tag{3.19}$$

For fixed installations:

$$E_s = \frac{1}{2}(m_s + a_s)v_s{}^2 \tag{3.20}$$

And for articulated installations:

$$E_s = \frac{1}{2}(m_s + a_s)\frac{(1 - \frac{v_i}{v_s})^2}{1 + \frac{m_s z^2}{J}} \tag{3.21}$$

The structural response of the ship and the installation can be plotted as a function of the deformation. This has been done in figure 12. In the plot, the relationship between the strain energy dissipated in the ship and the installation is shown. It is also worth mentioning that the area under the graph represents the strain energy dissipated by the two structures under the same load condition, this can also be expressed as an equation:

$$E_s = E_{s,s} + E_{s,i} = \int_0^{w_{s,max}} R_s dw_s + \int_0^{w_{i,max}} R_i dw_i \tag{3.22}$$

As it is difficult to know the exact load level of a collision before it occurs, it is in general a need for an incremental procedure. Establishing the load-deformation curves for the ship and the installation is done by assuming that the other installation is completely rigid. In the approach describes here, it is common that the stronger structure will experience a little less damage than this method yields, and the ductile one will suffer a little more damage than predicted. When the weaker structure deforms, the stronger structure will experience a larger resistance to the impact, as the forces from the impact will be distributed over a larger area.
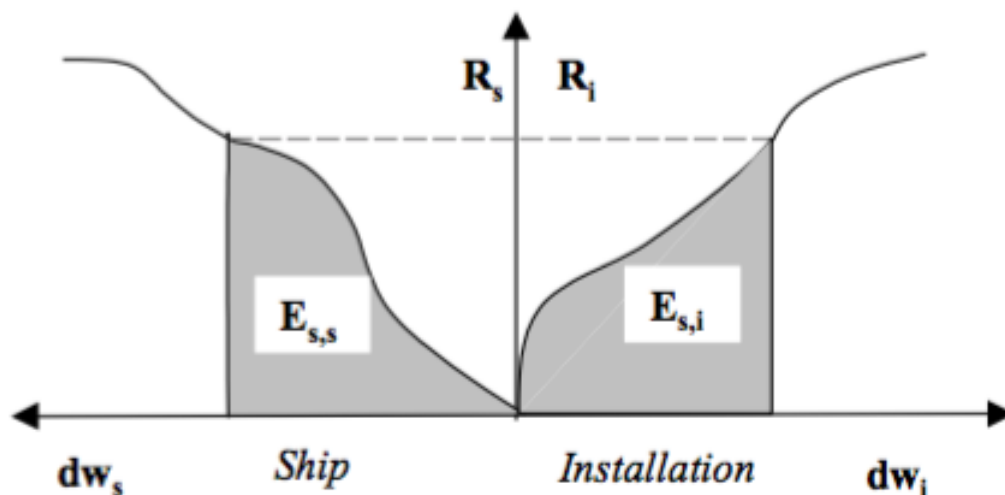

Figure 12: Dissipation of strain energy in ship and platform (Veritas, 2010)

In the practice, DNV recommends that a vessel with a mass of 5000 tons and a velocity

of $2\frac{m}{s}$ is used for the calculations. The deformation curve that is recommended to use for a vessel of this size and velocity is shown in figure 13. The figure has curves for beam, bow and stern impacts. In the graph the curves for the broad side and stern collision is for a scenario where an infinitely rigid wall is penetrated. This curve is therefore very usable for jacket legs. The plot of the stern corner is based on the penetration of an infinitely rigid cylinder. This is therefore applicable to column impacts, where the column has a large diameter. The last curve is that of the bow impacts. This is for an impact with an infinitely rigid wall, and has the same usage area as for the stern corner impact. The last one should not be used for a collision with tubular braces.
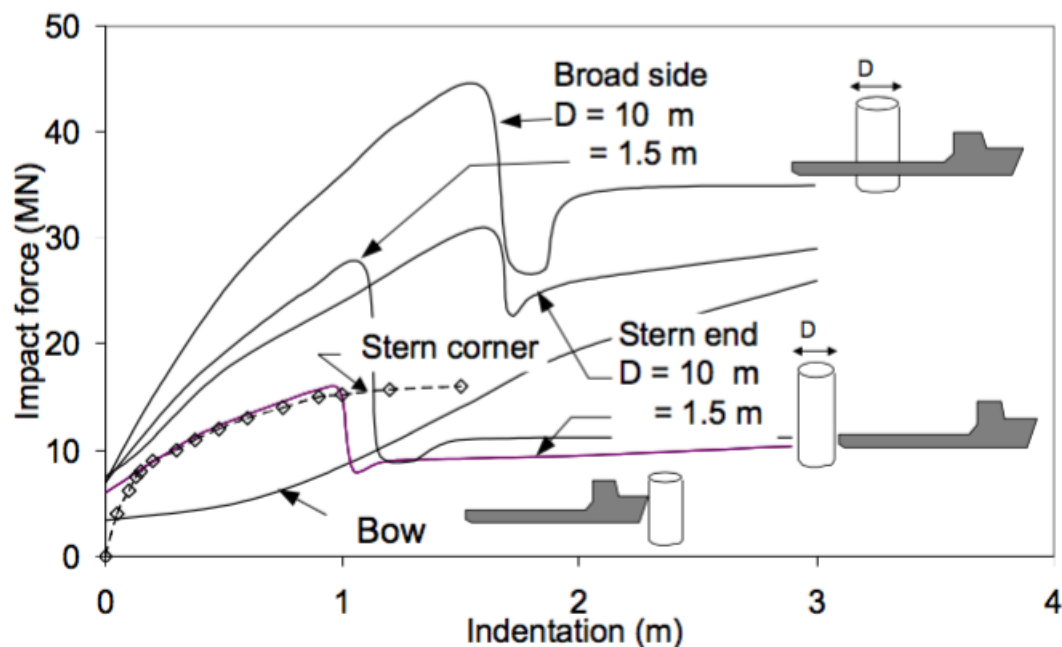

Figure 13: Recommended deformation curve for beam, bow and stern impact (Veritas, 2010)

As we can see from the figure, it is an impact with the broad side that will generate the largest impact forces.

3.4   Ship collision risk studies for crossing Sognefjorden

To be able to build a bridge across one of the broad Norwegian fjords, it is of vital importance to know something about the ship traffic in the fjord (Randrup-Thomsen et al., 2013). The more vessels that travel in the fjords, the more likely it will be that a collision happens. Larger vessels will result in an impact with a lot more energy, that yields larger damages to the bridge. A risk analysis can be done by making a risk model based on existing data, such as bathymetry, geography, bridge geometry, weather, current and very detailed ship traffic recordings (AIS data) as well as . This model can then be used to estimate the probability that a collision will occur, and be used as a design basis for the bridge and the design loading requirements for the bridge.

Because of the ongoing Ferjefri E39 project, Rambøll has established a ship collision risk model for this usage. To find out how many ships that pass through Sognefjorden, the Automatic Identification System(AIS) data was used. The system registers ship movements automatically to identify and locate vessels. It should be noted that the AIS do not register smaller vessels, but these will not contribute to a fatal damage on the bridge either.

For the distance where the new bridge is supposed to cross Sognefjorden there are today four important sailing routes. These routes can be seen a dependent on the vessel types. They can therefore be divided into 3 main categories given here as:

- Commercial ships, which also includes cruise ships

- High Speed Passenger crafts (HSC)

- Local traffic

These traveling routes in relation to where the bridge is going to cross the fjord is shown in figure 14.
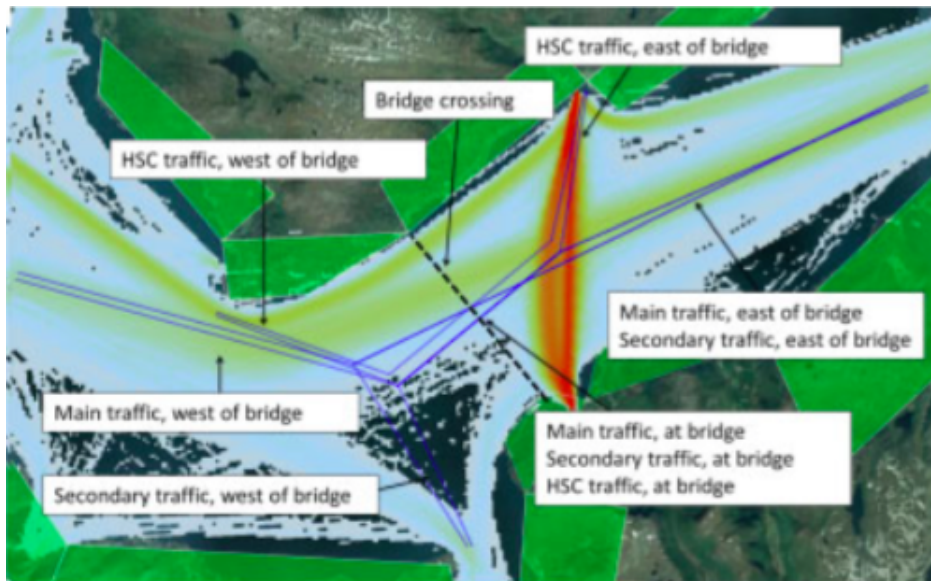
Figure 14: Intensity plot of current ship traffic in Sognefjorden, and estimated sailing routes when the bridge has been built (Randrup-Thomsen et al., 2013)

To use the collected data, each ship on a route had to be assigned a GT class, and a forecast was developed for the year 2030. Specially cruise ship traffic is expected to increase the next years. Other ships are also foreseen to increase in size, with a rate that is related to the national economic growth.The forecast for 2030 is given in figure 15.
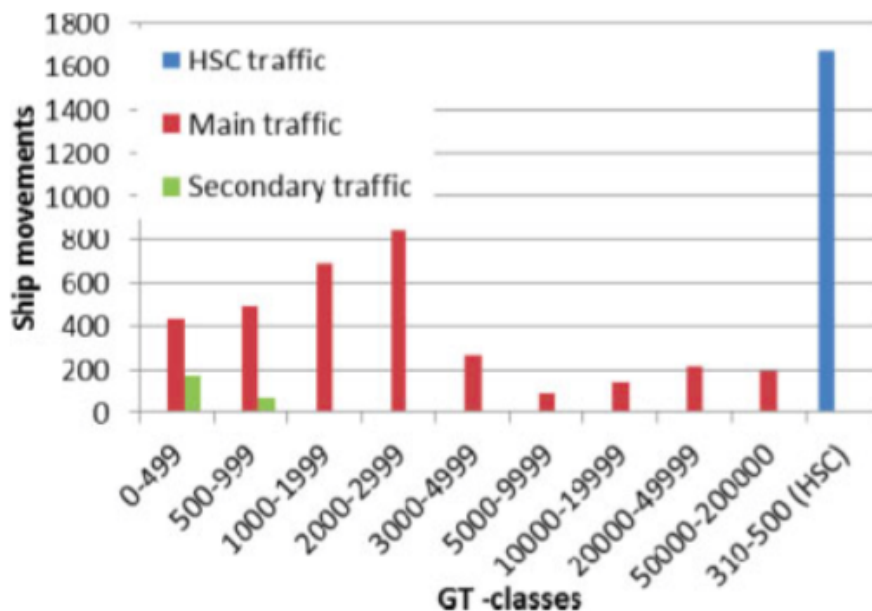

Figure 15: Distribution of ships in GT classes. Forecasted for 2030 (Randrup-Thomsen et al., 2013)

The risk of an impact occuring between a ship and an obstacle is dependent on two factors given by (Randrup-Thomsen et al., 2013) as:

1. *The probability of a ship being on a collision or grounding course*

2. *The probability that the navigator(s) does not make evasive actions in due time*

For a floating bridge crossing Sognefjorden, the final collision frequency for the total floating bridge is 9.2×10^{-3}. This corresponds to a return period of about 100 years. From the study, head on collisions and sideways collision has the same collision frequencies. But the collision energy in a head on collision will be much larger than that of a sideways collision, and cause significantly more damage. The most damaging collision will give an impact energy of 2855 MNm.

4 Finite Element Method

ABAQUS base its calculations on the Finite Element Method (FEM). The method is a numerical approach where different general differential equations can be solved in an approximate manner. The physical problem that are to be considered must hold over a defined region, and may be in one, two or three dimensions. The entire structure that is under consideration is divided into smaller parts, or *finite elements*. The calculations are then done for each element, and the total sum of all of the finite elements is called a finite element mesh. The general idea is that with an increasing number of elements, the more accurate will the solution become. By determining the behavior of all the elements, the elements can be patched together and give the solution for the entire body (Saabye Ottosen and Petersson, 1992).

The Finite Element Method is based on fundamental laws. These laws are used for all structural problems, and the problem can be solved by using the following conditions (Moan, 2003).

- Equilibrium of all parts in the structure, for both stresses and internal forces

- Compatibility in the material, for displacements and strains

- Stress/strain relationship, meaning Hooke's law for a linearly elastic material has to apply

And the assumptions that:

- Displacements are small

- The material is linear and elastic

For the equilibrium condition, an infinitely small cube can be looked at, with all stress components present, this is shown in figure 16.
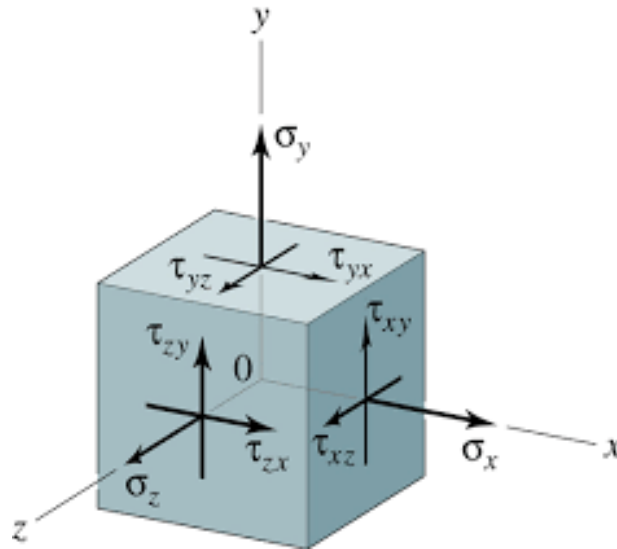

Figure 16: Stresses on a volume element (Recinto Universitaro de Mayaguez)

To obtain an exact solution to a problem, all of these small cubes inside of a meshed element has to be in equilibrium.

4.1   Main steps of the FEM

The FEM can be divided into six distinctive steps on how a problem is solved. These will be presented in here. Large parts of this chapter is found in (Moan, 2003).

4.1.1   Discretization

The first step of the method, is to divide the structure into several smaller parts, or finite elements. The results from the analysis will be greatly dependent on the number of finite elements the structure has been divided into.

4.1.2   Element analysis

This part has two conditions that has to be achieved. The first is to express the displacements within the elements, and the second is to maintain the equilibrium in the elements. Another important thing that has to be kept an eye on, is that compatibility is maintained by fulfilling the stress-strain relationships. Further, the displacements inside the element must be

expressed as shape functions. These functions are scaled by the node displacements. If the expressions for the shape function are assumptions, the displacement at any point inside the element can be found through the nodal displacements. The element stiffness relationship given below is established.

$$S = kv + S^0 \tag{4.1}$$

Where S is the generalized nodal point forces, k is the element stiffness matrix, v is the nodal point displacements and S^0 is the nodal point forces for external loads.

4.1.3 System analysis

In the system analysis a relationship between load and the nodal displacements must be established. This is done by requiring equilibrium in all nodal points in the structure. The following relationships then emerge:

$$R = Kr + R^0 \tag{4.2}$$

$$K = \sum_j a_j^T k_j a_j \tag{4.3}$$

$$R^0 = \sum_j a_j^T S_j^0 \tag{4.4}$$

4.1.4 Boundary conditions

The boundary conditions can now be introduced. This is done by applying the known node values to their respective nodes, or add spring stiffnesses.

4.1.5 Finding global displacements

To find the global displacements, the linear set of equations given above must be solved, this is done through the equation underneath.

$$r = K^{-1}(R - R^0) \tag{4.5}$$

4.1.6   Calculation of stresses

The stresses in the element can by found from the strains by usage of Hooke's law. The strains are found from the displacement functions inside of the element in combination with Hooke's law. Generally, this may be expressed as:

$$\boldsymbol{\sigma}(x, y, z) = \boldsymbol{DB}(x, y, z)\boldsymbol{v} \tag{4.6}$$

$$\boldsymbol{v} = \boldsymbol{ar} \tag{4.7}$$

where $\boldsymbol{D}$ is Hooke's law on matrix form and $\boldsymbol{B}$ is derived from $\boldsymbol{u}(x, y, z)$.

4.2   Shell elements

Shell elements are curved, and can be characterized by carrying the loads in a combination of in-plane (membrane) forces and bending moments. This interaction between forces and moments occurs because of the surface curvature. A general shell will carry the forces as membrane forces. The bending effects will occur because of the boundary conditions, or when the geometry does not match the variations in loading, for example when a concentrated force is applied to the structure. Shells can be categorized into the same two categories that plates are:

- Thin shell theory

- Thick shell theory

4.2.1   Kirchhoff theory

The Kirchhoff theory deals with thin shells, and has a base in the Kirchhoff thin plate theory. In the case of thin plates, the in-plane stresses in the element are expressed by the curvature of the shell. From this, it is implied that the lateral displacement together with its first derivatives must be continuous across the element to ensure compatibility. This yields that the Kirchhoff theory requires C^1-continuity Saabye Ottosen and Petersson (1992). In the thin plate theory, the shear forces cannot be determined from the displacements, which may be concerning, as shear stresses are important for the design check. The thin plate theory is based on two assumptions:

- The stress σ_z is negligible

- The deformation is in accordance with Kirchhoff-Navier's hypothesis

In the Kirchhoff-Navier hypothesis the deformations are described. It says that points on the midsurface z = 0 only moves in z-direction while the plate undergoes bending deformations. The next one is that a line that is straight and normal to the midsurface is assumed to remain straight and normal to the midsurface after bending, and yields that shear deformations must be assumed to be zero. Here, the theory contradicts itself between the existence of the shear stresses σ_{xz} and σ_{yz}, which are necessary to maintain equilibrium, and the shear strains γ_{xz} and γ_{yz}. This works well for thin plates because the real shear strains γ_{xz} and γ_{yz} are small. Because the stress is assumed to be zero in z-direction, the following stress-strain relationship is obtained:

$$\boldsymbol{\sigma} = \begin{bmatrix} \sigma_x \\ \sigma_y \\ \sigma_z \end{bmatrix} = \frac{E}{1-\nu^2} \begin{bmatrix} 1 & \nu & 0 \\ \nu & 1 & 0 \\ 0 & 0 & \frac{1}{2}(1-\nu) \end{bmatrix} = \boldsymbol{D\varepsilon} \tag{4.8}$$

4.2.2 Mindlin-Reissner theory

The Mindlin-Reissner theory is on thick shells. These types of elements only require C^0-continuity, and are applicable to both thin and thick plates. The main difference from thin plate is the assumption of the deformation pattern. Because the shear deformation is taken into account, it will give a better approximation for the shear forces and the corresponding stresses.

In Mindlin theory it is assumed that a line that is straight and perpendicular to the midsurface before deformation will remain straight, but not necessarily perpendicular to the midsurface after deformation, and thereby allowing for shear deformations. Also, the lateral stress component, σ_z is negligible. The stress-strain relationship for thick plates is then expressed as:

$$
\begin{bmatrix} \sigma_x \\ \sigma_y \\ \tau_{xy} \\ \tau_{xz} \\ \tau_{yz} \end{bmatrix} = \frac{E}{1-\nu^2} \begin{bmatrix} 1 & \nu & 0 & 0 & 0 \\ \nu & 1 & 0 & 0 & 0 \\ 0 & 0 & \frac{(1-\nu)}{2} & 0 & 0 \\ 0 & 0 & 0 & \frac{(1-\nu)}{2k} & 0 \\ 0 & 0 & 0 & 0 & \frac{(1-\nu)}{2k} \end{bmatrix} \begin{bmatrix} \varepsilon \\ \varepsilon \\ \gamma_{xy} \\ \gamma_{xz} \\ \gamma_{yz} \end{bmatrix} = \boldsymbol{D}_{MI}\boldsymbol{\varepsilon} \qquad (4.9)
$$

Where the k is a correlation factor set to 1.2 to ensure that the shear strain energy for the plate can correctly be represented by a uniform shear stress.

4.2.3   Shear locking and hourglassing

When using shell elements, shear locking may appear (Ehlers, 2013). The element will then appear as overly stiff under bending. This phenomenon arises when the linear elements in the shell can't accurately model the curvature present in the actual material during bending. This problem is then solved by introducing a shear stress, which do not appear in the real element. This additional shear stress in the element causes the element to reach equilibrium with smaller displacements, which means that it makes the body appear stiffer then it is in reality. This again gives smaller bending displacements than they are. Increasing the number of elements will allow a more accurate modeling of the curvature, and reduce the effects of shear locking.

Hourglassing often occur when you try to address the shear locking problem. Shear locking is often solved by introducing reduced integration. A reduced integration element is tolerant to shape distortions which makes it preferable in FEM modeling. Even though this gives a solution to the problem, a new one may arise. The reduced integration first order element has a numerical problem that makes it overly flexible. This problem is referred to as hourglassing. This phenomenon in FEM modeling gives hourglass modes in an element, it is especially prominent when coarse meshes are used. These modes are non-physical modes with zero energy. This means that they do not generate any stresses or strains, but they may affect the accuracy of the solution, and it is important to keep them under control.

4.3   Beam theory

A beam is dominated by it extension in the axial direction, and it it possible to make certain assumptions about the structural deformation, or the kinematic relationships of the beam to simplify the problem. In beams the deflection denoted as, w, is unknown. It therefore of interest to assume a displacement pattern of w inside of the element. Together with this the principle of virtual displacements has to be applied. This forms a basis for the beam theories that will be described in the next sections.

4.3.1   Bernoulli beam theory

The fundamental kinematic assumption for the Bernoulli beam, is that plane sections normal to the beam axis remain plane and normal to the beam axis during the deformation. Further it is assumed that Hooke's law for isotropic materials applies. The only strain that will not be zero is, ε_{xx}, and this can now be expressed as (Saabye Ottosen and Petersson, 1992):

$$
\begin{bmatrix} \sigma_{xx} \\ \sigma_{yy} \\ \sigma_{zz} \end{bmatrix} = \frac{E\varepsilon_{xx}}{(1+v)(1-2v)} \begin{bmatrix} 1-v \\ v \\ v \end{bmatrix}
\tag{4.10}
$$

With $\sigma_{xy} = \sigma_{xz} = \sigma_{yz} = 0$.

This means that σ_{xz} must be zero, but in reality this must be non-zero to be able to obtain a non-zero shear force, V. Therefore we have $\sigma_{xz} \neq 0$ and $\gamma_{xz} = 0$ and the constitutive relationship $\sigma_{xz} = G\gamma_{xz}$ Because of this, the assumption given below is used instead:

$$
\sigma_{xx} = E\varepsilon_{xx}
\tag{4.11}
$$

And we accept the contradiction $\sigma_{xz} \neq$ and $\gamma_{xz} = 0$, and shear deformations will therefore become negligible.

For this type of beam, the FE formulation is based on having a beam with a cross-sectional area, A, and a length, L. All of the beam properties has to be constant, and not change along the beam length or with time. The beam can only take up loads in the nodes, and if a dis-

tributed loading is applied, the load must be approximated as point loads in the nodes. The beam requires C^1-continuity. This can be expressed on the form:

$$\boldsymbol{K}^e \boldsymbol{a}^e = \boldsymbol{f}^e \tag{4.12}$$

where $\boldsymbol{a}$ is the vector with the nodal displacements and $\boldsymbol{f}$ is the force vector, consisting of the sum of the boundary vector $\boldsymbol{f}_b$ and the load vector $\boldsymbol{f}_l$. And these together with the stiffness matrix, $\boldsymbol{K}$, is expressed as:

$$\boldsymbol{K}^e = \int_a^b \boldsymbol{B}^{eT} EI \boldsymbol{B}^e \, dx \tag{4.13}$$

$$\boldsymbol{f}_b^e = [\boldsymbol{N}^{eT} V]_a^b - \left[\frac{d\boldsymbol{N}^{eT}}{dx} M \right]_a^b \tag{4.14}$$

$$\boldsymbol{f}_l^e = \int_a^b \boldsymbol{N}^{eT} q \, dx \tag{4.15}$$

For this system, the boundary conditions can be expressed as kinematic or static. The kinematic boundary condition is described by the deflection w of the beam, and its slope $\frac{dw}{dx}$. The static condition is on the other hand described by the moment, M and the shear force, V. The three equations can now be written out as:

$$\boldsymbol{K}^e = \frac{EI}{L} \begin{bmatrix} \frac{12}{L^2} & \frac{6}{L} & -\frac{12}{L^2} & \frac{6}{L} \\ \frac{6}{L} & 4 & -\frac{6}{L} & 2 \\ -\frac{12}{L^2} & -\frac{6}{L} & \frac{12}{L^2} & -\frac{6}{L} \\ \frac{6}{L} & 2 & -\frac{6}{L} & 4 \end{bmatrix} \tag{4.16}$$

$$\boldsymbol{f}_b^e = \begin{bmatrix} -V_{x=0} \\ M_{x=0} \\ V_{x=L} \\ -M_{x=L} \end{bmatrix} = \frac{6EI}{L^2} \begin{bmatrix} \frac{2EI}{L} \\ 1 \\ -\frac{2EI}{L} \\ 1 \end{bmatrix} \tag{4.17}$$

$$\boldsymbol{f}_l^e = \begin{bmatrix} \frac{1}{2} qL \\ \frac{1}{12} qL^2 \\ \frac{1}{2} qL \\ -\frac{1}{12} qL^2 \end{bmatrix} \tag{4.18}$$

4.3.2 Timoshenko beam theory

The theory in this section in mainly taken from (Tim). The Timoshenko beam theory is specially applicable to non-slender beams, and high-frequency responses. In this theory, the effects from shear together with the effect from rotation is added to the Euler-Bernoulli beam theory. In a slender beams these effects are negligible, but for thicker beams these must be taken into consideration. The fundamental kinematic assumption for a Timoshenko beam is that a plane section normal to the beam remains plane, but not necessarily normal to the beam axis during deformation. Because of the introduction of a shear forces together with the rotational effects, the stiffness matrix, $\boldsymbol{K}$, is divided into two parts. One for the material stiffness, $\boldsymbol{K}_M$, and one for the geometric stiffness, $\boldsymbol{K}_G$. This beam requires C^0-continuity. The material stiffness is a result of the variation in δz of the stress resultants, while $\boldsymbol{B}$ is fixed. And we get:

$$\delta z = \begin{bmatrix} \delta N \\ \delta V \\ \delta M \end{bmatrix} = \begin{bmatrix} EA_0 & 0 & 0 \\ 0 & GA_0 & 0 \\ 0 & 0 & EI_0 \end{bmatrix} \begin{bmatrix} \delta \varepsilon \\ \delta \gamma \\ \delta \kappa \end{bmatrix} = \boldsymbol{S} \delta \boldsymbol{h} \tag{4.19}$$

where $\delta \boldsymbol{h} = \boldsymbol{B} \delta \boldsymbol{u}$, and the term $\boldsymbol{B}^T \delta z$ becomes $\boldsymbol{B}^T \boldsymbol{S} \boldsymbol{B} \delta \boldsymbol{u} = \boldsymbol{K}_M \delta \boldsymbol{u}$. From this we obtain the expression for the material stiffness matrix as:

$$\boldsymbol{K}_M = \int_{L_0} \boldsymbol{B}^T \boldsymbol{S} \boldsymbol{B} dx' = \boldsymbol{K}_M^a + \boldsymbol{K}_M^b + \boldsymbol{K}_M^s \tag{4.20}$$

where $\boldsymbol{K}_M^a, \boldsymbol{K}_M^b$ and $\boldsymbol{K}_M^s$ are due to axial, bending and shear stiffness.

The geometric stiffness $\boldsymbol{K}_G$ is a result of the variation of $\boldsymbol{B}$ when the stress resultants in z are fixed. To get this to a closed form solution, $\boldsymbol{K}_G, \boldsymbol{B}, \boldsymbol{u}$ and z are denoted as K_{Gij}, B_{ki}, u_j and z_k. The indices i, j and k range over 1-6, 1-6 and 1-3 respectively, and we call the effective cross-sectional area, $\boldsymbol{A}^j = \frac{\delta \boldsymbol{B}}{\delta u_j}, j = 1,...,6$. And through the usage of the summation convention, we obtain:

$$K_{Gij} \delta u_j = \int_{L_0} \delta \boldsymbol{B}^T z dx = \int_{L_0} \frac{\delta B_{ki}}{\delta u_j} \delta u_j z_k dx = \int_{L_0} A_{ki}^j z_k dx \delta u_j \tag{4.21}$$

And we then get:

$$K_{Gij} = \int_{L_0} z_k A^j_{ki} dx'$$ (4.22)

We need to restore the matrix notation, and to do this, the following is defined:

$$W_{Nij} = A^j_{1i}$$ (4.23)

$$W_{Vij} = A^j_{2i}$$ (4.24)

$$W_{Mij} = A^j_{3i}$$ (4.25)

W_{Nij}, W_{Vij} and W_{Mij} are weighting matrices that isolate the stress resultants $z_1 = N, z_2 = V$ and $z_3 = M$. In W_{Nij}, W_{Vij} and W_{Mij} the jth column will come from the first, second and third row of A^j. We have that $\boldsymbol{W}_M$ is equal to zero, and we obtain the final expression for the geometric stiffness:

$$\boldsymbol{K}_G = \int_{L_0} (\boldsymbol{W}_N N + \boldsymbol{W}_V V) dx' = \boldsymbol{K}_{GN} + \boldsymbol{K}_{GV}$$ (4.26)

At last we obtain the equilibrium equation for the system:

$$(\boldsymbol{K}_M + \boldsymbol{K}_G)\boldsymbol{r} = \boldsymbol{R}$$ (4.27)

5   Plastic deformation

This chapter is, with the exclusion of the last sub chapter taken from my project thesis (Jansen, 2015). When a structure is loaded it will experience stresses and strains. Every material has a yield stress value, and after this has been reached, the material will experience plastic deformation instead of elastic. The elastic deformation process follows Hooke's law, which gives a linear relationship between the stresses and the strains in the material. A deformation in the elastic region will not be lasting, and the structure will therefore go back to its original shape after elastic deformation. Hooke's law in one dimension is given as (Saabye Ottosen and Petersson, 1992):

$$\sigma = E\varepsilon \tag{5.1}$$

Where E is Young's modulus. Since the deformation will follow the same path during loading and unloading, the material response is *path independent.* The elastic relationship is illustrated in the figure below.
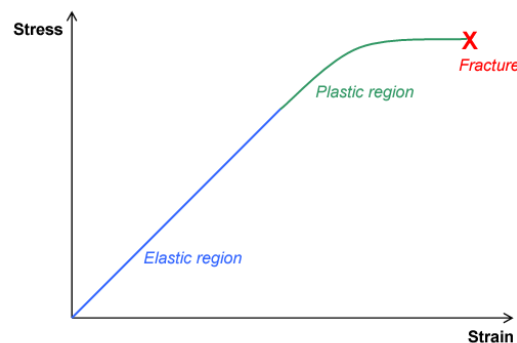
Figure 17: Illustration of Hooke's law (Alaa Kohja)

When the applied load is so large that you end up in the plastic region, the deformations will lead to lasting damage on the structure. The elasto-plastic behavior is characterized by the surpassing of the yield strength, a hardening rule where the yield condition is modified because of the strain hardening during plastic flow and a flow rule, which allow the determination of plastic strain increments at each point in the load history. (Moan, 2003). As for the elasticity theory, the material is assumed to be isotropic. Since the material no longer follows Hooke's law, some changes must be done. We have the expression (Kelly):

$$d\sigma = K' d\varepsilon \tag{5.2}$$

where K' is the plastic tangent modulus, and is the slope of the stress-strain curve in the plastic region. The modulus will change, as the slope of the curve changes during the deformation, and is therefore not a constant. $d\sigma$ is the incremental stress and $d\varepsilon$ is the incremental strain. The relationship is shown in the figure below.
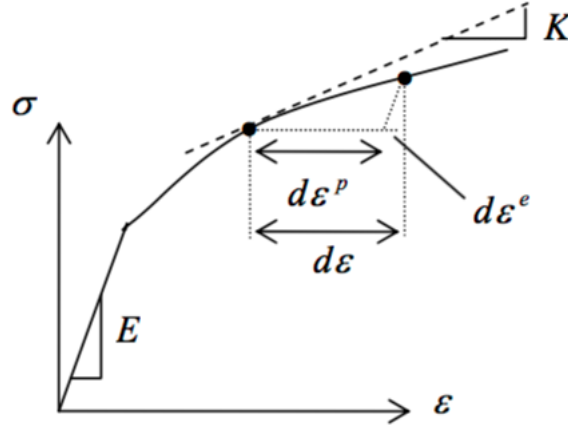

Figure 18: Figure of the tangent modulus (Kelly)

In plasticity theory it has been shown useful to split the stresses and strains into two components. For the stresses, it is the deviatoric and hydrostatic stress. Where the hydrostatic stress is the mean stress, and the component that contributes to the elastic compression or expansion of a stressed body. Whether a body deforms plastically or not is not dependent on the magnitude of the mean stress, but it is determined by the deviatoric stresses in the body. The hydrostatic stress is defined as following (Thaulow and Valberg, 2015)

$$\sigma_m = \frac{\sigma_x + \sigma_y + \sigma_z}{3} \tag{5.3}$$

And the deviatoric stress can be expressed as:

$$\sigma_d = \begin{bmatrix} \sigma_x - \sigma_m & \tau_{yx} & \tau_{zx} \\ \tau_{xy} & \sigma_y - \sigma_m & \tau_{zy} \\ \tau_{xz} & \tau_{yz} & \sigma_z - \sigma_m \end{bmatrix} = \begin{bmatrix} \frac{2\sigma_x - \sigma_y - \sigma_z}{3} & \tau_{yx} & \tau_{zx} \\ \tau_{xy} & \frac{2\sigma_y - \sigma_z - \sigma_x}{3} & \tau_{zy} \\ \tau_{xz} & \tau_{yz} & \frac{2\sigma_z - \sigma_x - \sigma_y}{3} \end{bmatrix} \tag{5.4}$$

The same applies for the strains, which now can be expressed in the same way. For the hydrostatic strain on the nominal form we have:

$$e_m = \frac{e_x + e_y + e_z}{3} \tag{5.5}$$

And for the deviatoric strain on nominal form:

$$e_d = \begin{bmatrix} e_x - e_m & e_{yx} & e_{zx} \\ e_{xy} & e_y - e_m & e_{zy} \\ e_{xz} & e_{yz} & e_z - e_m \end{bmatrix} = \begin{bmatrix} \frac{2e_x - e_y - e_z}{3} & e_{yx} & e_{zx} \\ e_{xy} & \frac{2e_y - e_z - e_x}{3} & e_{zy} \\ e_{xz} & e_{yz} & \frac{2e_z - e_x - e_y}{3} \end{bmatrix} \tag{5.6}$$

As mentioned, the nominal value of the strain component has been used in these equations, but they can easily be exchanged with the true strain values.

Another value that has importance in plastic deformation is the strain rate, which is the time derivative of strain. For nominal and true strains, it can be expressed as:

$$\dot{e} = \frac{de}{dt} \tag{5.7}$$

or

$$\dot{\varepsilon} = \frac{d\varepsilon}{dt} \tag{5.8}$$

And these can again be expressed in tensor form as:

$$\dot{e} = \begin{bmatrix} \dot{e}_{xx} & \dot{e}_{yx} & \dot{e}_{zx} \\ \dot{e}_{xy} & \dot{e}_{yy} & \dot{e}_{zy} \\ \dot{e}_{xz} & \dot{e}_{yz} & \dot{e}_{zz} \end{bmatrix} \tag{5.9}$$

In the theory of plasticity, the terms of effective, or equivalent values of stress, strain and strain rate are common terms. These values can be considered as the 'resultant' value that incorporates the total effect of all the stress, strain or strain rate components acting on a volume of the material.These values are convenient to define, as they can be used for comparison of two values for stress, strain or strain rate instead of trying to compare all of the components separately. The effective values are defined as given below:

Effective stress:

$$\bar{\sigma} = \frac{1}{\sqrt{2}} \sqrt{(\sigma_x - \sigma_y)^2 + (\sigma_y - \sigma_z)^2 + (\sigma_z - \sigma_x)^2 + 6(\tau_{xy}^2 + \tau_{yz}^2 + \tau_{zx}^2)} \tag{5.10}$$

Effective strain:

$$\bar{\varepsilon} = \sqrt{\frac{2}{3}(\varepsilon_x^2 + \varepsilon_y^2 + \varepsilon_z^2 + 2(\varepsilon_{xy}^2 + \varepsilon_{yz}^2 + \varepsilon_{zx}^2))} \tag{5.11}$$

Effective strain rate:

$$\dot{\bar{\varepsilon}} = \sqrt{\frac{2}{3}(\dot{\varepsilon}_x^2 + \dot{\varepsilon}_y^2 + \dot{\varepsilon}_z^2 + 2(\dot{\varepsilon}_{xy}^2 + \dot{\varepsilon}_{yz}^2 + \dot{\varepsilon}_{zx}^2))} \tag{5.12}$$

The two equations for the strain and the strain rate can often be seen expressed as incre-
ments ($d\varepsilon$ and $d\dot{\varepsilon}$) instead. This is done to show that they evolve after the end of the initial
elastic deformation. When large plastic deformations occur, the elastic deformations can be
taken as negligible in comparison to the plastic deformations. When working in the plastic
domain it is used increments of strain, instead of the total amount of strain (Thaulow and
Valberg, 2015).

5.1   Von Mises yield condition

As mentioned, the material has to reach the yield stress to become plastic. This can be de-
termined with the yield criterion (Moan, 2003). Here I have chosen to look more into the von
Mises yield criterion, but there are several other that can be used as well, for example Tresca.
The condition defines the limit of purely elastic behavior under any combination of stresses.
The condition can be expressed as:

$$f = \bar{\sigma} - \sigma_y = 0 \tag{5.13}$$

Where f is the loading function, σ_y is the initial yield stress and $\bar{\sigma}$ Is the effective stress
found in equation 5.10.

5.2   Hardening rule

By using the von Mises yield criterion, we can obtain the yield criterion in connection with
hardening. This can be written as (Moan, 2003)

$$\sigma_y = K(\bar{\varepsilon}^p) \tag{5.14}$$

where the equivalent plastic strain is:

$$\bar{\varepsilon}^p = \int_0^{\bar{\varepsilon}^p} d\bar{\varepsilon}^p \tag{5.15}$$

and the effective strain was found in equation 5.11, but with the use of incremental values instead. Here, we will introduce the plastic work as well:

$$W^p = \int_0^{\varepsilon_{ij}^p} \sigma_{ij} d\varepsilon_{ij}^p = \int_0^{\varepsilon_{ij}^p} \bar{\sigma} d\bar{\varepsilon}^p \tag{5.16}$$

There are two models that can be used to describe the hardening. The first one is isotropic, and the second one is kinematic or generally in an anisotropic manner. Through experiments with metals, it has been observed that a phenomenon called Baushinger effect occurs. This phenomenon involves that the material yields at a lower stress level when the loading is reversed, than at the initial yield. This yield condition can be written as:

$$f = \bar{\sigma} - K(\bar{\varepsilon}^p) = 0 \tag{5.17}$$

Which indicates that the hardening of the material has been taken into account for the new yield stress.

5.3   Deformation theory of plasticity

The relationship between stresses and plastic strains is mainly obtained from the two different plasticity theories. They are the deformation theory and the flow theory. The flow theory is used for cyclic and reversed loading, which an impact is not. Furthermore, ABAQUS uses the theory of deformation, and this will therefore be described further here. The theory is based on the Ramberg-Osgood relationship, which gives a representation of non-linear behavior. For one-dimension we have the expression (Hibbitt et al., 1992):

$$E\varepsilon = \sigma + \alpha \left(\frac{|\sigma|}{\sigma_0}\right)^{n-1} \sigma \tag{5.18}$$

where σ is the stress, ε is the mechanical strain, E is Young's modulus, α is the yield "offset" (in the way that when $\sigma = \sigma_0$ then $\varepsilon = \frac{(1+\alpha)\sigma_0}{E}$), and n is the hardening exponent for the "plastic" non-linear term, $n > 1$. The material behavior described by this model, is non-linear for all stress levels. A linear-elastic relationship was used to find the first term in equation 5.18. Through the use of Mises stress potential and associated flow rule, the non-

linear term has been generalized to multiaxial stress states, and gives the multiaxial model expressed by:

$$E\varepsilon = (1+v)\sigma_d - (1-2v)\bar{\sigma}_m\boldsymbol{I} + \frac{3}{2}\alpha(\frac{\sigma_v}{\sigma_o})^{n-1}\sigma_d \tag{5.19}$$

Where ε is the strain tensor, σ_m is the effective hydrostatic stress, σ_v is the von Mises effective stress, σ_d is the deviatoric stress and v is Poisson's ratio.

5.4 Energy dissipation

The strain dissipation energy is the amount of energy absorbed per volume unit. If an elastic stretching scenario using a tensile test specimen is considered up to a strain of ε_x. The energy needed to perform this stretching operation can then be expressed as (Thaulow and Valberg, 2015):

$$W = \int_0^{\varepsilon_x} dW = \int_0^{\varepsilon_x} Fdl = \int_0^{\varepsilon_x} \sigma_x Adl = V\int_0^{\varepsilon_x} \sigma_x\frac{dl}{l} = V\int_0^{\varepsilon_x} \sigma_x d\varepsilon_x \tag{5.20}$$

By removing the loads from the specimen, the elastic energy will be released again. The energy dissipation, or the applied energy per unit of volume of material can now be expressed as:

$$U = \frac{W}{V} = \int_0^{\varepsilon_x} \sigma_x d\varepsilon_x \tag{5.21}$$

When only elastic deformation is considered, the energy dissipation expressed above can be reformulated to:

$$U = \int_0^{\varepsilon_x} E\varepsilon_x d\varepsilon_x = \frac{1}{2}E\varepsilon_x^2 = \frac{1}{2}\sigma_x\varepsilon_x \tag{5.22}$$

Under loading of the specimen up to a general complex elastic state, all stress components contribute to the energy dissipation. The applied energy energy per unit of volume of material can then be formulated as:

$$U = \frac{1}{2}(\sigma_x\varepsilon_x + \sigma_y\varepsilon_y + \sigma_z\varepsilon_z + 2\tau_{xy}\varepsilon_{xy} + 2\tau_{yz}\varepsilon_{yz} + 2\tau_{zx}\varepsilon_{zx}) \tag{5.23}$$

Now the energy consumption per unit of volume, during uniaxial stretching of a tensile

test specimen from initial plastic strain ε_a up to final strain ε_b can be expressed as:

$$U = \int_{\varepsilon_a}^{\varepsilon_b} \sigma_x d\varepsilon_x \tag{5.24}$$

When loading is performed up to a general stress state, all stress components contribute to energy consumption. The dissipated energy per unit of volume is given below on infinitesimal form.

$$dU = \sigma_x d\varepsilon_x + \sigma_y d\varepsilon_y + \sigma_z d\varepsilon_z + 2\tau_{xy} d\varepsilon_{xy} + 2\tau_{yz} d\varepsilon_{yz} + 2\tau_{zx} d\varepsilon_{zx} \tag{5.25}$$

By integration of this equation over the added plastic strain region, the expression for the energy consumption per unit of volume due to plastic deformations emerge:

$$U = \int_{\varepsilon_a}^{\varepsilon_b} \bar{\sigma} d\bar{\varepsilon} \tag{5.26}$$

Dissipated energy per unit of volume and unit of time (the applied power) can now be found through the equation:

$$d\dot{U} = \sigma_x d\dot{\varepsilon}_x + \sigma_y d\dot{\varepsilon}_y + \sigma_z d\dot{\varepsilon}_z + 2\tau_{xy} d\dot{\varepsilon}_{xy} + 2\tau_{yz} d\dot{\varepsilon}_{yz} + 2\tau_{zx} d\dot{\varepsilon}_{zx} \tag{5.27}$$

6 Nonlinear Finite Element Method

This section is based on (Moan, 2003). Section 4 described the Finite Element Method for application to linear cases. For structures undergoing large deformations, this theory will not be applicable, as Hooke's law is no longer valid. This means that the assumptions about small displacements and a linear-elastic material have to be changed. The conditions that are applied to the linear theory, is still used for the non-linear FEM. The new thing is a change in the stiffness term for the non-linear elements. Non-linearity can occur due to a change in three different properties. The first is a change in geometry, the second a change in the material properties and the last a change in boundary conditions. The changes in the material properties has been studied in the previous section, and will not be explained further here. Some of the equations stated in section 4.1, must be altered to an incremental form to be used for these procedures. For the resultant of the internal forces, we get:

$$\boldsymbol{R}_{int} = \sum_i (\boldsymbol{a}^i)^T \boldsymbol{S}^i \tag{6.1}$$

And the total equilibrium can be found from:

$$\boldsymbol{R}_{int} = \boldsymbol{R} \tag{6.2}$$

The equations for a total and incremental equation of equilibrium can then be formulated:

$$\sum_i (\boldsymbol{a}^i)^T \boldsymbol{S}^i = \boldsymbol{R} \tag{6.3}$$

$$\boldsymbol{K}_I(\boldsymbol{r}) d\boldsymbol{r} = d\boldsymbol{R} \tag{6.4}$$

6.1 Change in geometry

When displacements become large, they no longer follow the linear assumption of small deformations, and every change in geometry needs to be accounted for. If this is done when the equilibrium equations are established and the strains are calculated from the displacements, the geometrical behavior can be seen as accounted for.

The stiffness term accounts for the effect of the change in geometry. This term will become more complex with time, and must be recalculated with every time step of an analysis.

6.2   Change in boundary conditions

When large deformations lead to contact between surfaces. It is implied that there has been a change in the boundary conditions from the initial configuration to the new, deformed one. When non-linear boundary conditions occur, it means that there has been a change in the boundaries, and it is no longer a linear function of the load.

6.3   Solution techniques

There are several different ways to solve a non-linear problem. Here, I will describe three different methods. These are:

- Incremental procedures

- Iterative procedures

- Combined methods

6.3.1   The Euler-Cauchy method

This method is a load incremental method. This means that a stepwise application of the external loading is used to give a solution to a non-linear problem. In each step, the increment of the displacement, Δr is determined by equation (6.4). To obtain the total displacement, all of the increments for the displacements are added together. The incremental stiffness matrix, K has to be determined based on the known displacements and stress conditions. This has to be done before a new load increment is applied, and it must be kept constant during an increment. For a load increment of the number (m + 1) we have the following expressions:

$$\Delta \boldsymbol{R}_{m+1} = \boldsymbol{R}_{m+1} - \boldsymbol{R}_m \tag{6.5}$$

$$\Delta \boldsymbol{r}_{m+1} = \boldsymbol{K}_I(\boldsymbol{r}_m)^{-1} \Delta \boldsymbol{R}_{m+1} \tag{6.6}$$

$$\boldsymbol{r}_{m+1} = \boldsymbol{r}_m + \Delta \boldsymbol{r}_{m+1} \tag{6.7}$$

These equations have the initial condition, $r_0 = 0$. Through this method, the load can be incremented up to the desired load level. The method can then be illustrated as shown in figure 19.
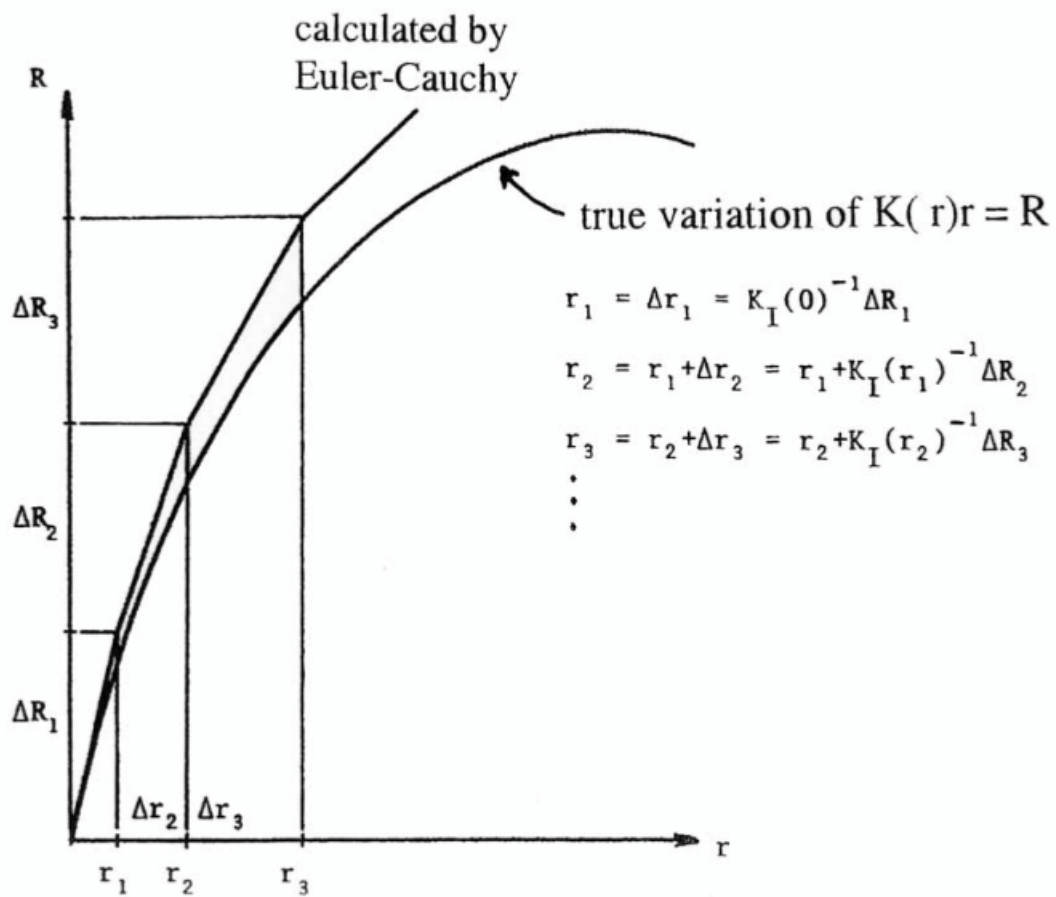
Figure 19: Illustration of the Euler-Cauchy incrementation method (Moan, 2003)

The method will not fulfill the total equilibrium equation given in equation (6.3). This is shown by the deviation between the true and approximated $K(r)r = R$. To improve this error, the increment size may be decreased together with an alteration of the load increment according to the degree of non-linearity.

6.3.2   The Newton-Raphson method

The Newton-Raphson method is an incremental procedure used to solve non-linear structural problems. The procedure of the method, is to solve x for a problem. For f(x) = 0 we have:

$$x_{n+1} = x_n - \frac{f(x_n)}{f'(x_n)} \tag{6.8}$$

Where $f'(x_n)$ is the derivative of $f(x_n)$ with respect to x. This algorithm is illustrated in the figure shown below.
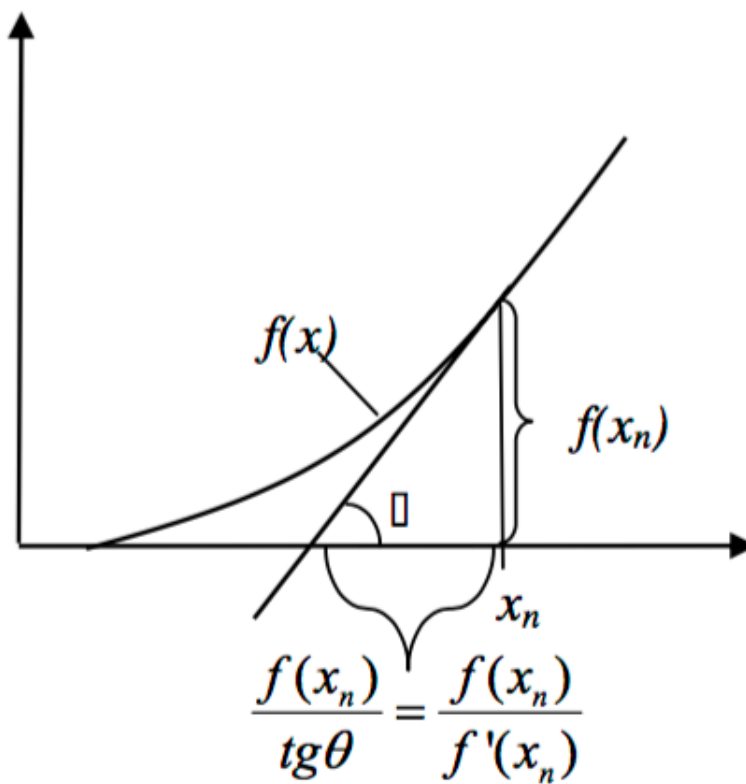
Figure 20: Illustration of the Newton-Raphson algorithm (Moan, 2003)

In Newton's method for a single d.o.f. $K_I(r)$ will represent the generalization of $\frac{\delta f}{\delta x}$. Equation (6.9) then needs to be solved.

$$d\sigma_{ij} = D_{ijkl}^{ep} d\varepsilon_{kl} \tag{6.9}$$

Where D are given in equation (6.10) for the elastic region, and equation (6.11) for the elasto-plastic region:

$$D = E \tag{6.10}$$

$$D = E_t \tag{6.11}$$

For the elasto-plastic E_t we have the following expression, wkere K' are given by equation (5.2).

$$E_t = E\left(1 - \frac{E}{E + K'}\right) \tag{6.12}$$

Equation (6.9) is then solved through the iteration method given below:

$$\boldsymbol{r}_{n+1} - \boldsymbol{r}_n = \Delta \boldsymbol{r}_{n+1} = \boldsymbol{K}_I^{-1}(\boldsymbol{r}_n)(\boldsymbol{R} - \boldsymbol{R}_{int}) \tag{6.13}$$

The basic principles behind the Newton-Raphson method is shown in the figure below.
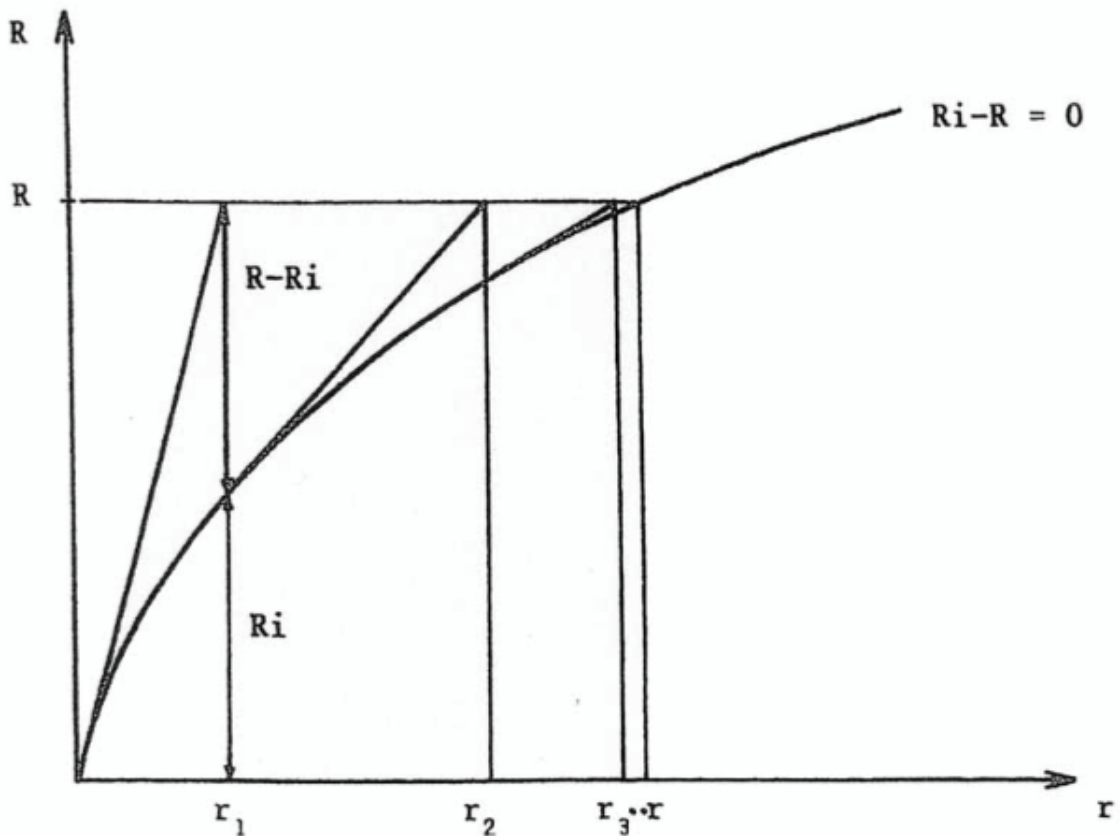
Figure 21: Illustration of the Newton-Raphson iterative procedure (Moan, 2003)

In this method $\boldsymbol{K}$ must be found before $\Delta\boldsymbol{r}_{n+1}$ is solved from the equation:

$$\boldsymbol{R} - \boldsymbol{R}_{int} = \boldsymbol{K}_{I(n)}\Delta\boldsymbol{r}_{n+1} \qquad (6.14)$$

for every iterative step.

6.3.3 Combined methods

This method combines the two procedures that have been described previously. In this method, the external load is applied in increments, and then the increments equilibrium is calculated through iteration. This has been desbribed in figure 22.
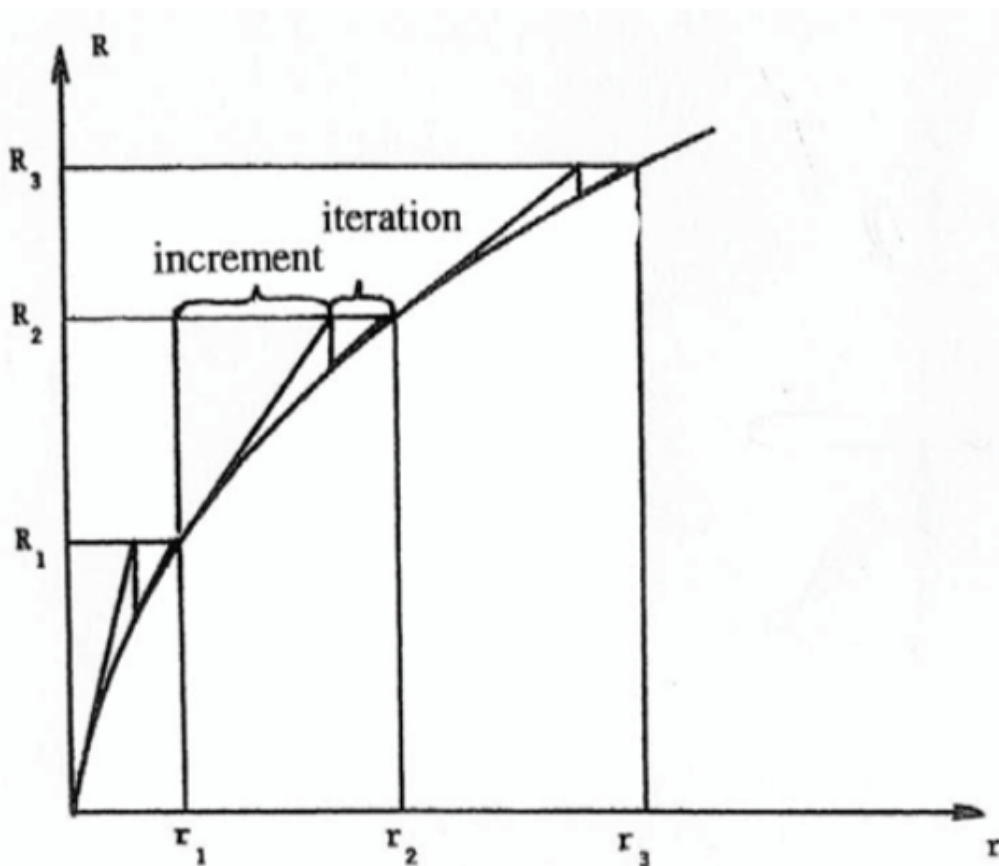
Figure 22: Illustration of the combined method (Moan, 2003)

This method is very applicable, as long as the load curve are increasing monotonically with the displacements. If not, special procedures need to be used instead.

7   Explicit dynamic analysis

Also this chapter is mainly taken from my project thesis, but has some smaller improvements (Jansen, 2015). An explicit method is based on the fact that the state a structure is in at the end of an increment is only based on the values of the displacements, velocities and accelerations at the start of the increment. The explicit dynamic analysis in ABAQUS is based on the implementation of an explicit integration rule. The equations of motions for the body are then integrated by using the central explicit central difference integration rule. This rule is then used to integrate the equations of motion explicitly through time, using the kinematic conditions at one increment to calculate the kinematic conditions for the nxet increment. At the beginning of the increment, it is solved for dynamic equilibrium. This means that the nodal mass matrix $\boldsymbol{M}$ multiplied with the nodal accelerations $\boldsymbol{\ddot{u}}$ will be equal to the net nodal forces. The net nodal forces is the difference between the external applied force $\boldsymbol{F}$ and the internal element forces $\boldsymbol{I}$. And the relationship becomes (Hibbitt et al., 1992):

$$\boldsymbol{M\ddot{u} = F - I} \tag{7.1}$$

In this explicit procedure a diagonal lumped mass matrix is used, and to solve the accelerations can be viewed as trivial, since there are no simultaneous equations to solve. This yields that the acceleration at each node is determined only by its mass and the net force acting on it. Therefore, the accelerations are integrated through time by usage of the central difference rule. This will calculate the changes in velocity under the assumption that the acceleration is constant. The change in the velocity is then added to the velocity in the middle from the last increment to find the velocities in the middle of the current increment.

$$\boldsymbol{\dot{u}}^{(i+\frac{1}{2})} = \boldsymbol{\dot{u}}^{(i-\frac{1}{2})} + \frac{\Delta t^{(i+1)} + \Delta t^{(i)}}{2}\boldsymbol{\ddot{u}}^{(i)} \tag{7.2}$$

The next step is to integrate the velocities through time, and they are then added to the displacements at the beginning of the increment to determine the displacements at the end of the increment:

$$\boldsymbol{u}^{(i+1)} = \boldsymbol{u}^{(i)} + \Delta t^{(i+1)}\boldsymbol{\dot{u}}^{(i+\frac{1}{2})} \tag{7.3}$$

Where $\boldsymbol{\dot{u}}$ is the velocity and $\boldsymbol{\ddot{u}}$ is the acceleration. By satisfying the dynamic equilibrium

at the beginning of the increment the accelerations can be obtained. We also have the superscript (i) that refers to the increment number and the reference to the mid increment value given by: $i - \frac{1}{2}$ and $i + \frac{1}{2}$. The central difference integration operator is explicit because the kinematic state can be known in advanced using known values of $\dot{\boldsymbol{u}}^{(i-\frac{1}{2})}$ and $\dot{\boldsymbol{u}}^{(i)}$ from the previous increment. The explicit integration rule is in itself quite simple, but it does not give the computational efficiency associated with the explicit dynamics procedure. To obtain this efficiency it is optimal to use the diagonal mass matrix, because the inversion of the mass matrix that is used in the computations of the accelerations at the beginning of the increment is triaxial:

$$\ddot{\boldsymbol{u}}^{(i)} = \boldsymbol{M}^{-1} (\boldsymbol{F}^{(i)} - \boldsymbol{I}^{(i)}) \tag{7.4}$$

It is required to to use special treatment of the mean velocities $\dot{\boldsymbol{u}}^{(i-\frac{1}{2})}$ and $\dot{\boldsymbol{u}}^{(i+\frac{1}{2})}$ when used for initial conditions, certain constraints and presentation of results. For the last case, the state velocities are stored as a linear interpolation of the mean velocities:

$$\dot{\boldsymbol{u}}^{(i+1)} = \dot{\boldsymbol{u}}^{(i+\frac{1}{2})} + \frac{1}{2} \Delta t^{(i+1)} \ddot{\boldsymbol{u}}^{(i+1)} \tag{7.5}$$

The central difference operator do not start by itself, because the value of the mean velocity $\dot{\boldsymbol{u}}^{(-\frac{1}{2})}$ must be defined. In ABAQUS, the initial values of the acceleration and the velocity at t = 0, is set to 0 as well, as long as any other values has not been given by the user. The following condition is then asserted:

$$\dot{\boldsymbol{u}}^{(+\frac{1}{2})} = \dot{\boldsymbol{u}}^{(0)} + \frac{\Delta t^{(1)}}{2} \ddot{u}^{(0)} \tag{7.6}$$

And by substituting the expression into the updated expression for $\dot{\boldsymbol{u}}^{(i+\frac{1}{2})}$ we will get the following definition of $\dot{\boldsymbol{u}}^{(-\frac{1}{2})}$:

$$\dot{\boldsymbol{u}}^{(-\frac{1}{2})} = \dot{\boldsymbol{u}}^{(0)} - \frac{\Delta t^{(0)}}{2} \ddot{u}^{(0)} \tag{7.7}$$

The explicit procedure integrates through time by dividing the time range into several smaller time increments.

8   ABAQUS

The simulations in this thesis has been conducted using the Finite Element Analysis (FEA) program ABAQUS. The program uses the Finite Element Method as a basis for its calculations. In ABAQUS the entire bridge was modeled, but with some simplifications. The bridge that was used as a starting point for the model was one that was proposed to the Norwegian Public Roads Administration as a solution for the crossing (Veg), and a model of this is shown in the figure below. As well as the bridge, the outline of a ship hull with stiffeners was modeled. This was to make a more realistic impact, as an applied force will not be able to give the same contact area. In the middle of the bridge, there is a 400 meter long opening for ships to pass through. Because it is more probable that a vessel will hit one of the pontoons near the opening, these have a larger dimension value then the rest.

Figure 23: Suggested bridge for crossing Bjørnafjorden (Veg)

8.1 Modeling of parts

Different elements was used for the different parts. The pontoons, cylinders and the ship hull was modeled using shell extrusion elements. The part is then drawn in 2D, before it is extruded into 3D by giving the drawing a depth. The pontoons are also given 5 bulkheads, so that it can be penetrated without losing its buoyancy. This has also been done with the hull, to prevent it from buckling and giving unrealistic results, which was done in the project thesis and the vessel buckled profusely. It has been specially reinforced in the bow, as ship often have extra strength there. The drawings of the hull and the pontoon are shown in figure 24 and 25 with dimensions. All of the dimensions are given in table 3 and 4.

Table 3: Dimensions of the ABAQUS models

	L_{sq}	L_{curve}	L_{tot}	B	D
Hull	120 m	60 m	180 m	60 m	40 m
Pontoon	50 m	20 m	70 m	20 m	16 m
Pontoon top	50 m	20 m	70 m	20 m	0.02 m
Large pontoon	60 m	30 m	90 m	30 m	20 m
Large pontoon top	60 m	30 m	90 m	30 m	0.02 m

The pontoon and cylinder tops are on the other hand modeled as 3D planar shell elements. This means that they are drawn in 2D, and are not in 3D before they are given a thickness when a section is assigned to the part.

Table 4: Dimensions of the cylinders

	H_{cyl}	R_{cyl}
Cylinder	74 m	10 m
Cylinder top	0.02 m	10 m
Large cylinder	74 m	15 m
Large cylinder top	0.02 m	15 m

The last part that was modeled was the road. For simplicity, this part has only been made as a wire to connect the pontoons.
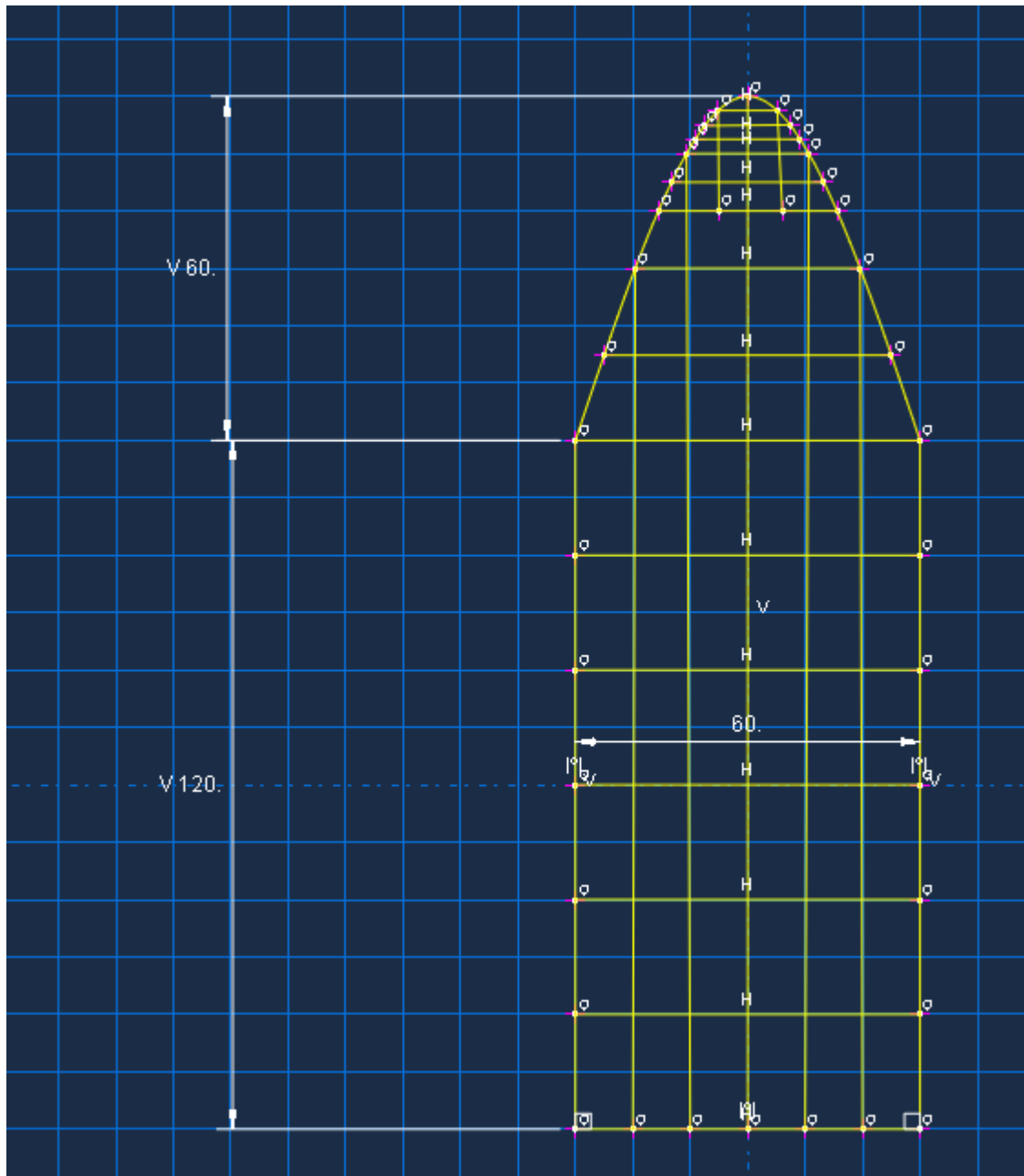
Figure 24: Hull dimensions

Table 5: Dimensions of the road

	L_{road}	L_{curve}	$L_{opening}$
Road	4200 m	400 m	400 m

8.2 Materials

The next step of the modeling is to define the materials. All of the elements is assumed to be steel, because it has several good features for marine installations, and are extremely usable.
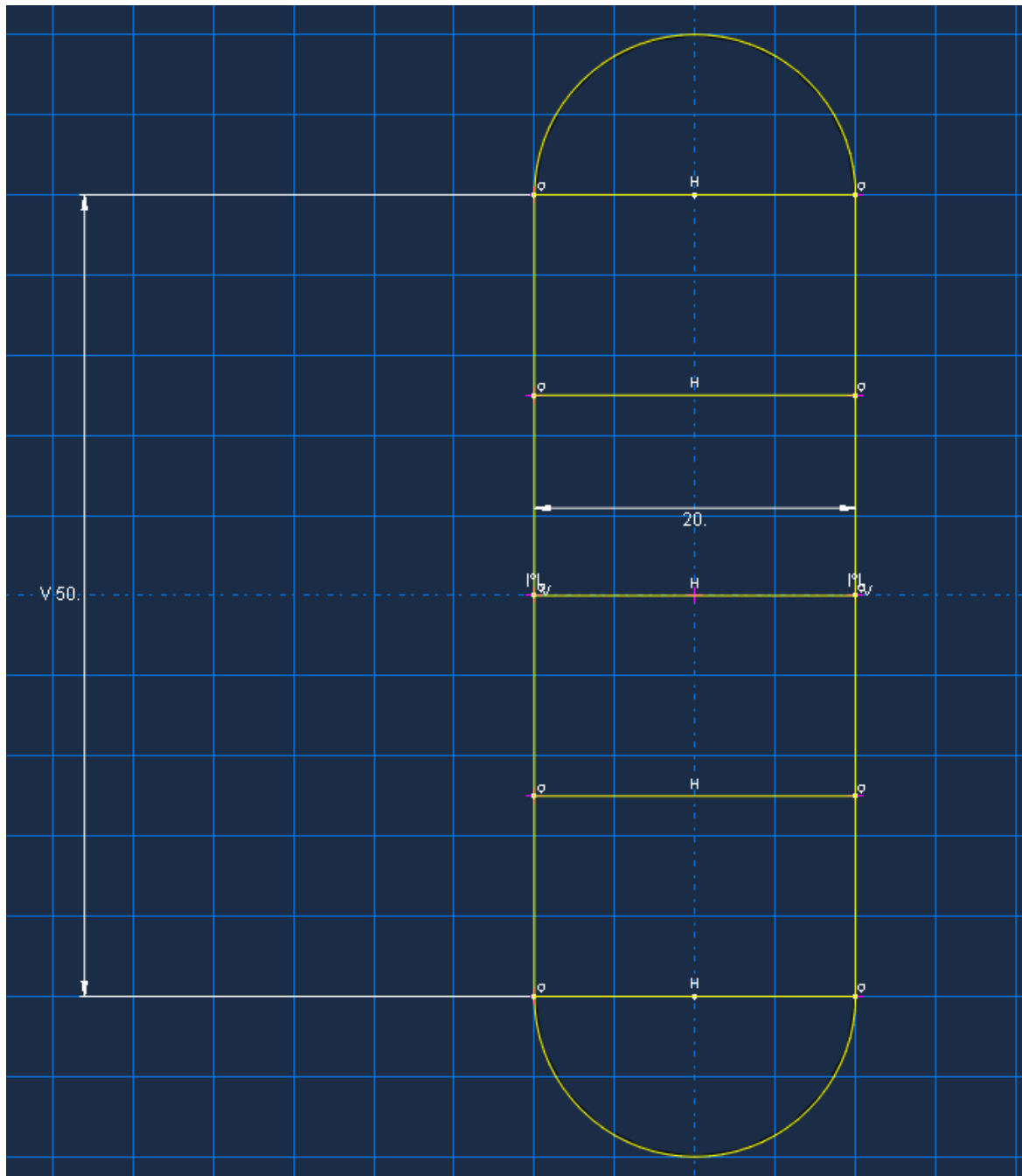
Figure 25: Pontoon dimensions

The properties given to the material is presented in the table below.

As can be seen from the tables, the materials has been given plastic properties. By letting the plastic strain go from 0 to 1, the material will exhibit elastic perfectly plastic traits. This means that the stresses in the structure will not go above the yield stress given to the material. So the maximum stress levels will be 235 MPa. The road was also given steel properties, but is was given through a generalized beam profile. When a generalized profile is used, several parameters are needed. These are the area, the second moment of area about the x-and y-

Table 6: Given properties of steel

Property		Value
Density	ρ	7850 $\frac{kg}{m^3}$
Young's modulus	E	210 GPa
Poisson's ratio	ν	0.3
Yield stress	σ_y	235 MPa
Plastic strain	Start value	0
Plastic strain	End value	1

axes, as well as the product moment of area and the torsional constant, which for a circle is equal to the polar moment of inertia. For a circle these constants was found from the equations, with the following resulting values for a radii of 5 meters:

$$A = \pi r^2 = 78.5 m^2 \tag{8.1}$$

$$I_x = I_y = \frac{\pi r^4}{4} = 490.625 m^4 \tag{8.2}$$

$$I_{xy} = 0 \tag{8.3}$$

$$I_P = J = \frac{\pi r^4}{2} = 981.25 m^4 \tag{8.4}$$

The cross-sectional area of the beam has then been established, and the next step can be processed.

8.3 Material assignment to parts

When the materials and profiles has been defined, these need to be assigned to sections. The shell elements are modeled as shells and are again defined as shells, and given the material properties of steel and a thickness. The steel in the hull was set to be 1 cm, and the steel in the pontoon and cylinder element a thickness of 2 cm. This is very simple to do in the profile section later, when the parameter study on the significance of the thickness is conducted. The road on the other hand was modeled as a wire, and here given beam properties. This section then needs input from the profile made from the beam, the Young's modulus, mate-

rial density and Poisson's ratio for steel. The shear modulus also has to be assigned, and this is found from the equation below.

$$G = \frac{E}{2(1 + \nu)} = 80.77 GPa \tag{8.5}$$

The defined sections are then applied to their respective elements. All of the pontoons and cylinders are given the shell section with a thickness of 2 cm, the ship hull the shell section with a thickness of 1 cm, and the road are assigned the beam section. When all of the parts had been assigned sections, their masses could be found. This was data that was needed later in the modeling process.

Table 7: Masses of model parts

Type of element	Mass [kg]	Number of elements in model	Total mass [kg]
Pontoon	536440	18	9655920
Pontoon top	206323	36	7427628
Road	387463520	1	387463520
Large cylinder	1094970	2	2191940
Large cylinder top	110977	2	221954
Large pontoon	1143738	2	2287476
Large pontoon top	393577	4	1574308
Cylinder	729981	18	13139658
Cylinder top	49323	18	887814
Shiphull	7317487	1	7317487
Total bridge			425070172

As can be seen from the masses, the weight of the bridge is very large compared to the weight of the ship, as should be expected. The weight of the ship is 7317,5 tons, which is higher then the recommended displacement of 5000 tons recommended in the DNV standard. But on the other hand, cruise ships that more and more frequently visit Norwegian fjords, has a large displacement which may easily exceed this weight.

It is also in this part that the added mass is given to the structure. This was done by assigning a non-structural inertia force to all of the parts. This was set to a factor of 0.5. This factor uses the total mass of the element, and distributes its mass proportional in the element. Because the bridge is a buoyant structure, springs need to be attached to the pontoons to prevent it from rotating, because of the resistance it will experience from the surrounding

water. The spring constants then has to be calculated, which has been done, through the usage of MatLab. The code from MatLab is attached in the appendix, but the main steps will be presented here and the equations are from (Amdahl et al., 2015).

The first thing that must be found, is the volume of water that is displaced by the bridge, and by each of the pontoons. This is done by the usage of Archimedes principle, which states that a body submerged in water will experience an upward force, the buoyancy, when the body is at rest, the magnitude of this force is equal to the weight of the volume fluid that is displaced by the body. Since the weight of the bridge and the pontoons modeled in ABAQUS is known, the displaced volume for both bodies can be found from:

$$\nabla = \frac{\Delta}{\rho} \tag{8.6}$$

Where ∇ is the displaced volume in m^3, Δ is the mass of the bridge in kilograms and ρ is the density of the fluid the body is submerged in, which is $1025 \frac{kg}{m^3}$ for seawater.

The next step is to find the area of the waterline of the submerged body.To do this The area of the pontoons is calculated and multiplied by the number of pontoons in the bridge, which is 18 small, and two large ones. The area for each pontoon will also be used later. From these results, the draft of the bridge can be calculated by the equation below.

$$T = \frac{\nabla}{A_{wl}} \tag{8.7}$$

The draft of the bridge, will not be used yet, so now the second moment of area for the pontoons will be looked at. First the area of the circular ends of the pontoons must be calculated. As theses are half circles, the area is found by usage of equation 8.1, and dividing it by two. To calculate the second moment area of area about the x-axis, the distance from the axis the circle center must be found. This consists of half the distance of the square part of the pontoon in y-direction, here denoted as h, added together with the distance to the area center of the halfcircle. This distance is found from the equation given below from (Irgens, 2010) together with the next equations.

$$y_c = \frac{4r}{3\pi} \tag{8.8}$$

So the total length becomes:

$$a = \frac{\frac{h}{s}}{2} + y_c \tag{8.9}$$

The next step is now to calculate the second moments of inertia about the x- and y-axes. For the square part of the pontoon these are given as:

$$I_x = \frac{bh^3}{12} \tag{8.10}$$

$$I_y = \frac{b^3 h}{12} \tag{8.11}$$

These will give different values for the large and the small pontoons, but these must also be found for the half circles at the end of the pontoons. These values can be calculated from:

$$I_{x,circle} = \frac{9(\pi^2 - 64)r^4}{72\pi} \tag{8.12}$$

$$I_{y,circle} = \frac{\pi r^4}{8} \tag{8.13}$$

When all of the second moment of areas are found, they can be added together. In the x-direction, the area center of the half circles has an offset from the x-axis, and therefore the parallel axis theorem has to be used. This is given by:

$$I = I_{circle} + a^2 A \tag{8.14}$$

Where a is the perpendicular distance between the x-axis and the area center for the half circles. Because there are two of these, one in each end, the expression above has to be multiplied by 2. And in x-direction the total second moment of area for the pontoon is obtained:

$$I_{x,total} = I_x + 2(I_{x,circle} + a^2 A) \tag{8.15}$$

In y-direction on the other hand, the area center of the half circles lies on the y-axis, and the inertia moments can just be added together without the use of the parallel axis theorem. We then get the expression:

$$I_{y,total} = I_y + 2I_{y,circle} \tag{8.16}$$

Now, we have enough information to find the distance between the buoyancy canter and the meta center, the BM value, for the pontoons in both transverse and longitudinal direction. These values can be calculated from (Pettersen, 2004):

$$BM_T = \frac{I_{x,total}}{\nabla_{pontoon}} \tag{8.17}$$

$$BM_L = \frac{I_{y,total}}{\nabla_{pontoon}} \tag{8.18}$$

Then the distance between the keel and the buoyancy, the KB value, can be found as half the distance of the draft:

$$KB = \frac{1}{2}T \tag{8.19}$$

And the distance between the keel and the gravity center, KG, is half the depth of the pontoon, because of symmetry:

$$KG = \frac{1}{2}D \tag{8.20}$$

Now, all the values needed to calculate the spring stiffness in roll and pitch motion has been calculated. And the expression for the spring stiffness in roll motion is:

$$C_{44} = \rho g \nabla GM_T = \rho g \nabla (KB + BM_T - KG) \tag{8.21}$$

And for pitch motion we have:

$$C_{55} = \rho g \nabla GM_L = \rho g \nabla (KB + BM_L - KG) \tag{8.22}$$

And the values presented in the table below are obtained as spring stiffness' for the pontoons.

These values for the spring stiffness are then applied to the pontoons in ABAQUS. When springs are applied in ABAQUS, this can be done either in a point to connect it to the ground, or along a line. Because this is a dynamic explicit analysis, the only form of spring that is al-

Table 8: Spring stiffness'

	C_{44}	C_{55}
Small pontoon	4.82×10^9	4.18×10^8
Large pontoon	1.49×10^{10}	1.73×10^9

lowed is a spring that connects to points and create a line between them. This is therefore the only choice I have to apply it. the C_{44} is therefore applied along a line in the transverse direction of the pontoon, and C_{55} in the longitudinal direction. When the thickness of the pontoons are changed, the change in mass will not make any significant change in the spring stiffness', and these can be equal as they were for the previous runs.

The last thing that has to be done before the next section is to assign the road a beam orientation. This is done by giving it the default coordinates that appears when the orientations is assigned, and has the same orientation as the global coordinate system.

8.4 Assembly

As the all of the parts has been modeled and given material properties and sections, they can be assembled together. This was done by working from the top and downwards. This proved to be the easiest solution, because of the curved shape of the road. The order of the assemble then became the road first, then the cylinder tops, next the cylinders, before the pontoon tops was put in place, and then the pontoon, and another pontoon top to form the bottom of the pontoon. The last element that was put in place was the ship. Along the road 18 smaller pontoons are connected to it, as well as two larger pontoons, all with a 200 meter spacing. In the middle, there is 400 meter gap, that will be used as an opening for vessels to pass through, where the large pontoons are located at each side of this. The total assembly can be seen in the figure below.
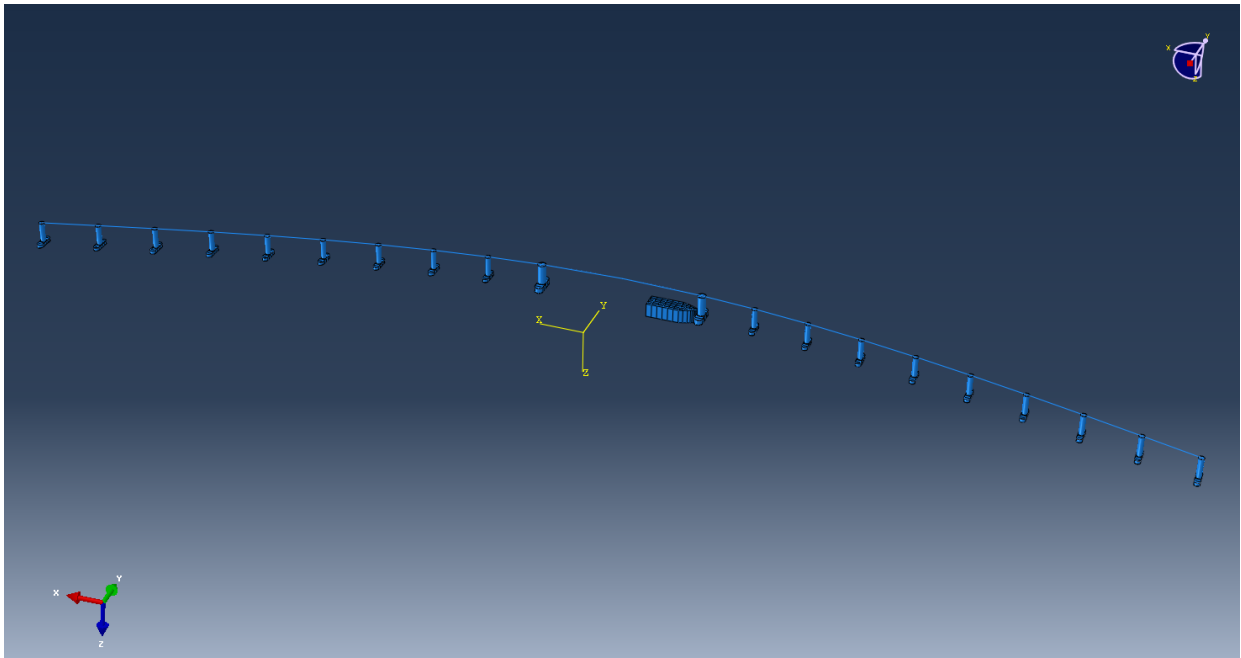
Figure 26: Assembled bridge

8.5 Boundary conditions

The bridge then had to be given the boundary conditions. Since the road is curved, there will not be a necessity to have an anchorage system along the bridge other than in both ends where it is connected to the land side. In both ends it is therefore restrained against all rotations and translations.

8.6 Steps

A time step is needed, because the simulation is time dependent. The time step was set to be an explicit dynamic step. The theory behind this integration method has been explained in section 7. The step has to be dynamic to be able to create an analysis that is time dependent, and was set to last for 20 seconds with 20 time intervals. The amount of time intervals is important for the number of frames that will be available in the results section later. However, it is not very important for the output data if the are exported to Excel later, as these will have a lot smaller intervals, and not make large time gaps. Because of the large deformations that will occur during an impact, it is necessary to make sure that the box with Nlgeom is on. This allows large deformations to occur during the analysis.
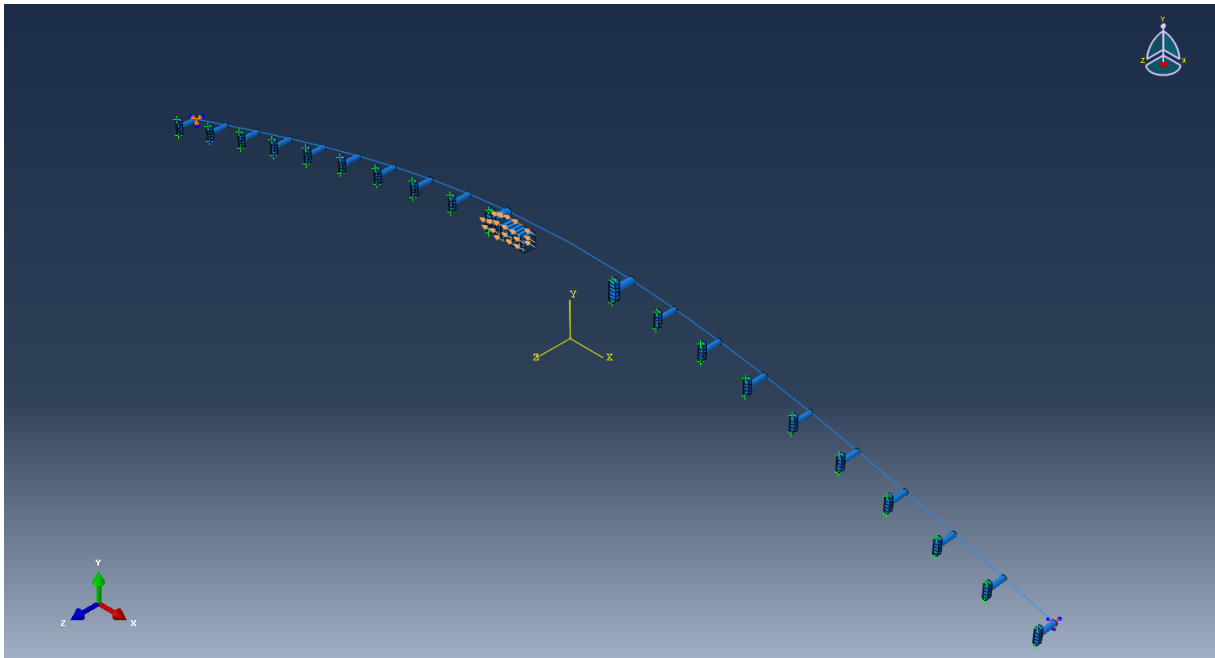
Figure 27: Boundary conditions on the bridge

Before we can move on to the next part, the field output requests has to be altered. ABAQUS will not automatically generate output for moments, forces and stresses in the beam, and these have to be asked for specifically. The last thing that is done is therefore to request output data for these as well as for the shell elements, which are generated automatically.

8.7   Interactions

The ship needs a velocity to collide into the bridge. This is given as a general contact interaction, where the entire surface of the hull is given a speed of $2\frac{m}{s}$. This was done because it is recommended in these calculations by the DNV standards. It may be a little conservative to apply this inside a Norwegian fjord, but it is probably better to be conservative in the calculations. Since it is an interaction, there has to be two different surfaces involved, here this is one of the large pontoons and the vessel. The interaction properties had to be defined, which is defined as a "hard contact", that lies underneath the normal contact behavior. This means that as long as the two elements are in contact with each other, there can be any pressure, and when the contact stops, the pressure will be zero as well. For this interaction the ship and the pontoon are allowed to separate after contact. The principle of hard contact is

demonstrated in the figure below.
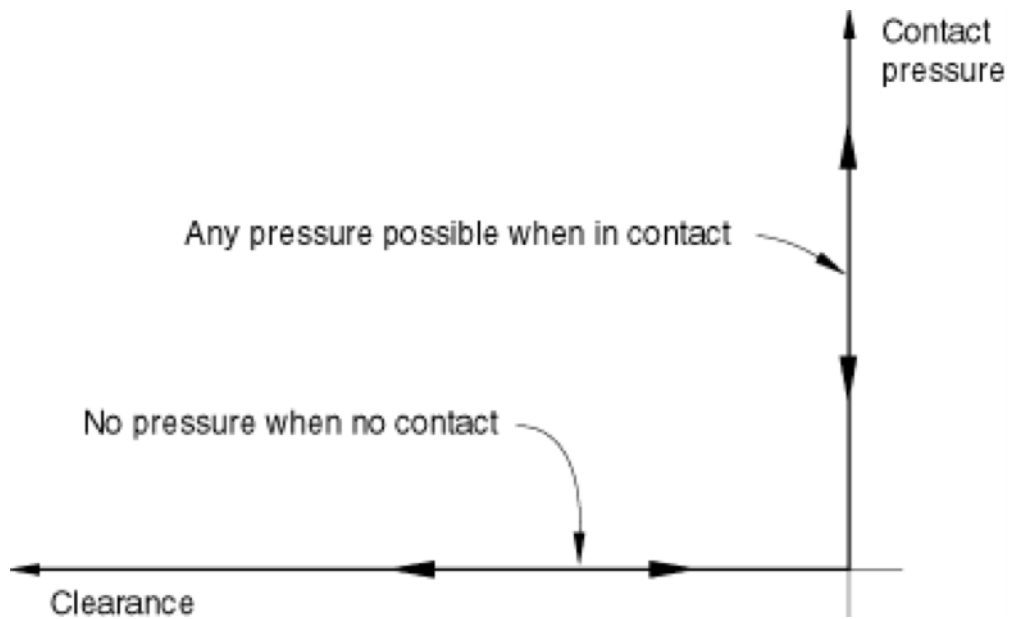
Figure 28: The "hard contact" option in ABAQUS (Hibbitt et al., 1992)

Because the cylinder must be able to transfer forces to the road, other interactions was created. ABAQUS only allows one general contact in each analysis, and therefore these had to be applied as surface-to-surface contacts. This was then done by connecting the surface of each cylinder top to the node of beam that lies in the middle of the cylinder top surface. When applying this contact, ABAQUS requires that the surfaces are continuous. The cylinders are separate, so each contact had to be applied one at a time. The elements are not allowed to separate after contact, to make sure the structure holds together. This is different from the pontoon-ship contact where this was allowed. Also there is a choice between the kinematic contact method and the penalty contact method, where the penalty contact method was used because it does not conflict with other types of constraints, and it works well with shell elements (Hibbitt et al., 1992).

8.8 Constraints

When the model was assembled, the different parts was not connected to each other. This became apparent after the analysis had been ran, and the parts fell from each other. It was therefore necessary to constrain the different parts, to make the model adhesive. This had to be done in one operation for the entire bridge to avoid conflict between the master and slave surfaces. Because of this, the cylinders with the cylinder tops was set to be the master surface, and the other parts as slave surfaces. When a constraint is applied the d.o.f.s that is in connection with the master nodes are deleted, and is made dependent on the master nodes d.o.f.s instead. Therefore their motions is coupled to the master nodes' motion (Hibbitt et al., 1992).
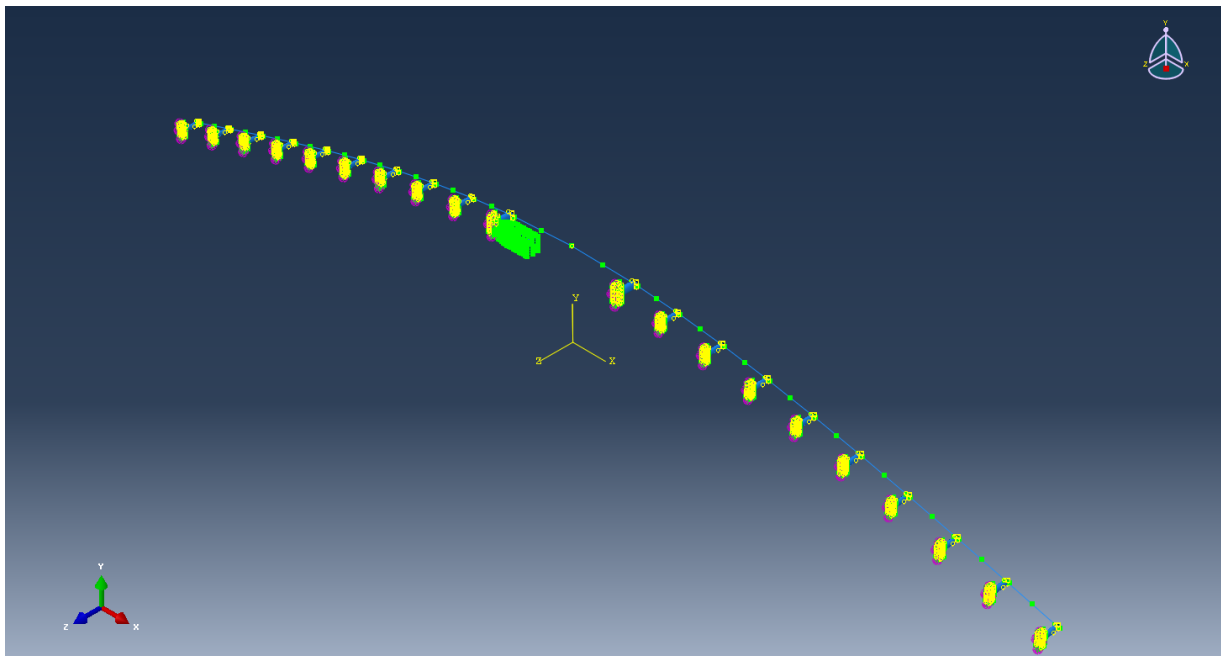
Figure 29: Applied constraints

8.9 Meshing

Before an analysis can run, it had to be meshed into smaller parts. This is because the finite element method is based on dividing the elements into several smaller parts. Because the goodness of the results is dependent on the mesh size, a convergence study of the mesh was conducted. By running the simulation several times, but with a smaller mesh size each time, the results should become more and more similar with each run. When the mesh size

is small enough, the results will converge towards the same solution, and the problem can be seen as solved. Each element had a different mesh size, and these are given in the table 9 for each run. Since it is the point of impact that will experience the largest amount of forces, it is most important that the colliding parts has a very fine mesh for accurate results. So after the normal mesh size all parts not connected to the collision area had the same mesh size, this was to save computational time, as the simulations needed a very long running time at the finest mesh sizes.

Table 9: Mesh sizes

Type of element	Coarse mesh [m]	Normal mesh [m]	Fine mesh [m]	Very fine mesh [m]
Pontoon	2.2	1.1	0.55	0.55
Pontoon top	10	5	2.5	2.5
Road	60	30	15	7.5
Large cylinder	8.4	4.2	2.1	1.05
Large cylinder top	8.4	4.2	2.1	1.05
Large pontoon	3.4	1.7	0.85	0.425
Large pontoon top	12	6	3	1.5
Cylinder	5.6	2.8	1.4	1.4
Cylinder top	5.6	2.8	1.4	1.4
Shiphull	5	2.5	1.25	0.625

In the mesh part of the set up for the analysis, the element type can be chosen. ABAQUS has several options here. All of the elements, except for the road are here chosen to be meshed as shell elements, and the road as a beam element. Further, for the shell elements, several options can be chosen. Because this is an explicit dynamic analysis, the elements are chosen as explicit, and not static. After the explicit element was chosen, it was set as a linear element. Quadratic can usually be chosen as well, but ABAQUS did not allow it in this analysis. The last selection that can be checked here is to determine if reduced integration is wanted or not. For this analysis reduced integration has not been used. The option was tried out, and it greatly reduced the computational time, but increased the presence of hourglassing too much. Because of these element selections, a S4 element is obtained. This element will converge towards shear flexibility for thick shells, and towards classical theory for thin shells, which means that ABAQUS determines if the element is calculated after Reissner-

Mindlin or Kirchhoff plate theory. For the beam, the same choices was made for an explicit, linear analysis without reduced integration. This gives a B31 element, which is a 2-noded linear beam in space, and its solution is found by the usage of Timoshenko beam theory. For all of the elements, element deletion had to be activated, which means that ABAQUS will re-move the element from the structure once the solution for the element has been calculated. This reduces computational time, and overly distorted elements are avoided. In this section it is also possible to regulate the hourglass control, if extensive hourglassing occurs in the el-ements occur, and it is a need to complete the analysis despite the large amount of artificial energy in the structure. To use this hourglass control should in this analysis be avoided, as the results where large hourglass modes was allowed gave an artificial energy value of up to 20% of the internal energy, and the results were not usable.
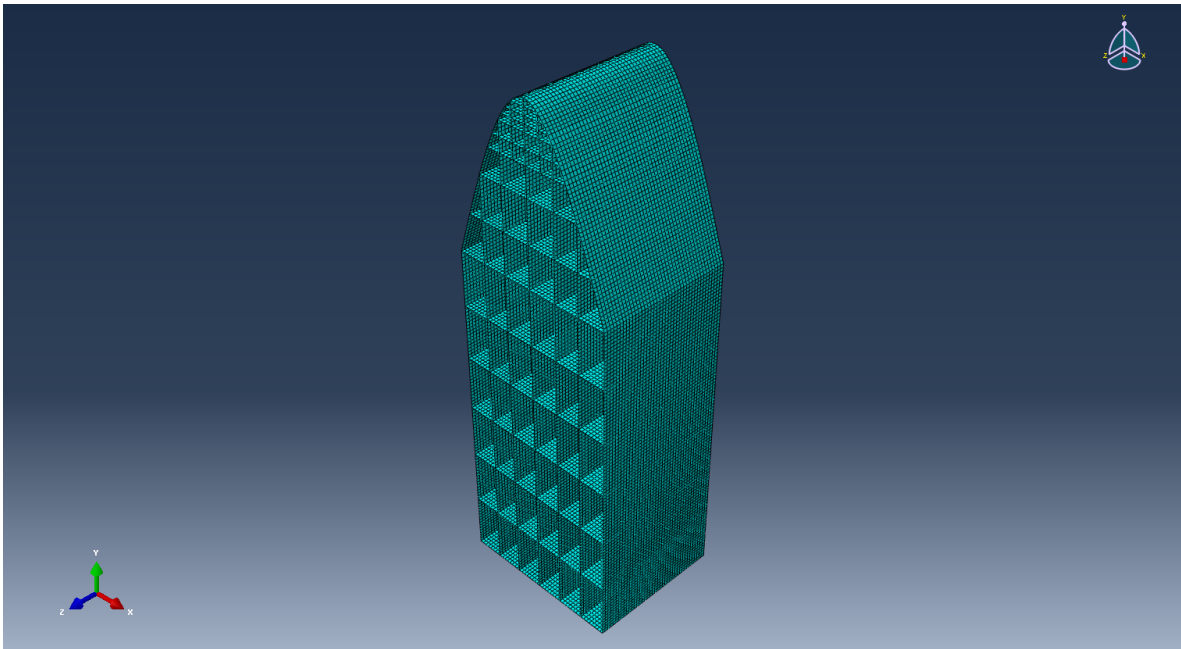
Figure 30: Meshed hull
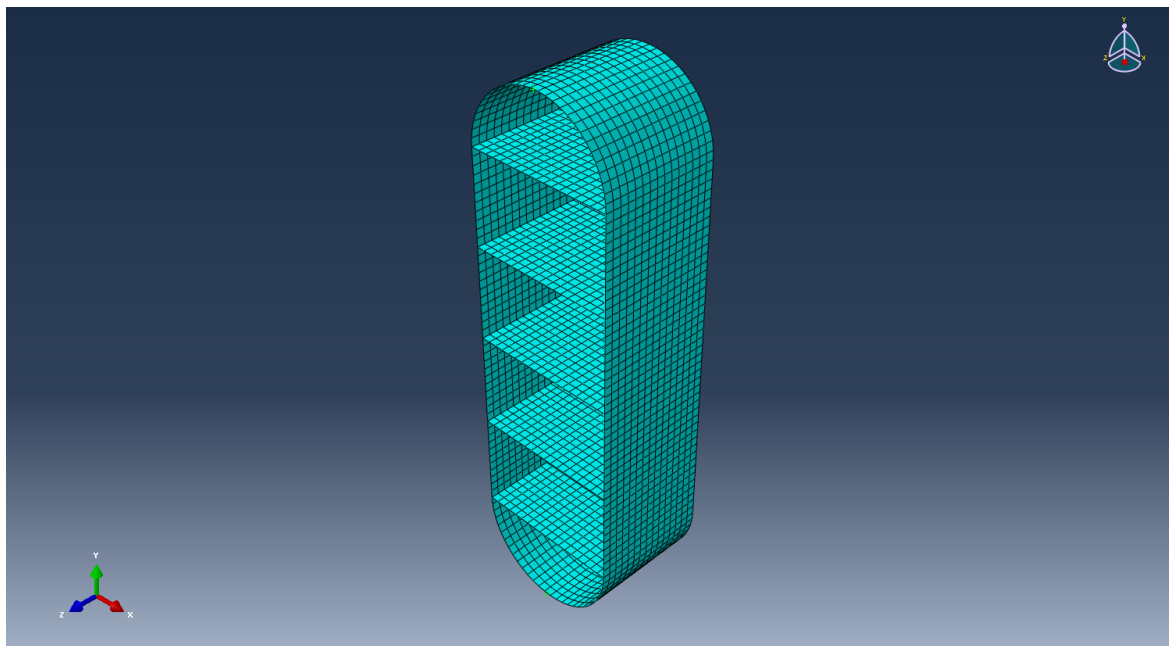
Figure 31: Meshed pontoon

When all of these steps has been performed, the file is ready to be submitted as a job. Abaqus will then perform the analysis, and the results can be taken out once the job is completed.

8.10   Taking out the results

When a job is completed, the results can be analyzed as they are in ABAQUS, or be exported from ABAQUS to Excel for further analysis and comparison. When the results part are opened the bridge is displayed in an undeformed shape, and with von Mises stress as the default parameter that shows its distribution in the structure. It is therefore useful to show it in the deformed shape. When the deformed shape is shown, it is possible to see how the stresses, displacements and forces distributes in the structure over time. As mentioned earlier, ABAQUS does not calculate forces, stresses and moments automatically, and by just looking at the time frames for the bridge, it will look like the beam do not experience any of these parameters at all. Therefore, these have to be looked at individually from the rest of the parameters that occur in the bridge.

To be able to export the data to Excel, XY data had to be made. This can be done in several ways, but for the energy components, this has to be done from the history output requests. ABAQUS then saves a file with the data of energy magnitude along the y-axis as a function of the time. This saved file, can then be exported. For the other parameters, that cannot be found in the history field output, such as stresses, strains, forces and moments, these has to be made into XY data from the field output request, where a point in the structure is chosen, and the output data for the element is plotted as a function of time, before they are exported. This was not done because it is of a larger interest to look at the entire bridge, and not the results for a single node.

8.11   Changing the geometry of the pontoon

To be able to perform the parameter study with a change in the number of bulkheads, this had to be done in the section sketch described previously in this chapter. When this done, the part has to be regenerated. When bulkheads are added, this means that not all elements of the pontoon has material properties assigned to them, so this has to be done again for the new part. For both pontoons, the spring that was attached has to be applied again, as it is removed as well. Below is a figure of the new pontoon with many bulkheads. The other model does not have any bulkheads at all.
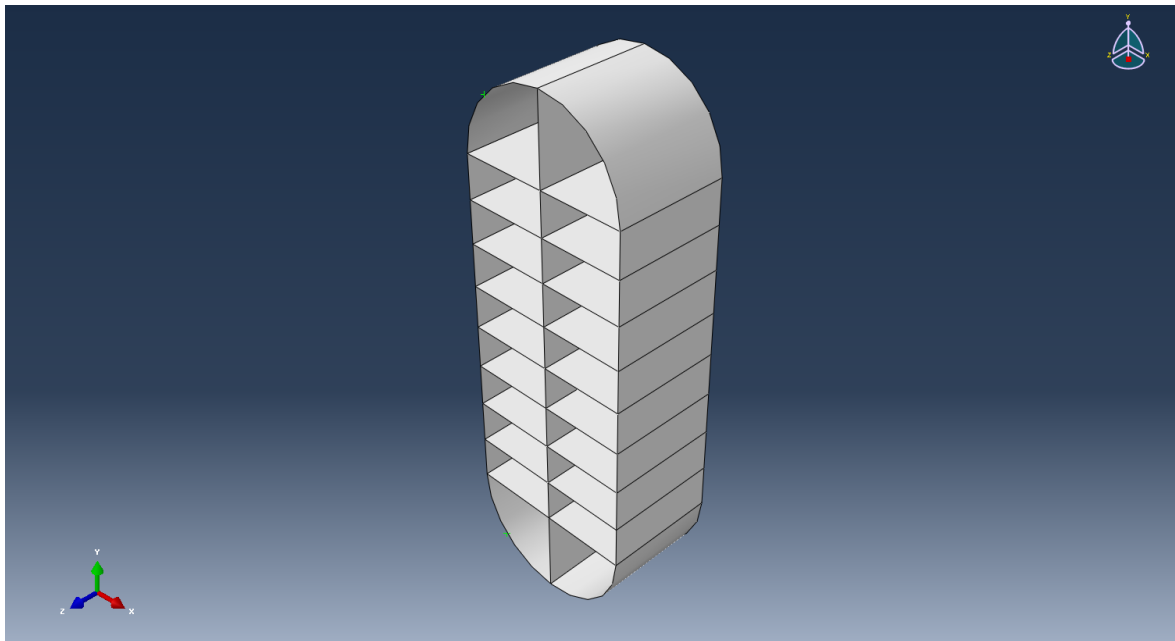
Figure 32: Pontoon with many bulkheads

9   Results

9.1   Stresses

The stresses in the structure can tell if the steel material has gone over in the plastic region or not. With a collision scenario the forces are very large, and plastic deformation should be expected.

9.1.1   Local stresses

For the local stress, the figure is of the pontoon that is exposed to the collision. It is in this part of the bridge that the largest stresses will occur, and this is the reason that this has been zoomed in at.
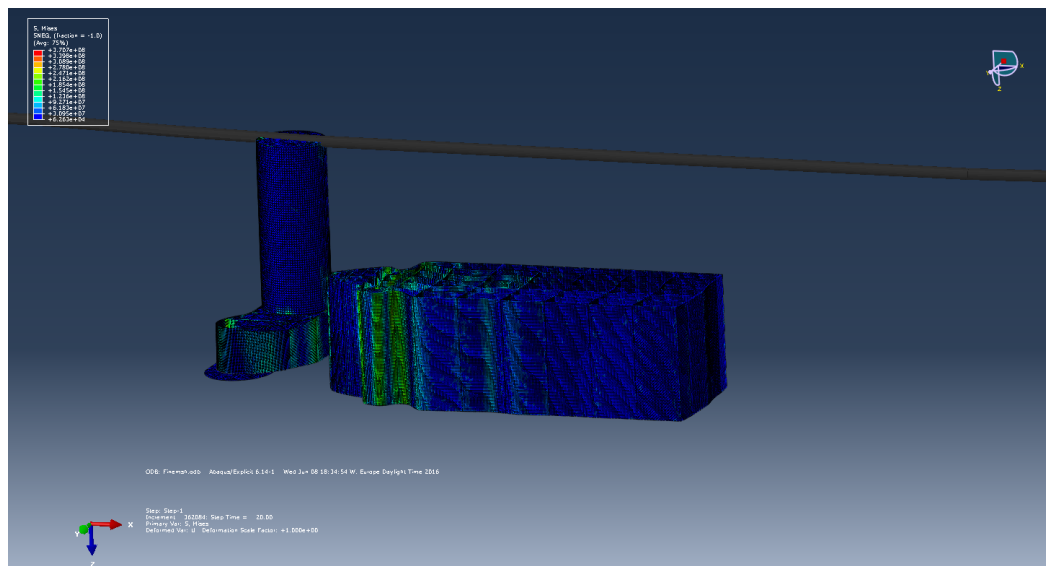
Figure 33: Local stresses at 20 seconds

From the figure it can be observed that both the vessel and the pontoon will deform plastically, but it is the ship that will end up with the highest stress values. The maximum value for the stress is in the ship, and this is 307 MPa, which is well above the yield stress of 235 MPa.

9.1.2 Global stresses

The global stresses are here shown in an overview from the side of the bridge, and in the other figure, connected pontoons have been zoomed in to. This was done because it was very difficult to see the stresses from the overview point. The small mesh size made the figure so dark, that the colors could not be distinguished.
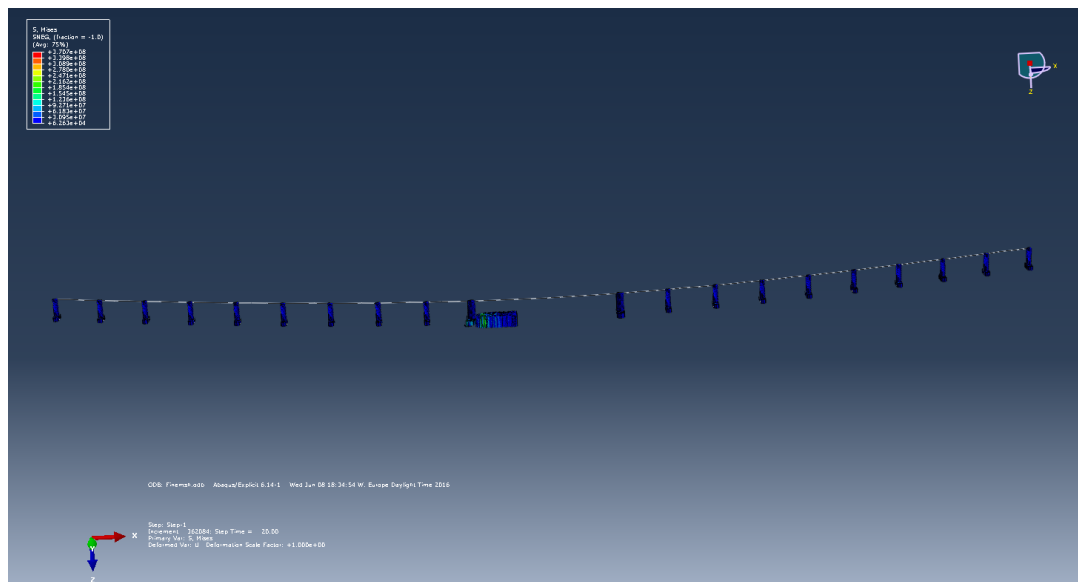
Figure 34: Overview of stresses at 20 seconds
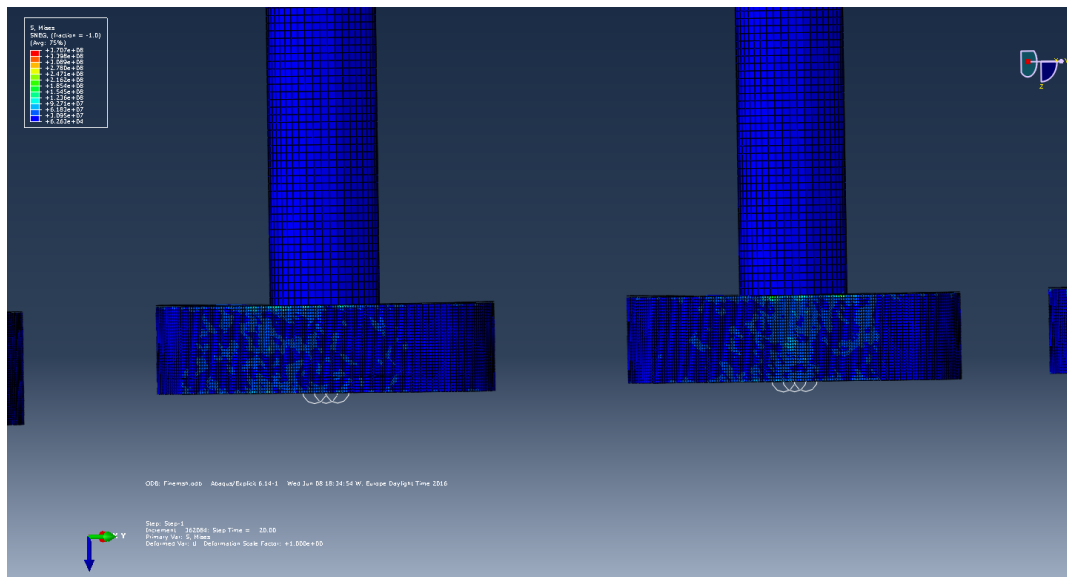
Figure 35: Global stresses at 20 seconds

From the figures it can be seen that the pontoon that the ship collides into has a lot more stresses in it than the other pontoons will. In the close up of the other pontoons, it can be

observed that it is the pontoons that will feel the forces. These forces are small compared to those in the main pontoon. Here, the maximum value is 154 MPa, and plasticity will not occur in them.

9.2 Forces in the road

Because ABAQUS does not output the beam values automatically, these have to be viewed separately from the other forces. Underneath the beam forces is shown for 10 and 11 seconds. These two time steps was chosen because it was here that the largest values occurred for the forces.
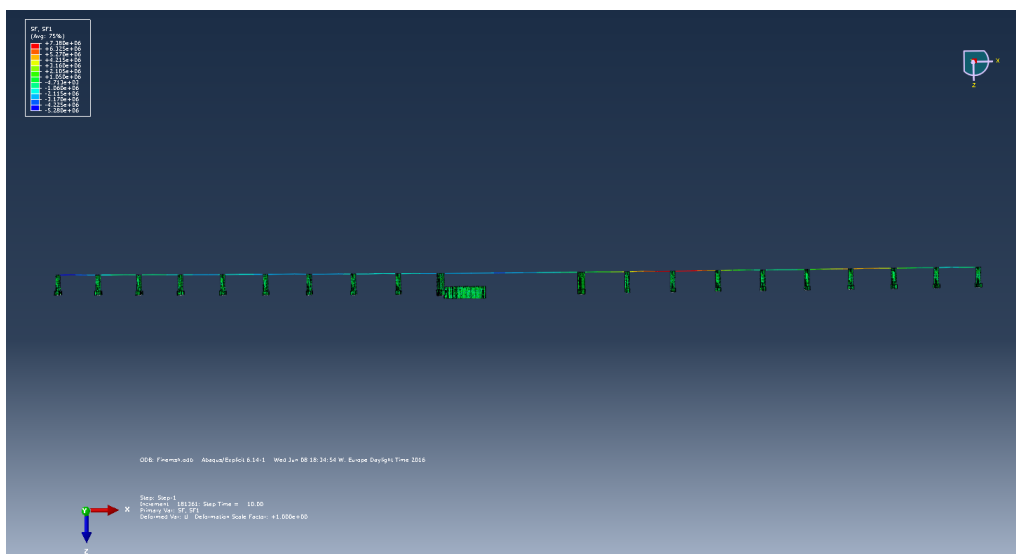
Figure 36: Beam forces at 10 seconds
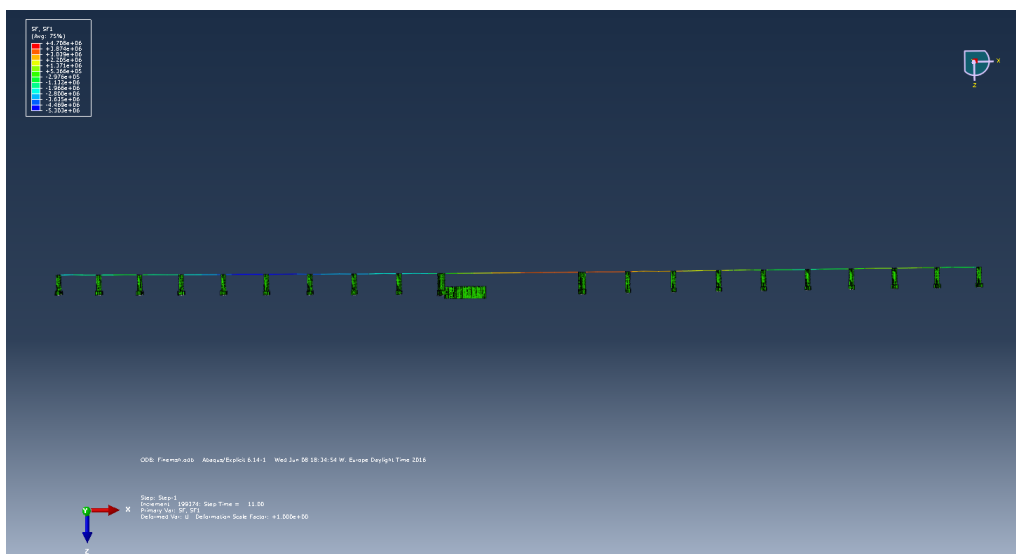
Figure 37: Beam forces at 11 seconds

From the two figures it can be observed that the largest force after 10 seconds occurs at the third pontoon to the right from the middle. At 11 seconds this forces will be be more distributed in the road. The maximum value that occurs in the bridge for the forces is 7.4 MN.

9.3   Moments in the road

The moments in the road is presented in the figures below for 5, 15 and 20 seconds. As for the forces, these values were not outputted from ABAQUS automatically, and had to viewed separately.
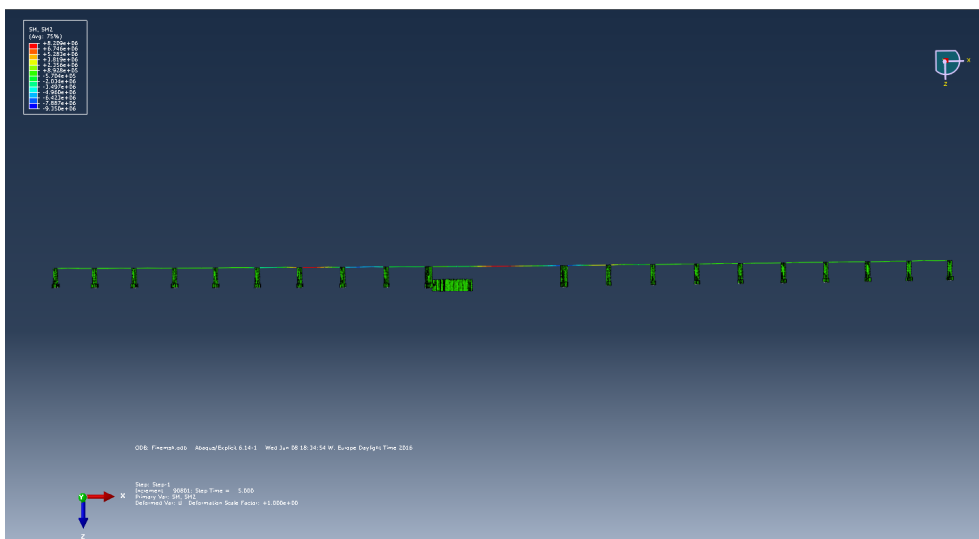
Figure 38: Beam moments at 5 seconds
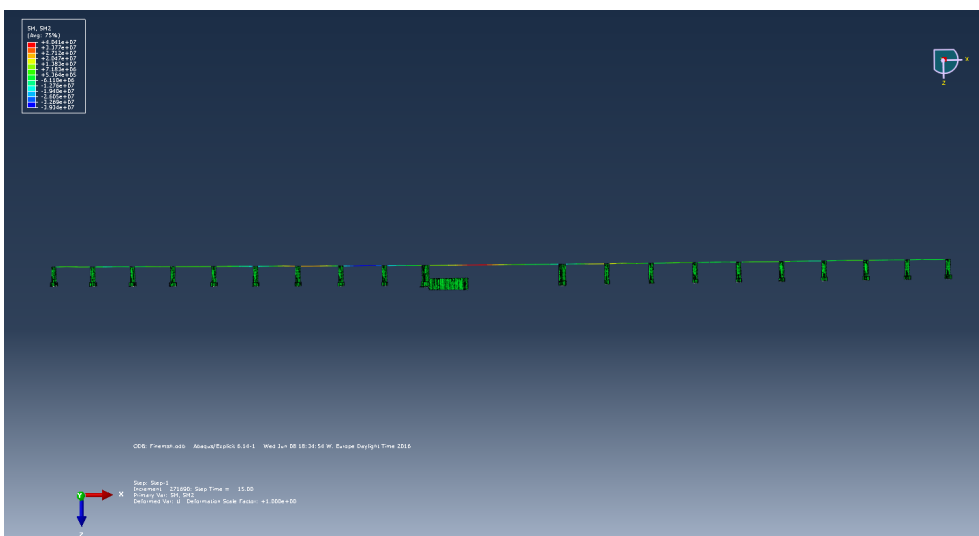
Figure 39: Beam moments at 20 seconds
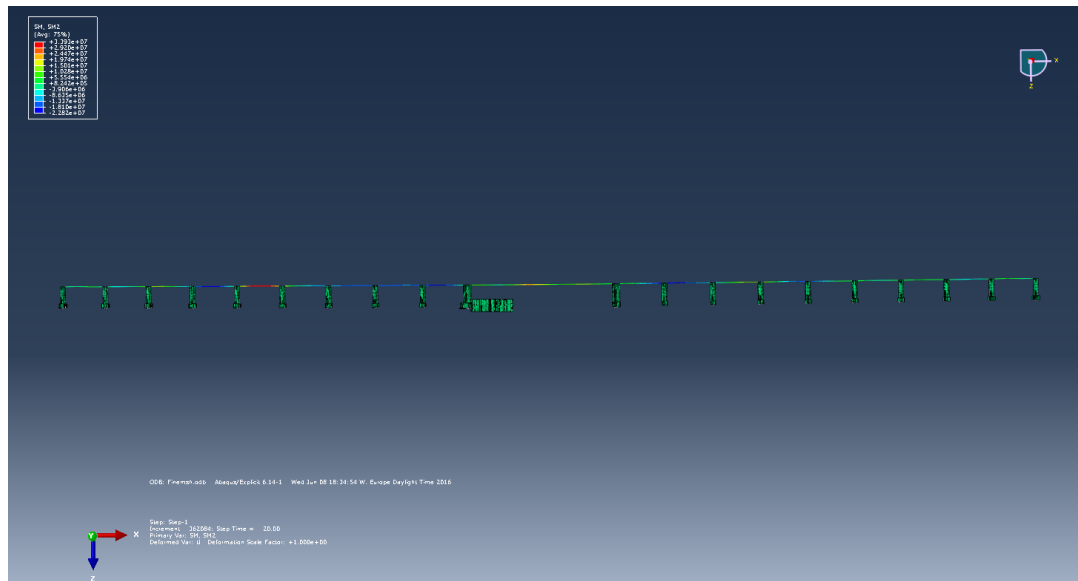
Figure 40: Beam moments at 5 seconds

The moment distributes in the beam with a periodic behavior. The moment in road will be generated from the point where it is connected to the cylinder experiencing the collision. From this point it will travel through the beam away from this point. The maximum value for the moment occurs at 15 seconds, with a magnitude of 40.4 MNm.

9.4   Displacements

Underneath in the figures are the displacements for the bridge show for 10 and 20 seconds.
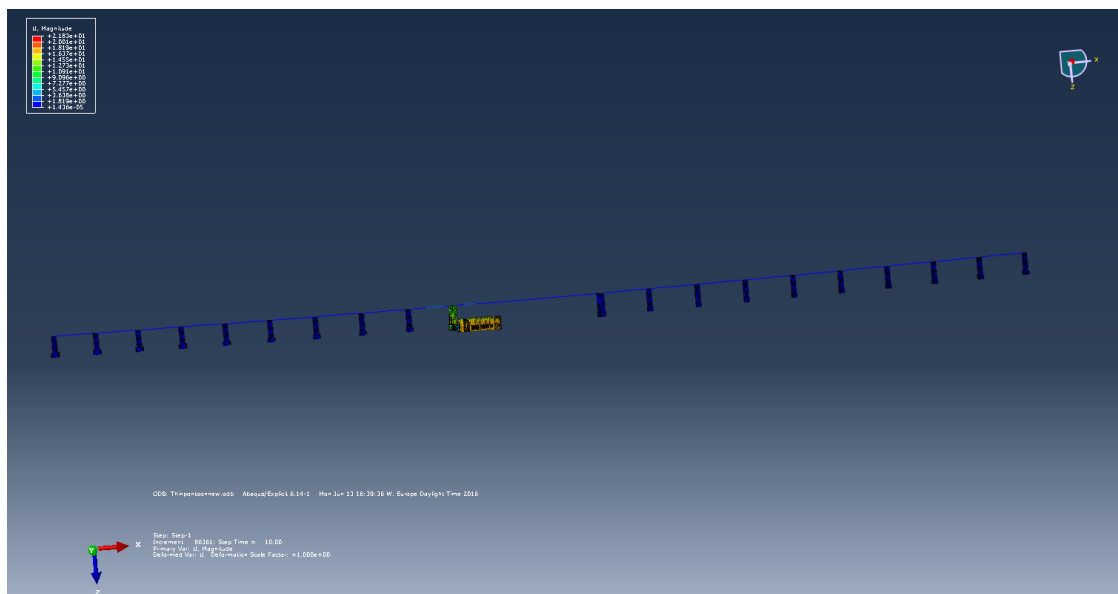
Figure 41: Global displacements at 10 seconds
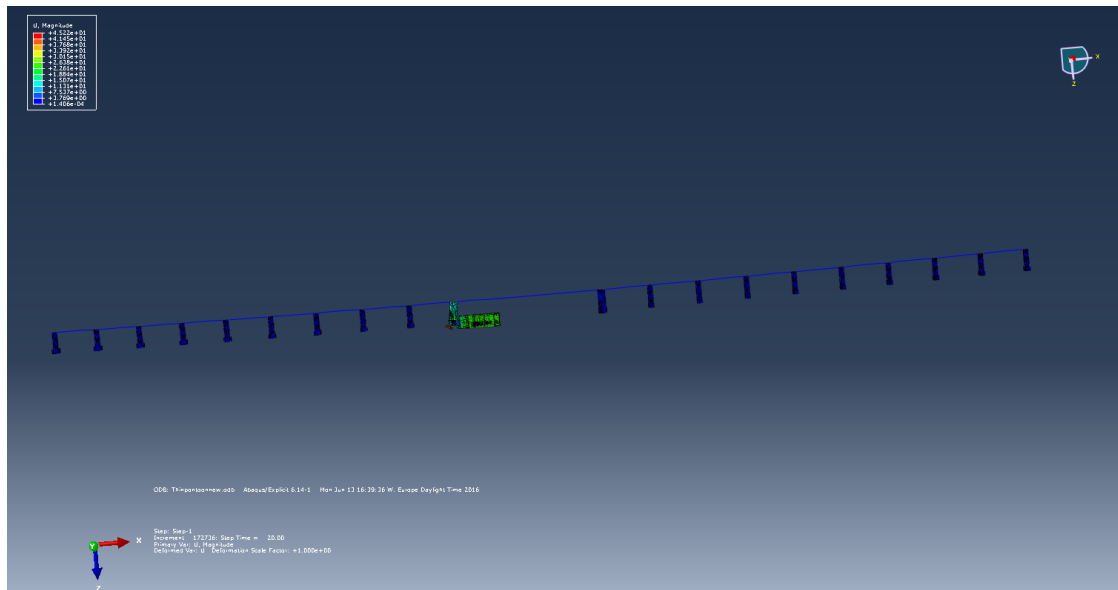
Figure 42: Global displacements at 20 seconds

As can be seen from the figures the displacement are very large, with some of them being as large as 1.5 meters. This will mean that the pontoon has been penetrated. The same pattern is shown for all of the analyses, and this figure will therefore just be shown here.

9.5 Energies

It is the energy levels in a structure that drives a collision. The kinetic energy in the impacting structure decides the amount of energy that has to be absorbed by the installation. Some parts may remain as kinetic energy, but most of it will be absorbed. Because the absorbed energy gives the deformation of the elements, it is an important factor too look more closely at. In ABAQUS there are several output energy that can be looked at, and they must all be in balance. This is given, as energy cannot disappear, only be transformed into another form. By looking at the balance, it is possible to see whether an analysis is giving an appropriate response. In ABAQUS, the energy balance is given as (Hibbitt et al., 1992)

$$E_I + E_V + E_{FD} + E_{KE} + E_{IHE} - E_W - E_{PW} - E_{CW} - E_{MW} - E_{HF} = E_{total} = constant \quad (9.1)$$

where E_I is the internal energy, E_V is the viscous energy dissipated, E_{FD} is the frictional energy dissipated, E_{KE} is the kinetic energy, E_{IHE} is the internal heat energy, E_W is the work done by the externally applied loads, $E_{PW}, E_{CW} and E_{MW}$ are the work done by contact penalties, constraint penalties and by propelling added mass. E_{HF} is the external heat energy through external fluxes. As can be seen from the equation, these energies added together, gives the total energy in the system, E_{total}. The total energy should be constant throughout the whole process, but is valid with a error less than 1%.

Since the creep dissipation energy, damage dissipation energy, frictional dissipation energy and the eternal work becomes zero from the analyses, they will not be presented here.

9.5.1 Kinetic energy

From the plot of the kinetic energy in figure 43, we can see that this energy will decrease with time. It reaches a plateau at 1.5 seconds, before it decreases further at 9.5 seconds. This is in agreement with the theory.
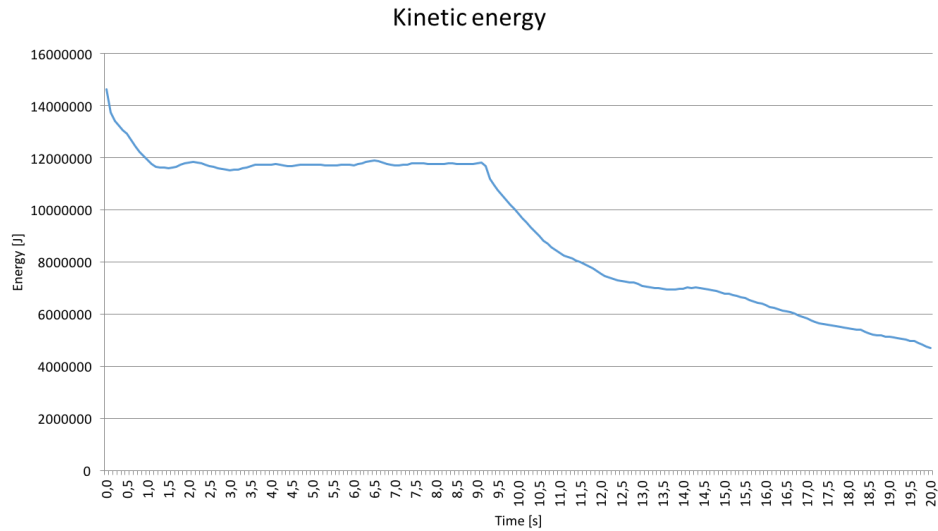
Figure 43: Kinetic energy at the finest mesh size

9.5.2   Internal energy

The internal energy in ABAQUS can be expressed through the equation (Hibbitt et al., 1992)

$$E_I = E_E + E_P + E_{CD} + E_A + E_{DMD} + E_{DC} + E_{FC} \tag{9.2}$$

Here, E_E is the recoverable strain energy, E_P is the energy dissipated through inelastic processes such as plasticity, E_{CD} is the energy dissipated through viscoelasticity or creep, E_A is the artificial strain energy, E_{DMD} is the energy dissipated through damage, E_{DC} is the energy dissipated through distortion control and E_{FC} is the fluid cavity energy.
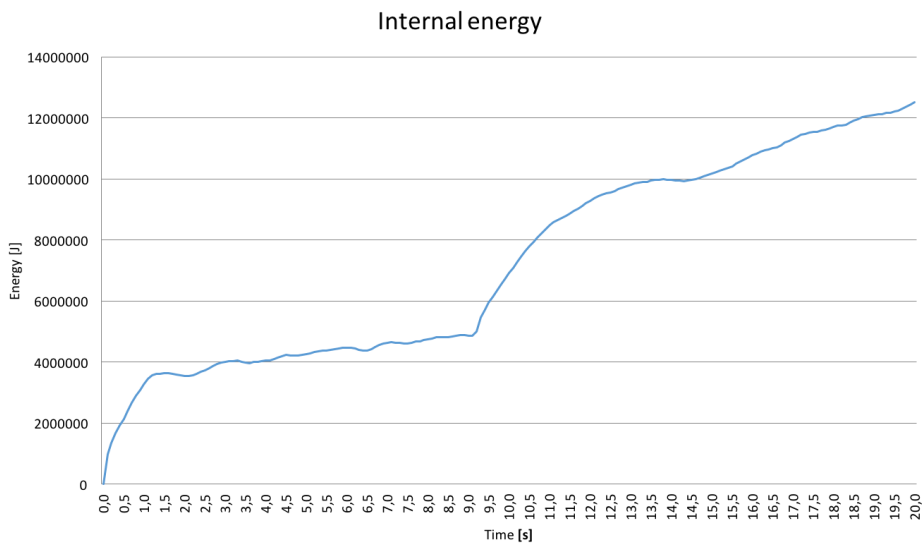
Figure 44: Internal energy at the finest mesh size

In the figure above, it can be seen that this energy will increase with time, and after 1.5 seconds the growth rate of the curve slows down, before it increases rapidly again at 9.5 seconds. The internal energy has to increase, because both the ship and the hull will absorb the impact forces as internal energy.

9.5.3   Kinetic and internal energies

From the plots in figure 50 an 85 it can be seen that these two are very similar, but are the opposites of each other, they are here plotted together.
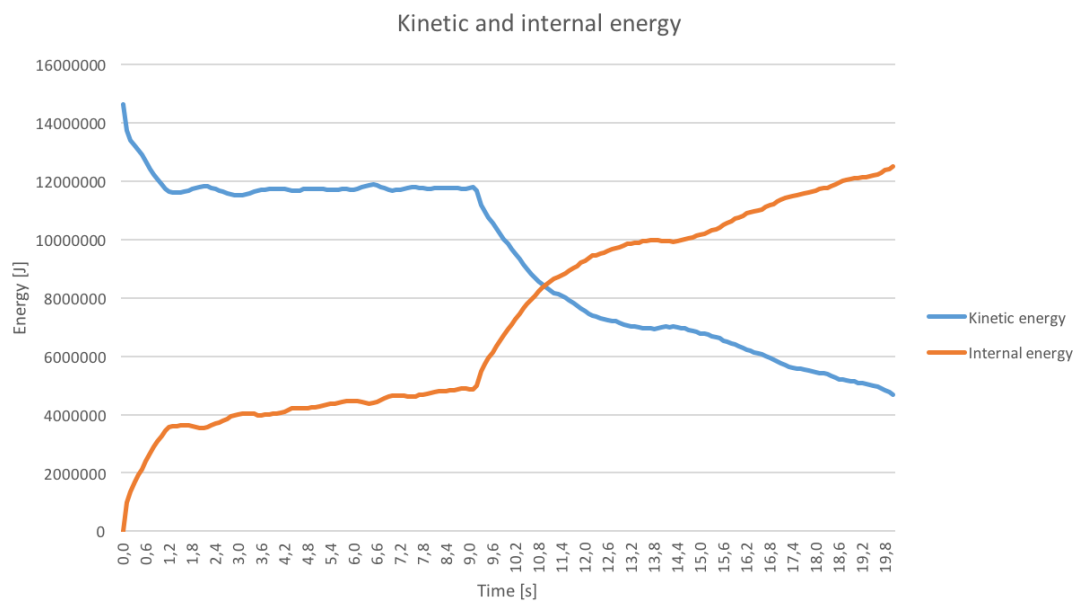
Figure 45: Internal and kinetic energy at the finest mesh size

From the graph, it is seen that this is correct. The kinetic energy that disappears from the system is transferred into internal energy in both the hull and the bridge.

9.5.4   Strain energy

The strain energy shows how much of the energy in the system that has been stored as energy in the strains.
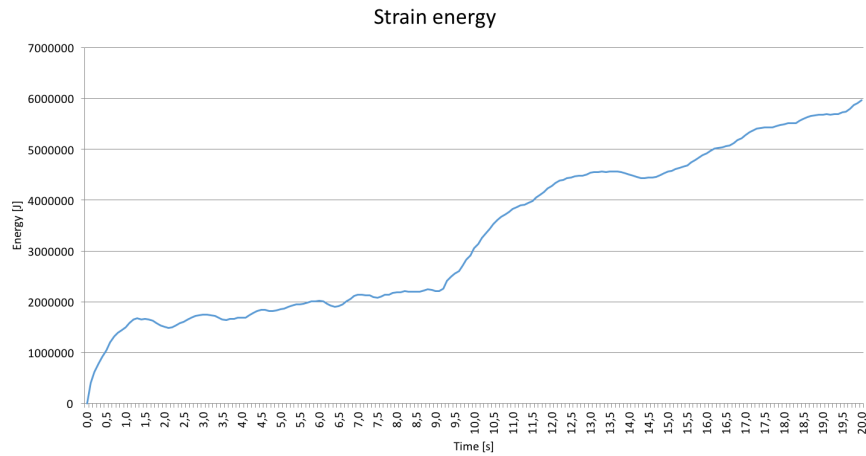
Figure 46: Strain energy at the finest mesh size

The plot is similar to the plot of the internal energy in figure 50. It starts out with a rapid increase in the strain energy level, before it plateaus, and starts to increase again.

9.5.5   Strain and internal energies

Because of the similarities between the curves of the internal energy and the strain energy, these two has been plotted together for comparison.
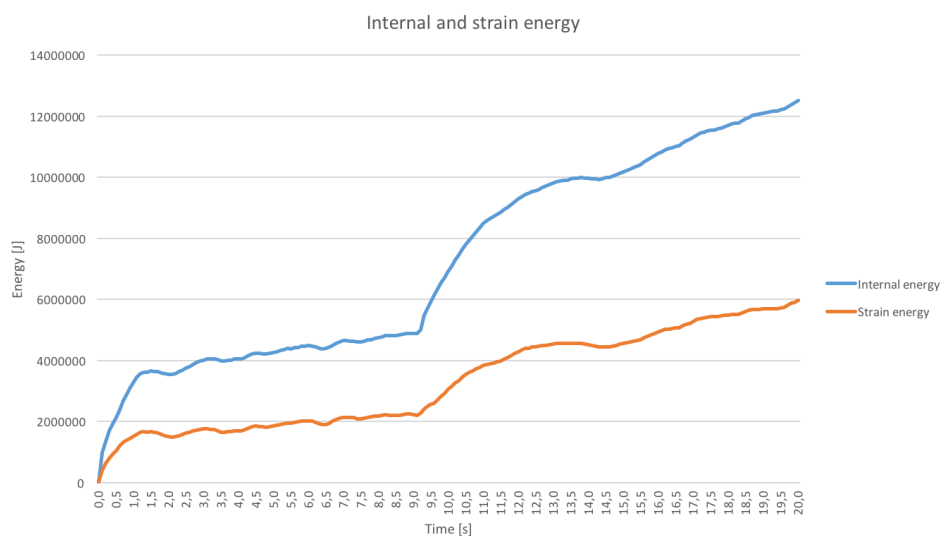
Figure 47: Internal and strain energy at the finest mesh size

In the plot, it can be seen that the curves of the two energies have the same shape, but a different magnitude. This tells us that the strain energy will be a large contributor to the internal energy, only with a smaller value.

9.5.6   Artificial energy

The artificial strain includes the energy that is stored in hourglass resistances and transverse shear in shell and beam elements, as presented in section 4.2.3. If a high value is obtained here, it is an indication that mesh refinement or other changes in mesh is necessary. It should be less than 5% of the internal energy for the results to be considered valid (Hibbitt et al., 1992).
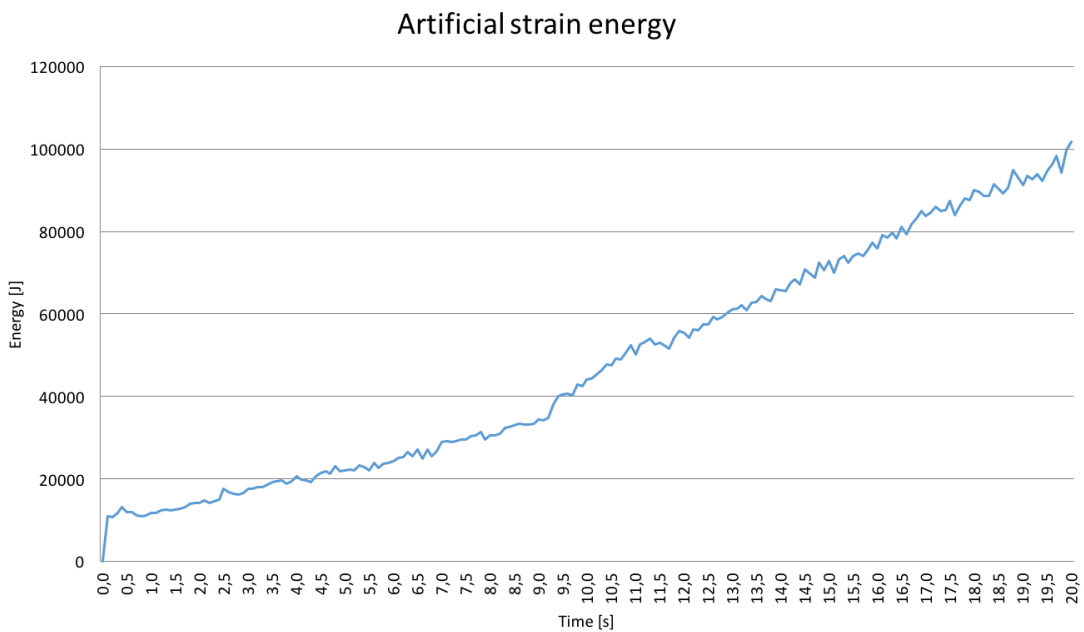
Figure 48: Artificial energy at the finest mesh size

For the artificial energy plot it can be seen that the energy will increase gradually with time, which could be expected as the hourglass modes do not disappear.To check if these results are small enough compared to the internal energy, the two have been plotted together below.
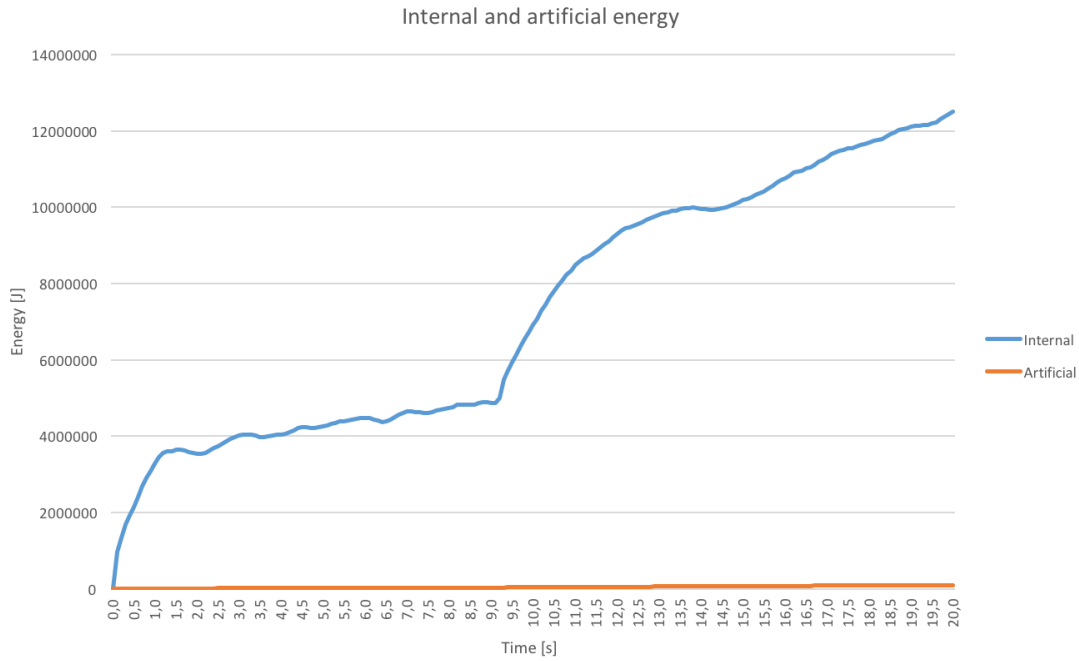
Figure 49: Artificial and internal energy at the finest mesh size

From this figure, we can see that the artificial energy will be less than 5% of the internal energy. The analysis is therefore not producing too large amount of hourglass modes during the analysis, and the results can be seen a usable.

9.5.7   Plastic dissipation

The plastic dissipation is a measurement of how much of the energy that is dissipated in inelastic processes. This will include plasticity processes (Hibbitt et al., 1992).
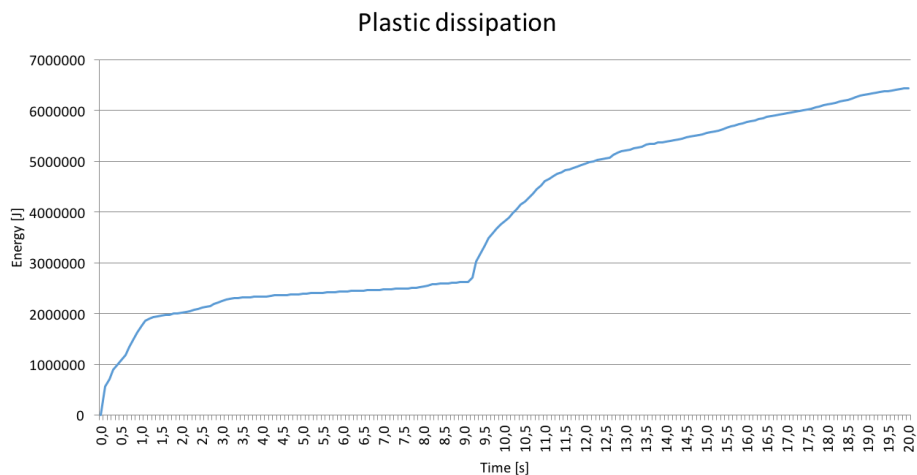
Figure 50: Plastic dissipation at the finest mesh size

In the plot it can be seen that a lot is dissipated in the first 1.5 seconds of the analysis, before the curve flattens out for a while, until it reaches 9.5 seconds and then again increases rapidly, before it starts to take a more linear behavior towards the end of the analysis.

9.5.8   Viscous dissipation

The viscous energy is the energy dissipated through damping mechanisms. It can be seen as a fundamental variable for the global energy balance, but it is not part of the energy dissipated through viscoelasticity or inelastic processes (Hibbitt et al., 1992).
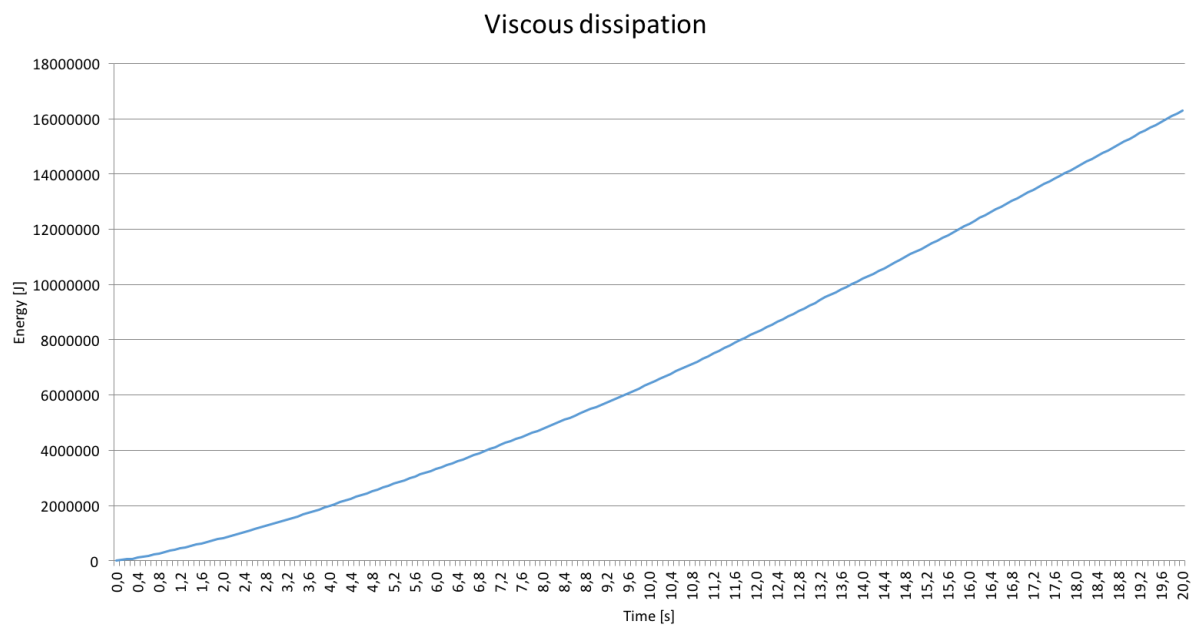
Figure 51: Viscous dissipation at the finest mesh size

In the plot it can be seen that the viscous energy will increase almost linearly throughout the entire process. This yields that energy must be dissipated through damping processes in a stable way.

9.5.9   Total energy

The total energy should be constant throughout the entire process. The results for the total
energy is presented in the graph below.
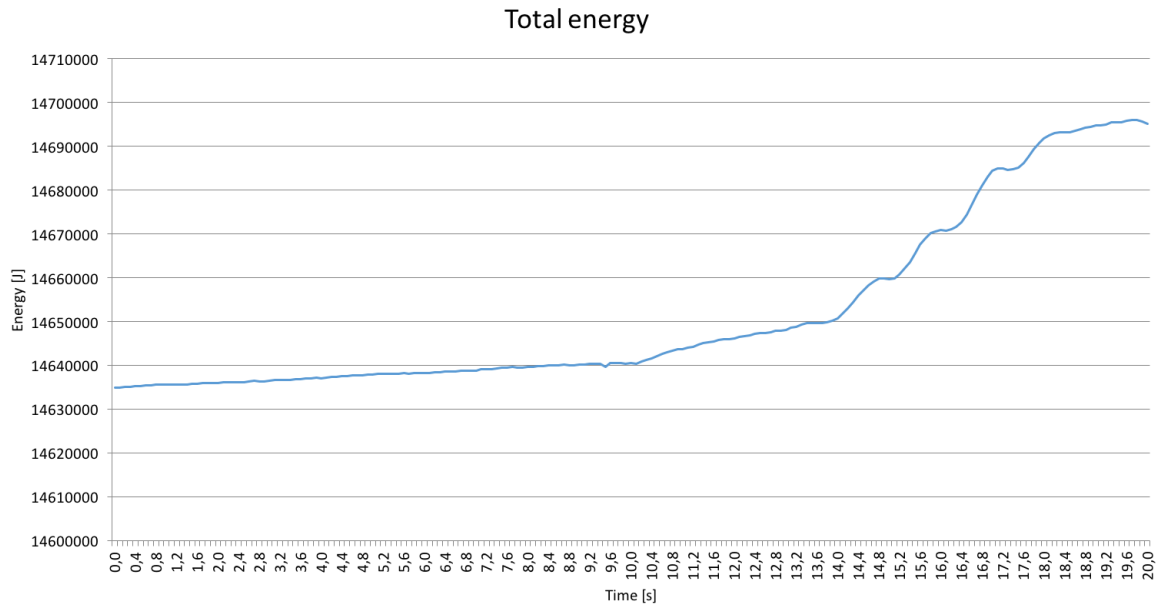
Figure 52: Total energy at the finest mesh size

As can be seen from the plot, the graph does not stay constant. But by looking more
closely at the y-values it can be seen that in reality, the changes in the total is very small
compared to the total value. This change can therefore be seen as negligible.

9.6   Mesh refinement

A mesh refinement study was conducted. To do do this, he analysis several times but with a smaller mesh size for each run. The purpose of this study is to see when the solution will converge towards the solution.

9.6.1   Kinetic energy

The first plot in the mesh refinement study is of the kinetic energy. This is shown in the figure below.
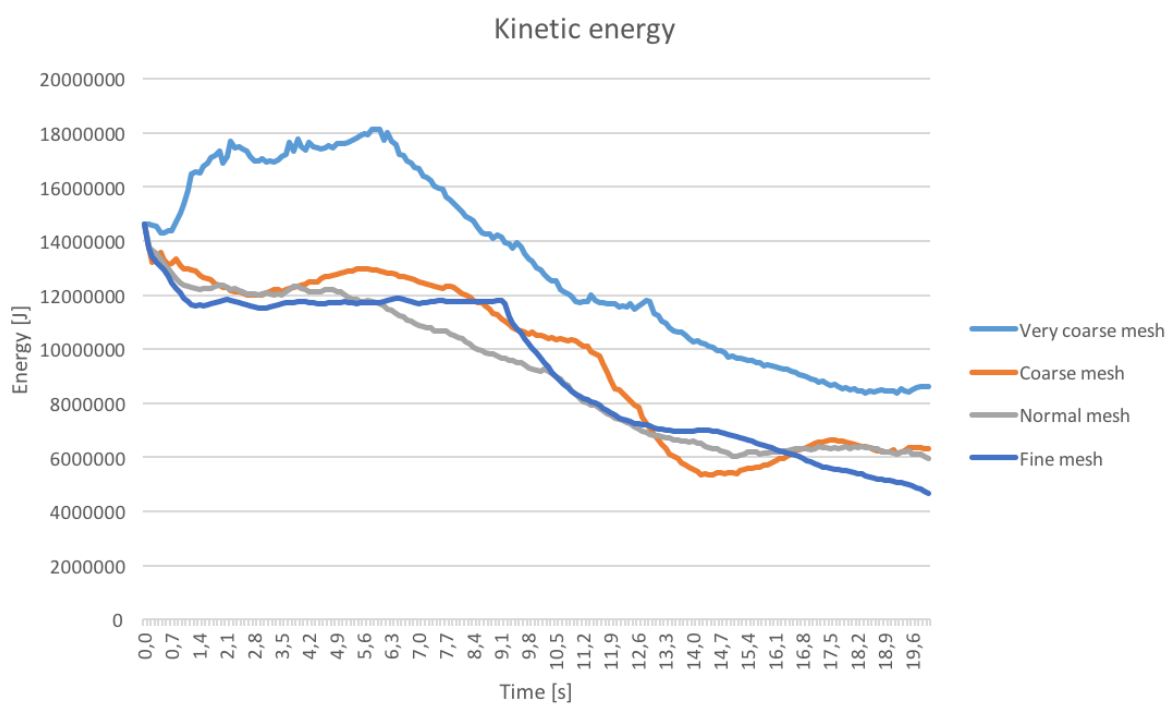
Figure 53: Mesh refinement study of kinetic energy

It can be seen that the curve for the very coarse mesh is very far from the three other analyses. The other three start to resemble each other. But they do not become equal to each other with the finest mesh size.

9.6.2   Internal energy

The next plot is of the internal energy, the results are plotted in the figure below.
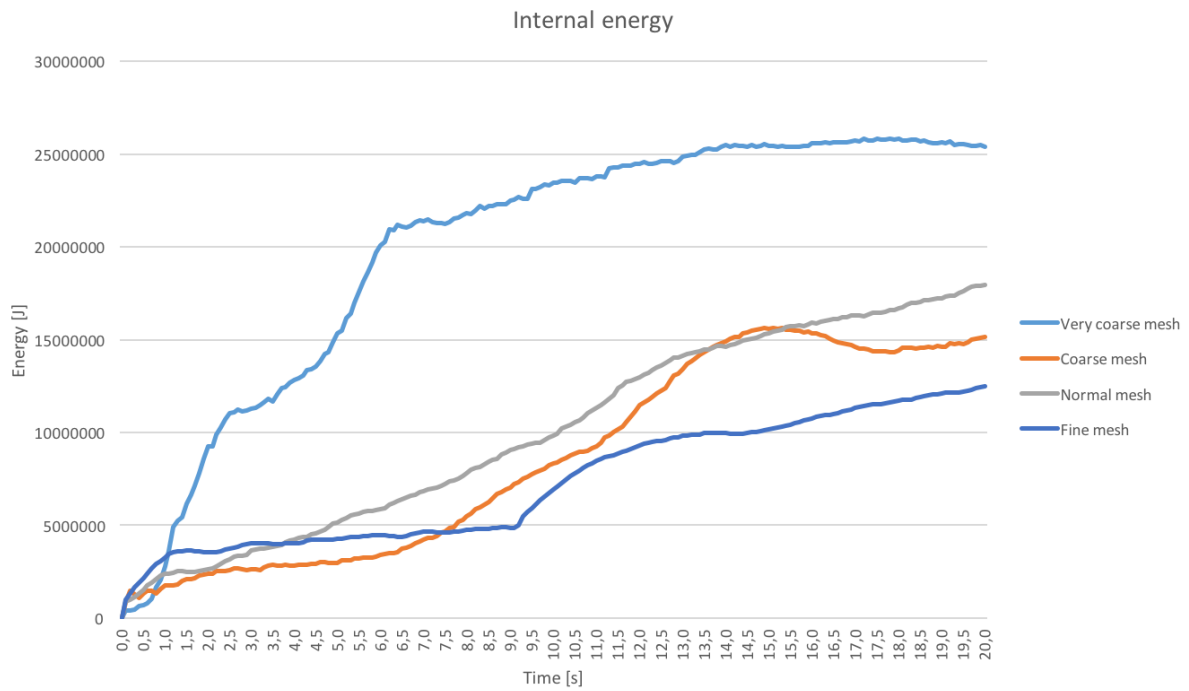
Figure 54: Mesh refinement study of the internal energy

As can be seen from the plot, the first analysis with a very coarse mesh size has results that is much larger than those for the other analyses. Even though complete convergence is not achieved, the results starts to resemble each other more and more with a smaller mesh size.

9.6.3   Strain energy

For the strain energy in the system, we have the plot shown below.
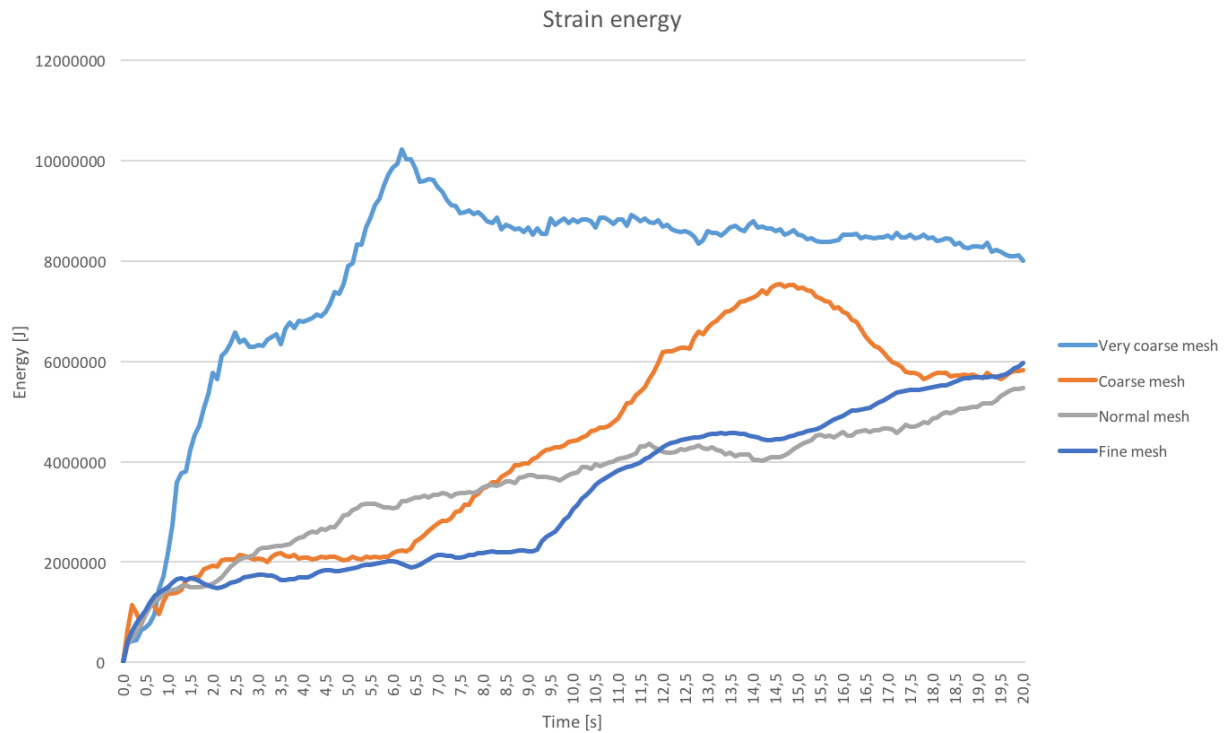
Figure 55: Mesh refinement study of the strain energy

In the figure, it can be seen that the curve for the very coarse mesh size is quite much larger than the other three. Here, also the coarse mesh size has a peak at around 14.5 seconds, which defers from the two other mesh sizes.

9.6.4   Artificial energy

The results for the artificial energy is plotted in figure 56.
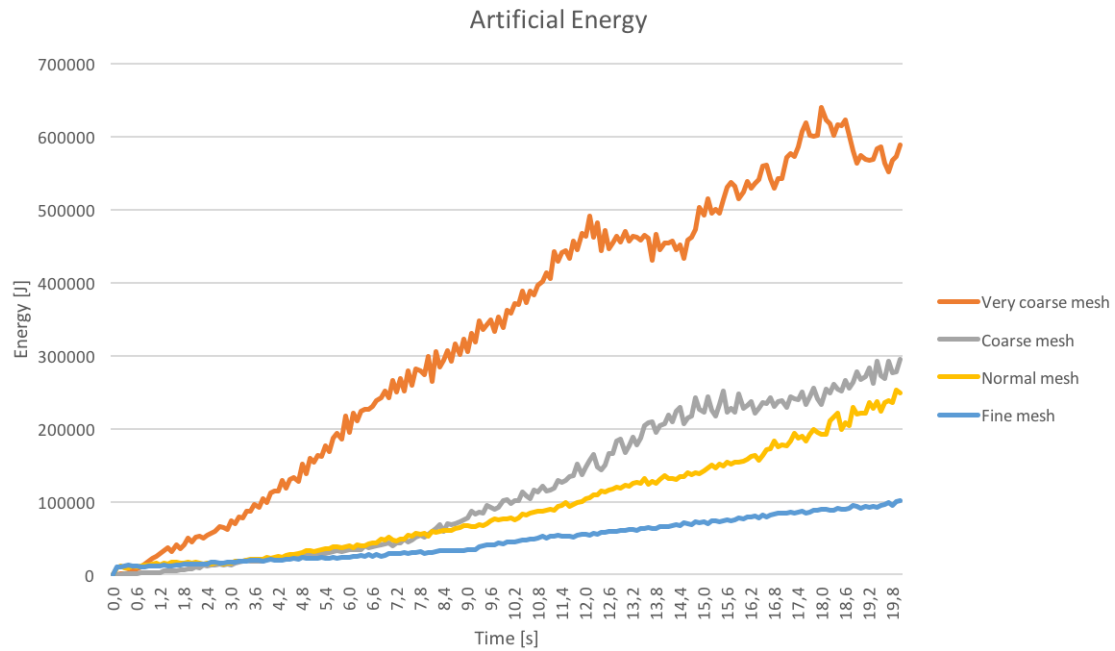
Figure 56: Mesh refinement study of the artificial energy

In this plot, the curves does not starts to resemble each other, but since this is a plot of the artificial energy, which is the zero-energy modes in the system, it is desired that this energy is as low as possible. The magnitude of this energy decreases with a finer mesh size, which may be a factor in the more accurate results with mesh refinement.

9.6.5   Plastic dissipation

Here, the plastic dissipation has been compared with different mesh sizes. The results are shown in the plot below.
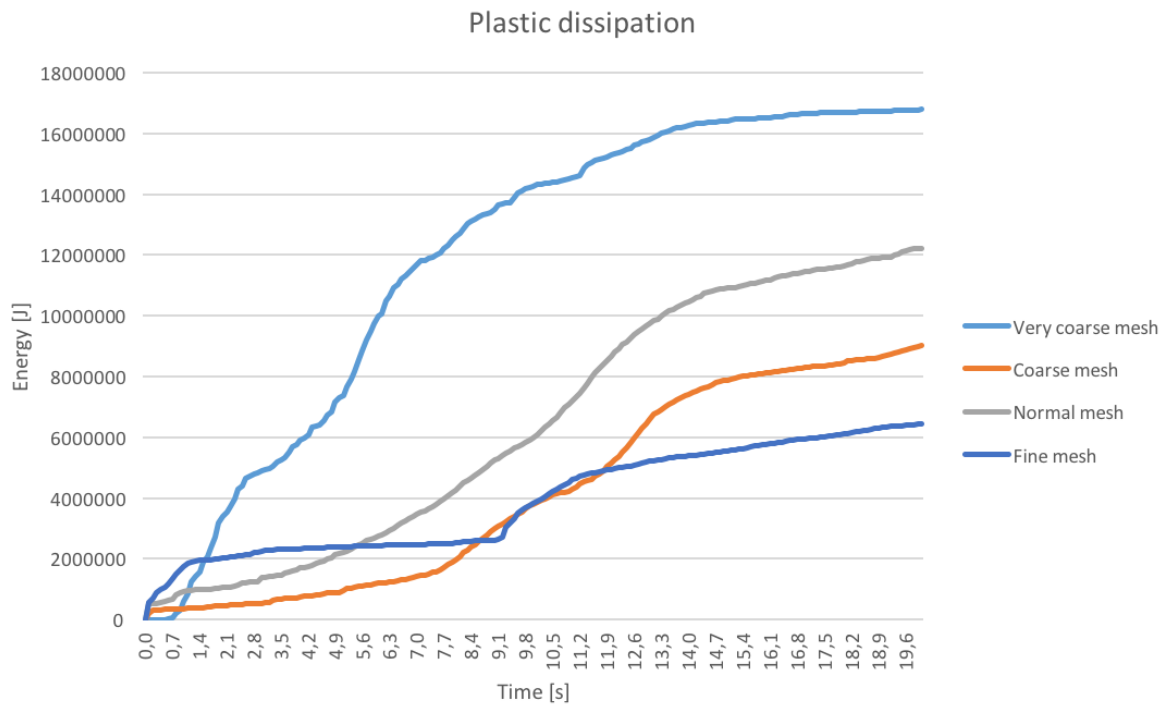
Figure 57: Mesh refinement study of the plastic dissipation

As for the earlier results from the mesh refinement study, the results for the very coarse mesh defers a lot from the other results. Here, the curve of the very fine mesh size is actually more similar to the results from the coarse mesh than the normal mesh. It it the very fine mesh that yields the lowest value for the plastic dissipation.

9.6.6 Total energy

Underneath the results for the mesh refinement study of the total energy is presented.
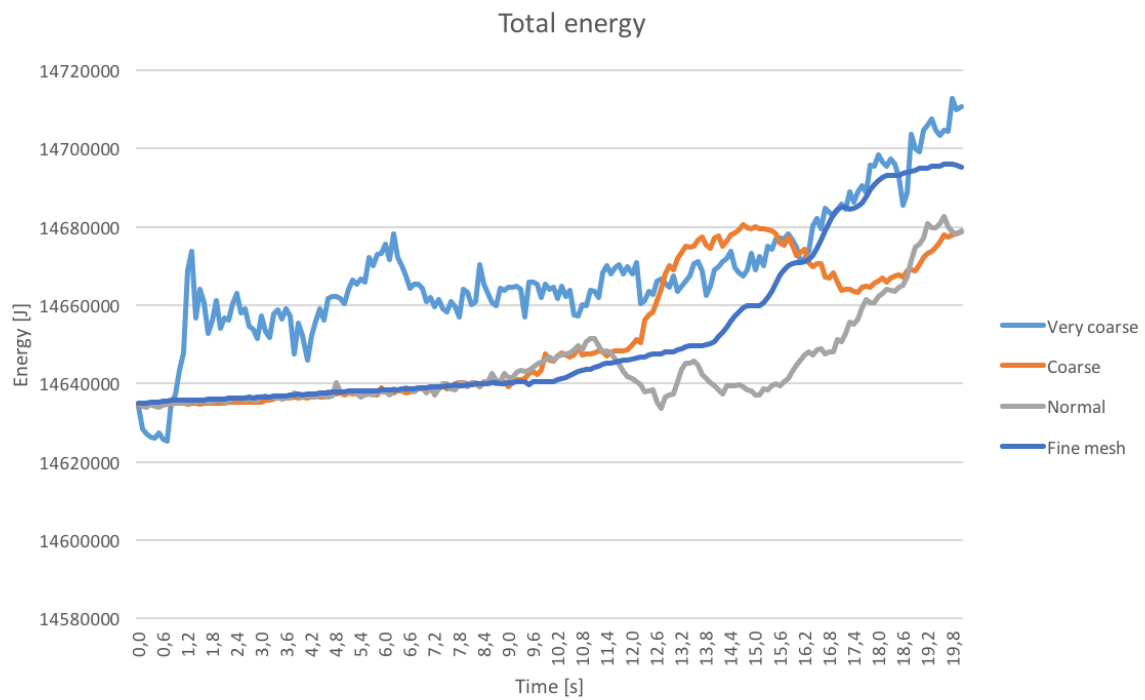
Figure 58: Mesh refinement study of the total energy

Just by looking at the plot, it looks like the total energy in the system does not stay constant during the analysis, but the changes in the total energy is in general very small, and can be seen as negligible. It can also be seen that the very fine mesh size lies between the normal and coarse mesh sizes for a while, before it ends up with a larger magnitude.

9.6.7 Viscous dissipation

The last plot for the mesh refinement study is of the viscous dissipation. These results are shown in plot below.
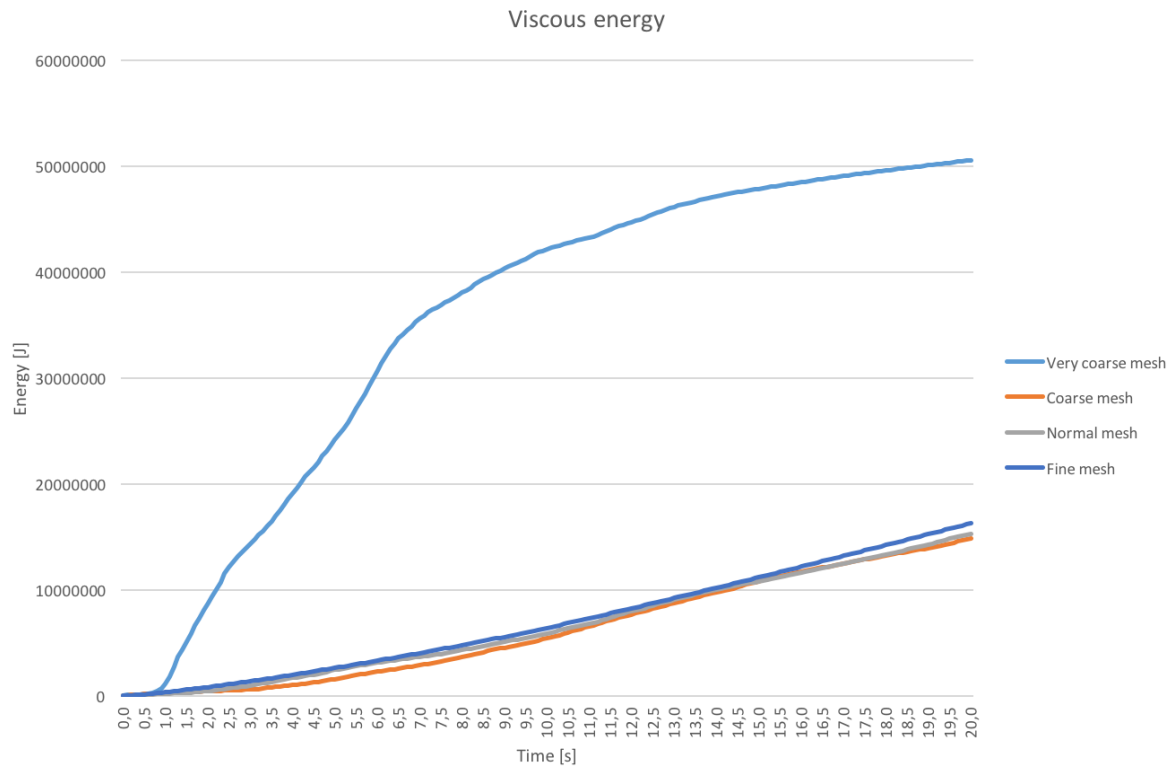
Figure 59: Mesh refinement study of the viscous energy

From this plot it becomes very clear that the first analysis of the very coarse mesh is significantly larger than the other three. These are on the other hand very similar to each other.

9.7 Significance of shell thickness

It was of interest to see how the results would be influenced by a change in the thickness of the shell element in the pontoons. The first simulations was ran with a thickness of 2 cm, and this was then changed to 1 cm for the thin option, and 4 cm for the thick one. The results that have been presented earlier, will here be compared to the new results for these two alternatives.

9.7.1 Local stresses

Here, the stresses for both the alternative with thick and thin shells are compared. They are both presented in the figures below.
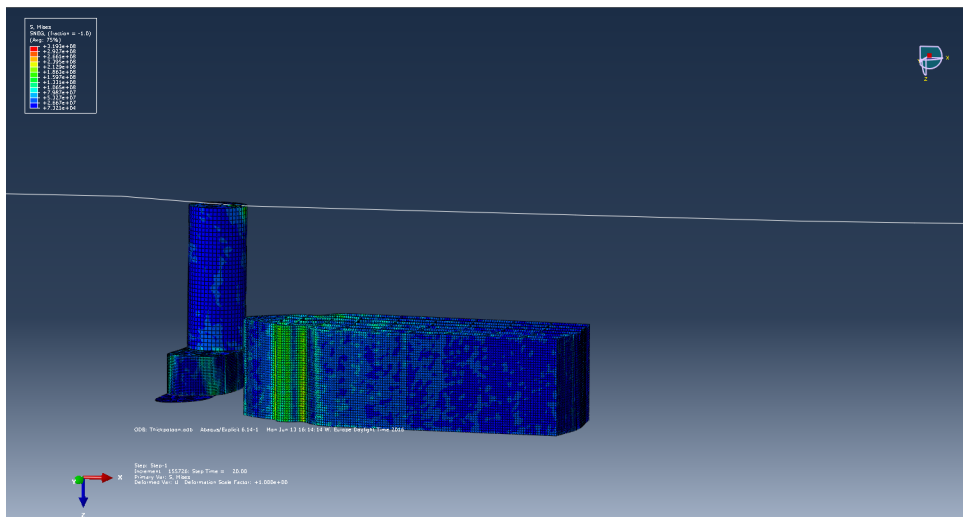
Figure 60: Local stress of collision area at 20 seconds for the model with a thick shell
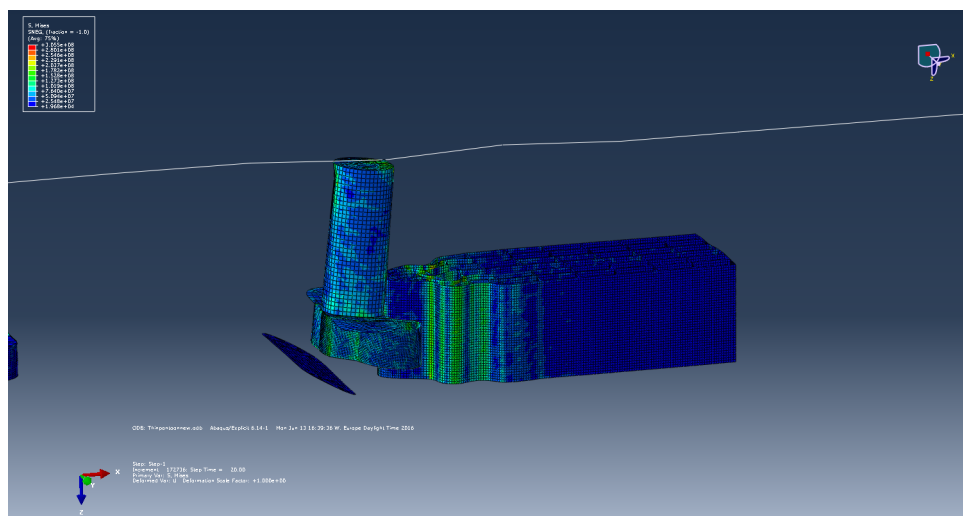
Figure 61: Local stress of collision area at 20 seconds for the model a thin shell

From the figures it can be seen that the pontoon with a thin shell clearly will experience a lot more forces than the model with a thick shell. Where the model with the thick shell will not deform significantly, this is not the case for the pontoon with a thin shell. The maximum stress that occurs in the pontoon with a thick shell is 213 MPa, is this value for the thin shell 305 MPa.

9.7.2 Global stresses

The global stresses for the thick and thin shell pontoons are shown in the figures underneath.
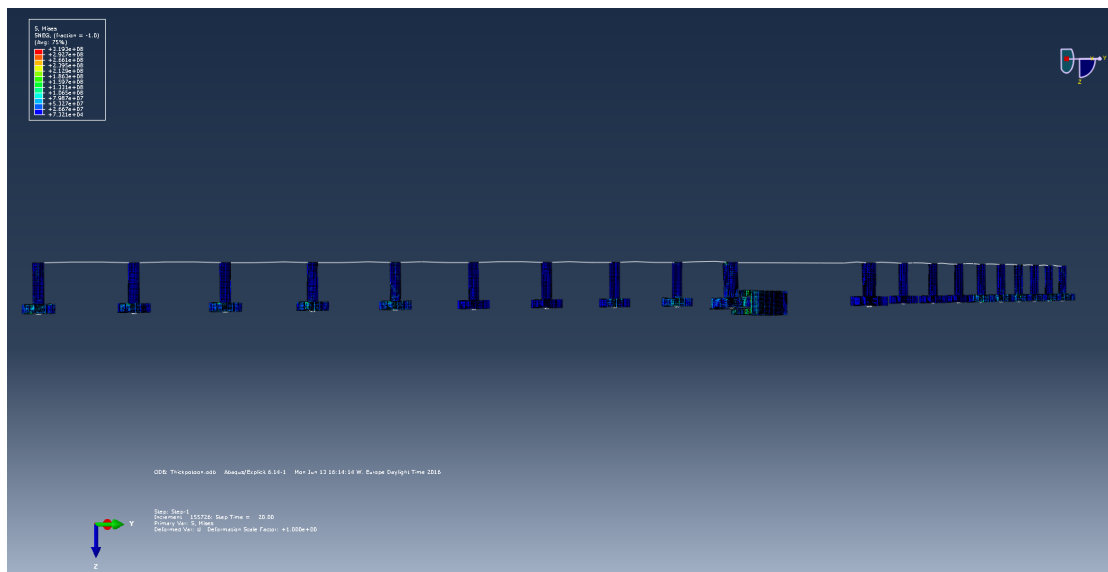
Figure 62: Global stresses at 20 seconds for the model with a thick shell
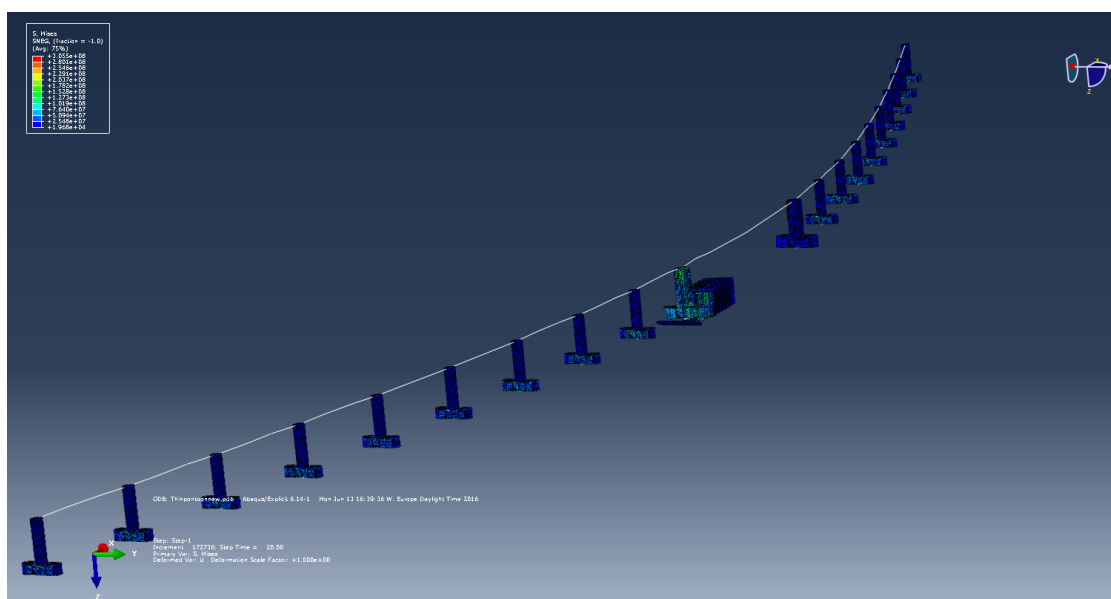
Figure 63: Global stresses at 20 seconds for the model with a thick shell

From the figures it can be seen that both of the model will distribute stress in the other pontoons, but the pontoons with thin shell elements will experience stresses in a larger scale than the thick pontoons will.

9.7.3 Forces in the road

The forces in the beams for the two alternatives with thick and thin shell are presented in the figures below.
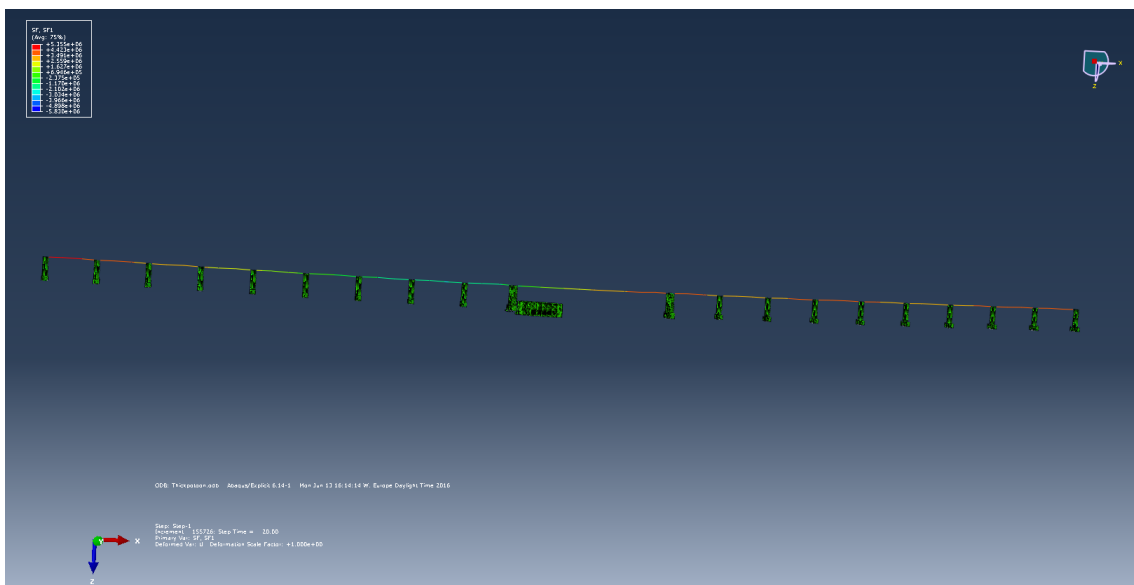
Figure 64: Beam forces at 20 seconds for the model with many bulkheads
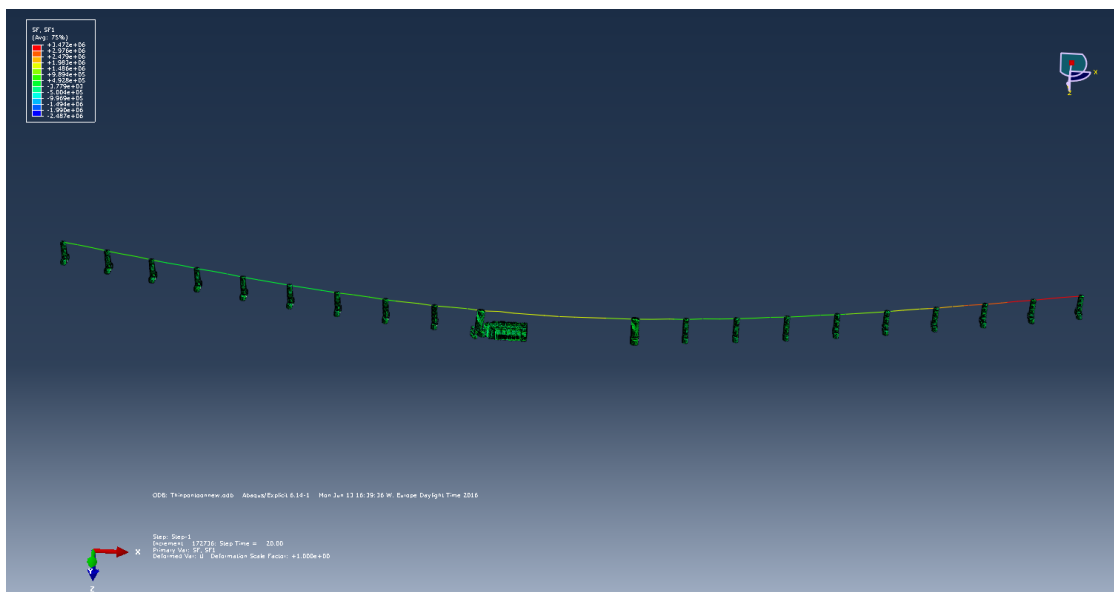
Figure 65: Beam forces at 20 seconds for the model without bulkheads

From the figures it looks a if the road for both cases experiences about the same force. But red color is not just red color, and the actual magnitude has to be looked more into. For the road in the model with a thick shell, the maximum force is 5.36 MN, and for the thin shell alternative it is 3.47 MN. This means that the model for the thick shell will experience the largest force, even though it is not very much higher than that of the thin model.

9.7.4 Moments in the road

In this section the moments in the road are presented for the model with thin and thick shell elements. These are given in the figures below.
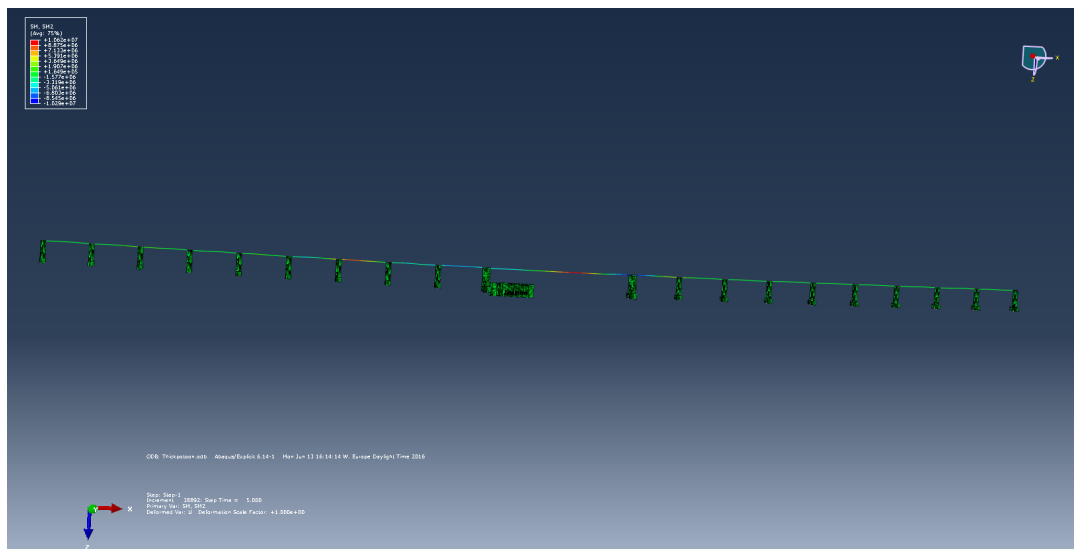
Figure 66: Beam moments at 5 seconds for the model with a thick shell element
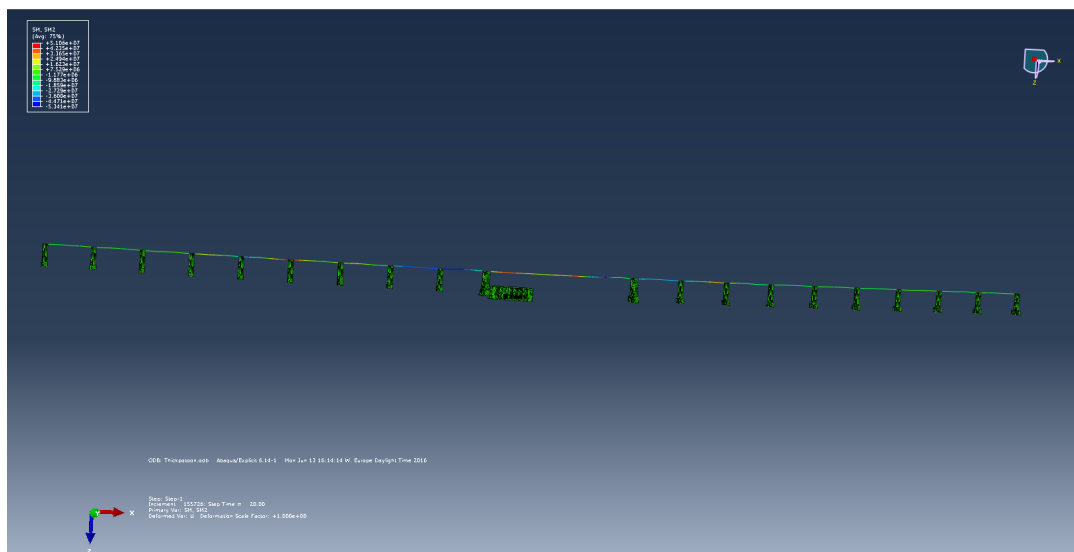
Figure 67: Beam moments at 20 seconds for the model with a thick shell element
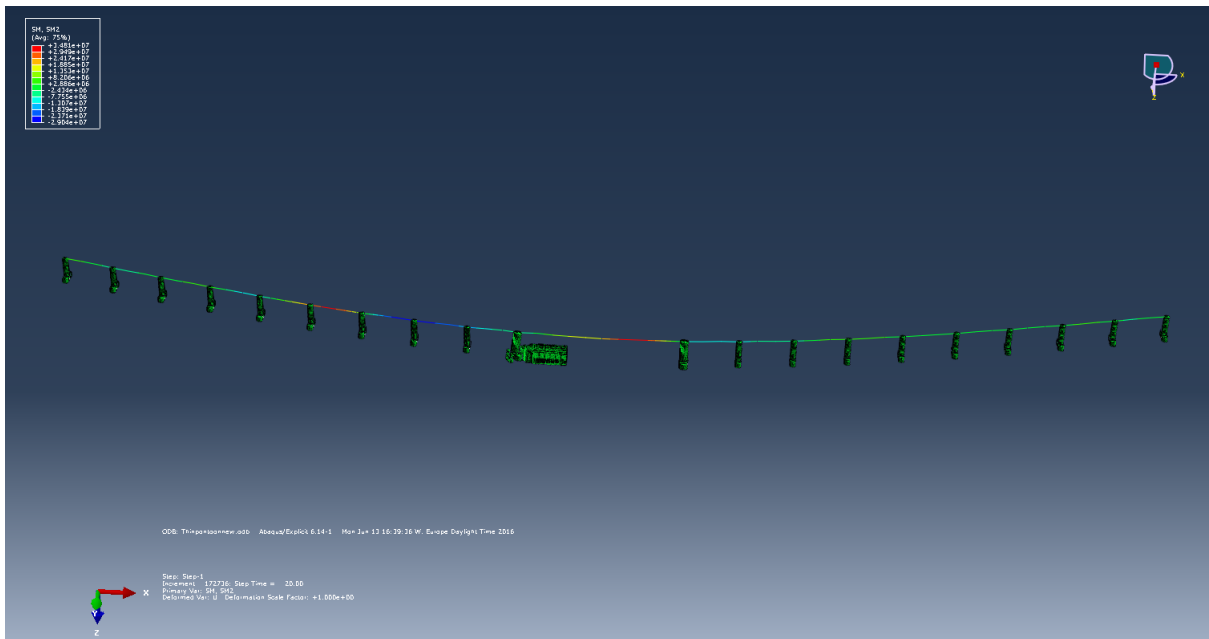
Figure 68: Beam moments at 5 seconds for the model with a thin shell element
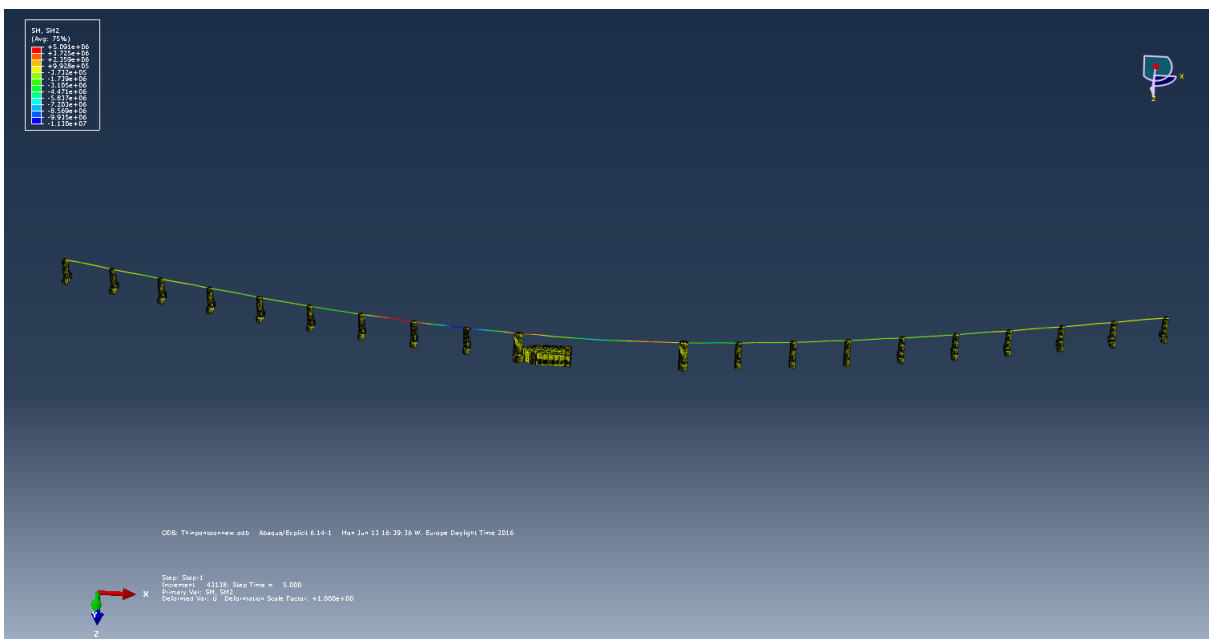

Figure 69: Beam moments at 20 seconds for the model with a thin shell element

The moment distributes in the beam with a periodic behavior. It will distribute in the same manner for both of the models, but with a different magnitude. For the thin shell model the maximum moment in the beam is 34.8 MNm, and for the thick model this value is 51 MNm.
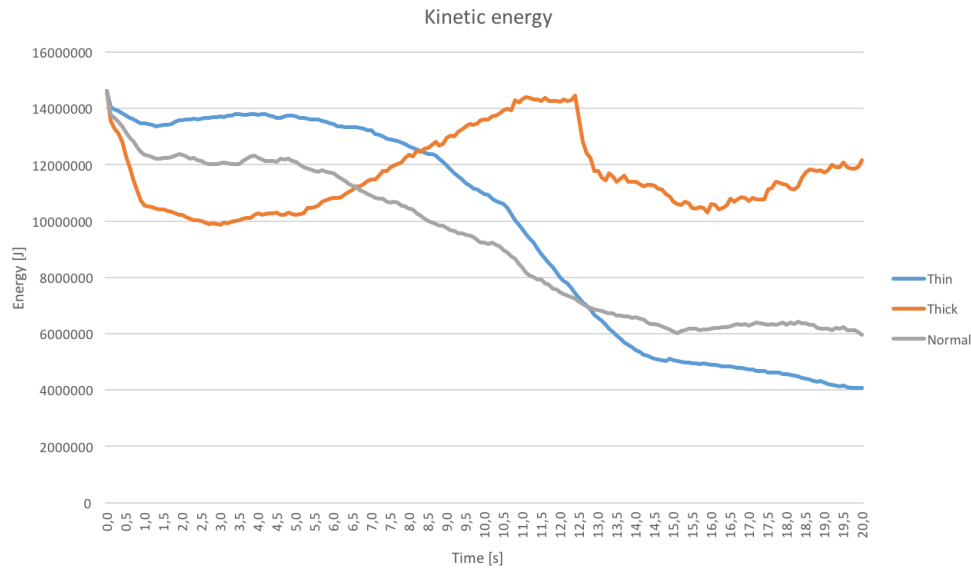
9.7.5   Kinetic energy

Figure 70: Significance of shell thickness on the kinetic energy

As can be seen from the plot, the thick shell will decrease much faster than the other two at the beginning, before kinetic energy again is added to the system, and it again will drop. The thick shell is the alternative that has the most kinetic energy remaining in the system after 20 seconds. As for the thin shell, this will not absorb the kinetic energy before some time has passed, but it ends up containing the least amount of kinetic energy of all of the alternatives.
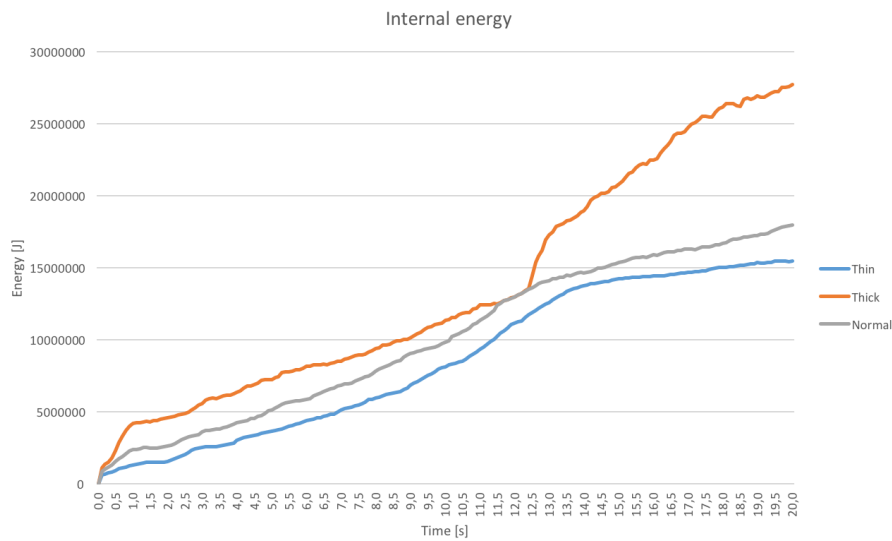
9.7.6 Internal energy

Figure 71: Significance of shell thickness on the internal energy

In the plot of the comparison of the internal energies, it can be seen that the thick shell will absorb most of the energy, and the thin shell the least. As more materials can hold a larger amount of internal energy is predictable.

9.7.7 Strain energy

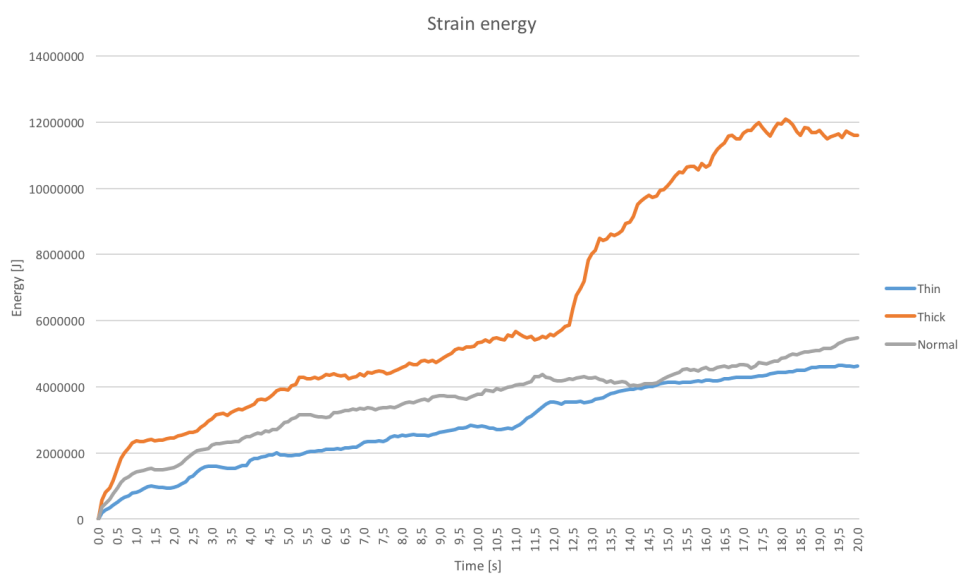Here, a comparison of the strain energies are presented.

Figure 72: Significance of shell thickness on the strain energy

As can be seen from the plot, the strain energy follows the same pattern as the internal energy does. This means that the thick shell will contain the largest amount of strain energy, and the thin shell, the least amount at the end of the time period.

9.7.8 Artificial energy

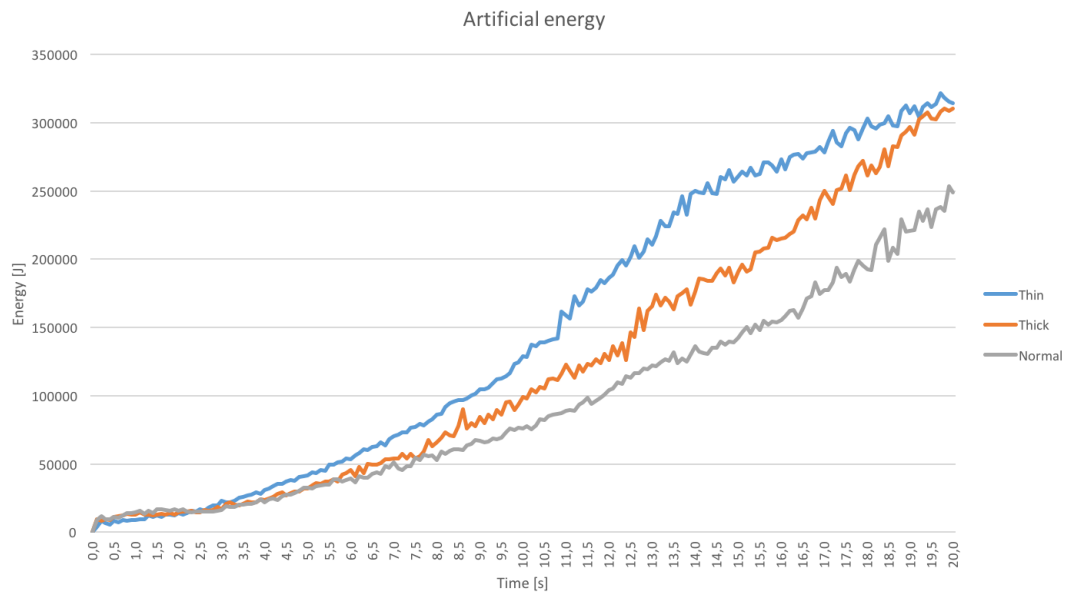The next plot is of the artificial energy.

Figure 73: Significance of shell thickness on the artificial energy

In the plots it can be seen that the analysis from the original analysis actually contains the least amount of artificial energy.

9.7.9   Plastic dissipation

For the plastic dissipation in the structure, the results is presented in the plot below.
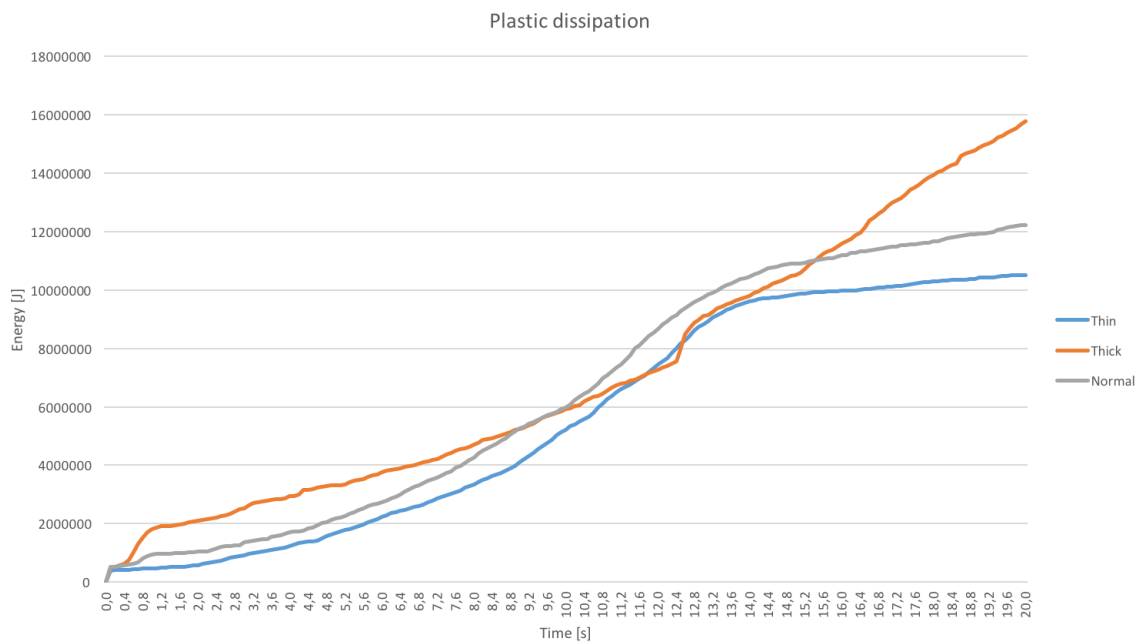

Figure 74: Significance of shell thickness on the plastic dissipation

In the plot it can be seen that the curves crosses each other several times, but in the end the thick shell will have the largest amount of plastic dissipation, and the thin shell the least. Both curves for the original and thin shell have a stable increase in the beginning, before the curves flattens out.

9.7.10 Viscous dissipation

The plot of the viscous energies, and the significance the shell thickness has on this energy is plotted in the figure below.
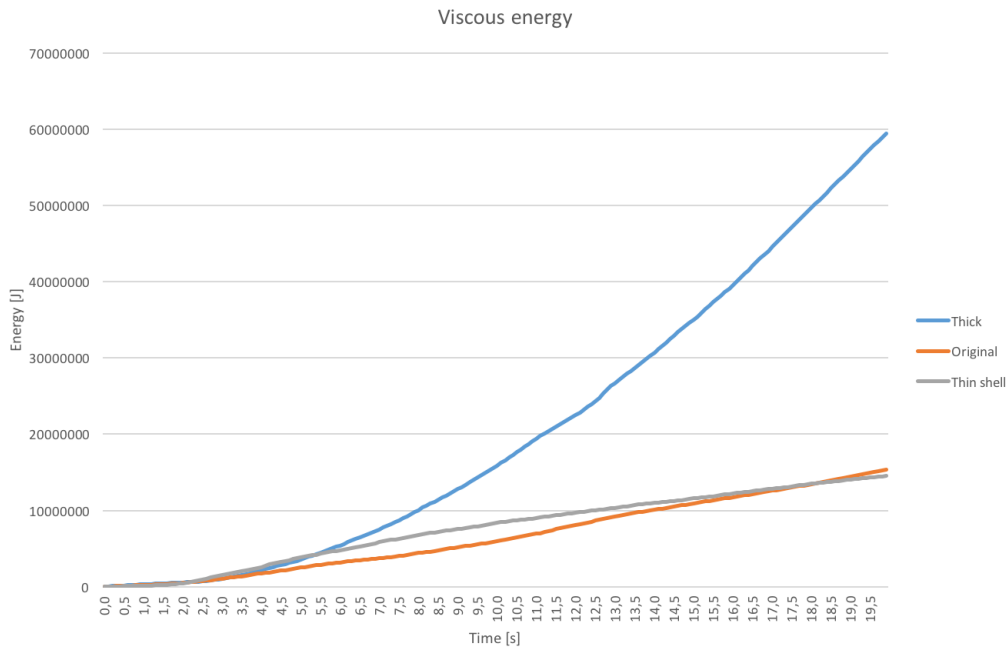

Figure 75: Significance of shell thickness on the viscous energy

From the figure it can be seen that the plot for the energy in the thick shell will be larger than the energies of the original run and of the thin shell.

9.8   Significance of amount of bulkheads

In addition to studying the significance of the thickness of shell, a study has also been conducted on the significance of the amount of bulkheads. The original run had 5, while there now has been a run with none and one with several more.

9.8.1   Local stresses

Here, the stresses for both the alternative with and without bulkheads are compared. They are both presented in the figures below.
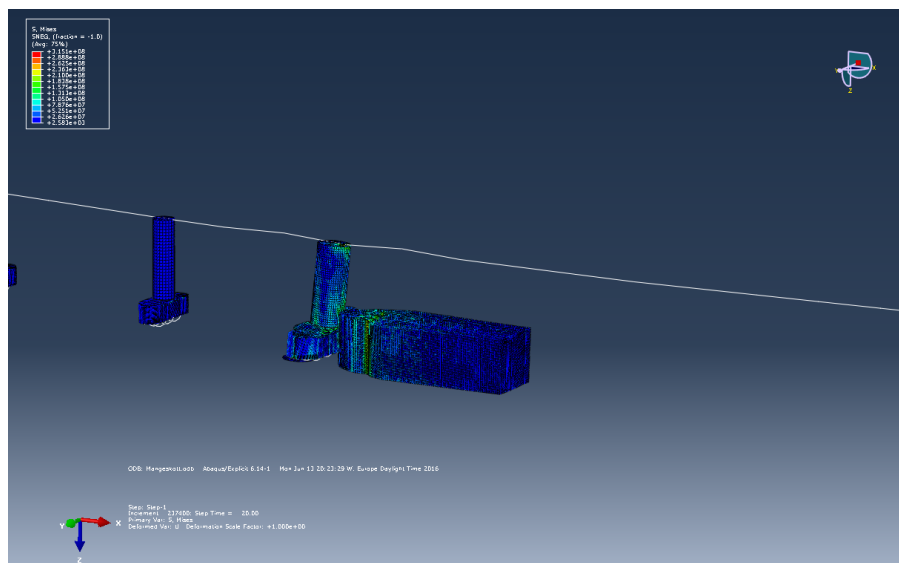

Figure 76: Local stress of collision area at 20 seconds for the model with many bulkheads
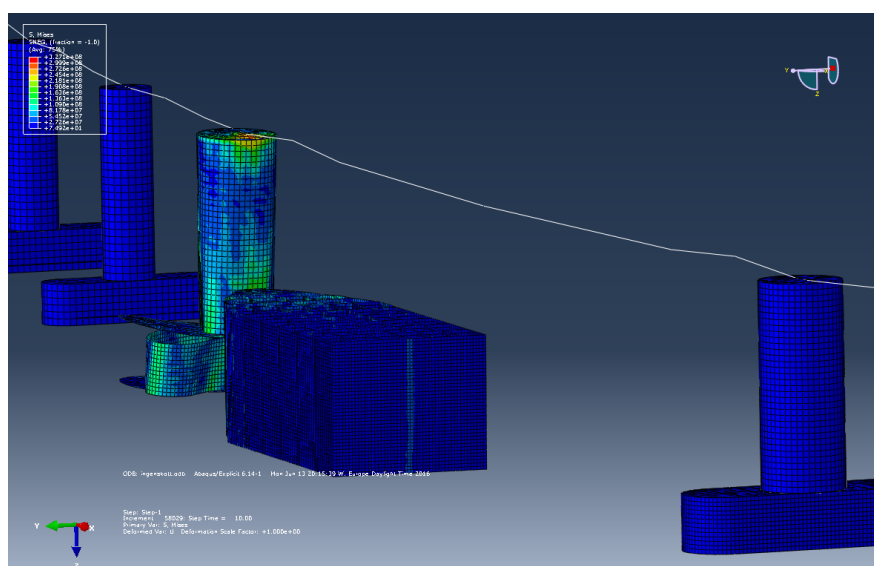

Figure 77: Local stress of collision area at 20 seconds for the model without bulkheads

From the figures it becomes clear that the model without any bulkheads will experience a lot more stress than the model with many. The stress reaches a maximum of 235 MPa for the model with extra bulkheads, compared to 330 MPa for the model without any.

9.8.2   Global stresses

The global stresses for the significance of bulkheads is shown in the
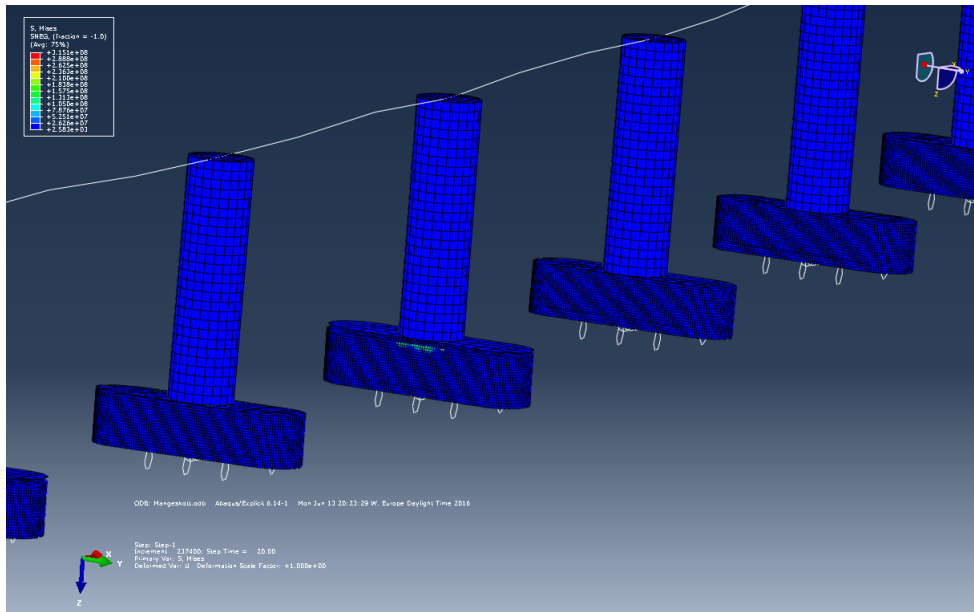

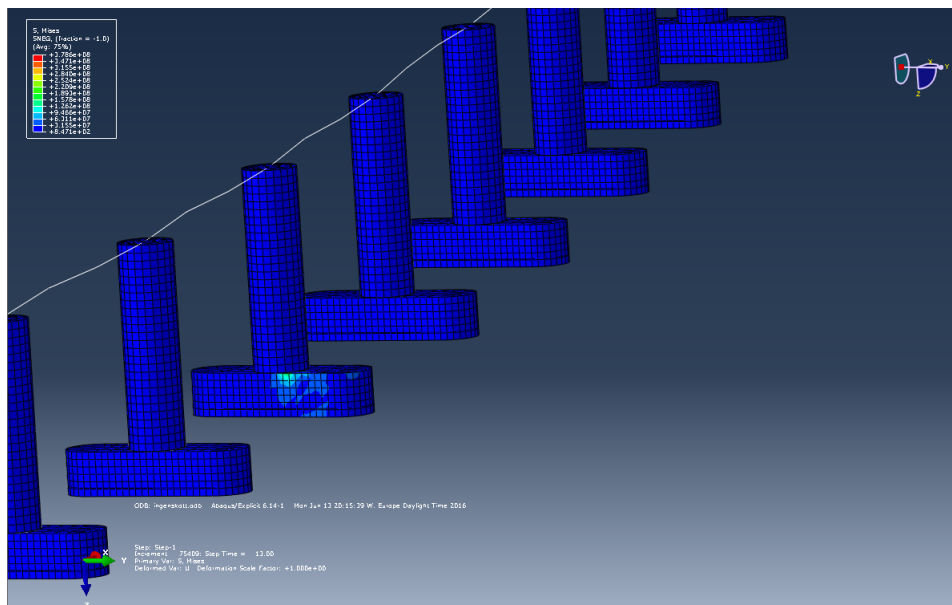Figure 78: Global stresses at 20 seconds for the model with many bulkheads

Figure 79: Global stresses at 20 seconds for the model without any bulkheads

As can be seen from the figures, the distribution of forces is limited, with only a small

speck at one of the pontoons for the model with many bulkheads, and a larger speck at the
pontoon for the model without.

9.8.3   Forces in the road

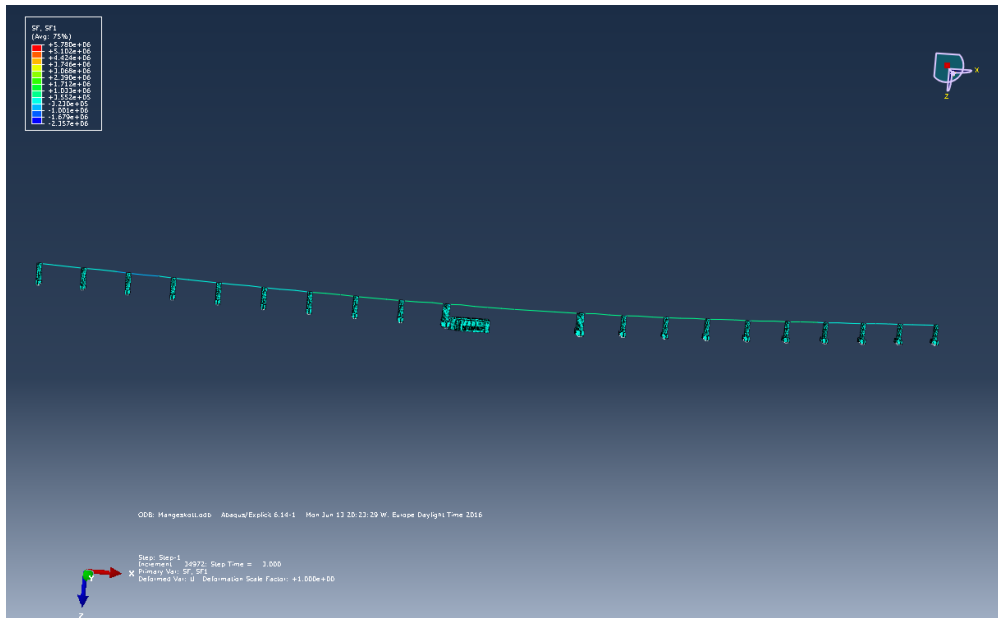The forces in the beams for the two alternatives are presented in the figures below.

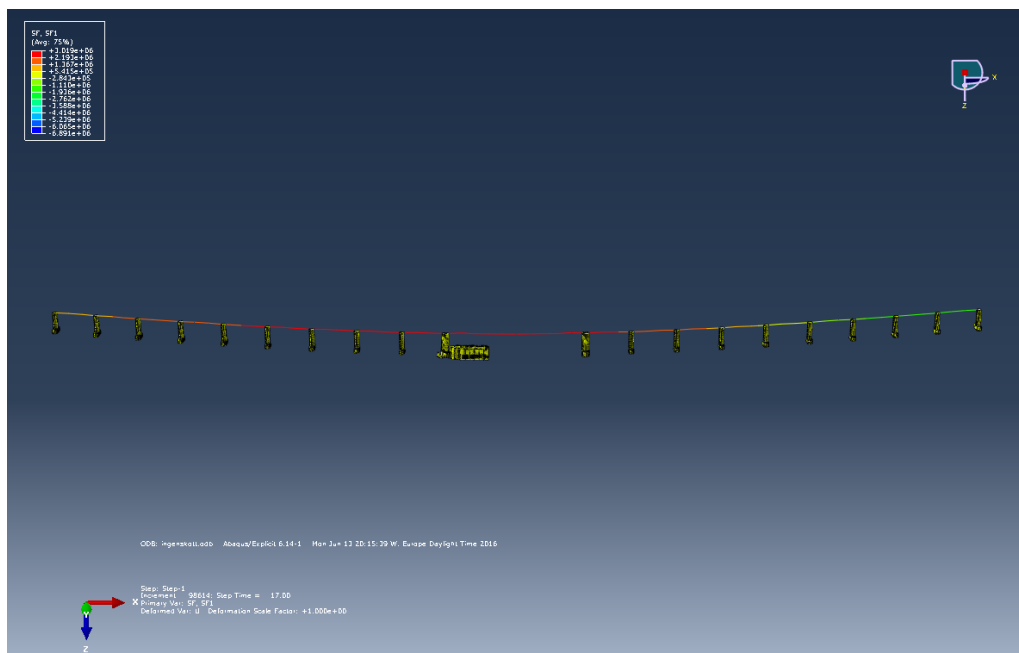Figure 80: Beam forces at 20 seconds for the model with many bulkheads

Figure 81: Beam forces at 20 seconds for the model without bulkheads

In the figures it can been seen that the model without any bulkheads has a lot more red

parts, than the one without many. The model without any bulkheads has almost no forces in the road at all. The maximum value for the forces is 3 MN for the model without bulkheads, and 0.35 MN for the model with bulkheads.

9.8.4   Moments in the road

In this section the moments in the road are presented for the model with and without bulkheads. These are given in the figures below.
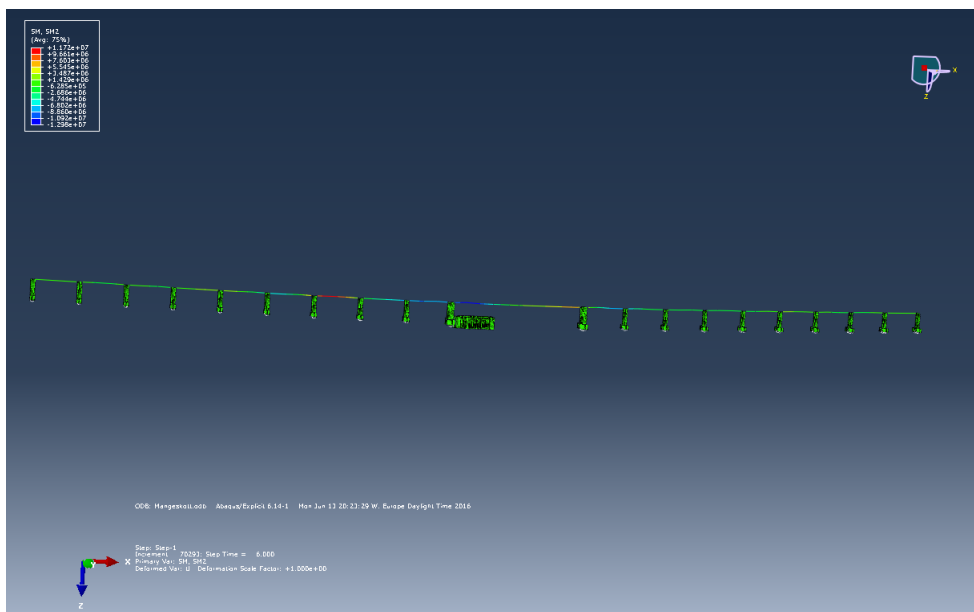
Figure 82: Beam moments at 5 seconds for the model with bulkheads
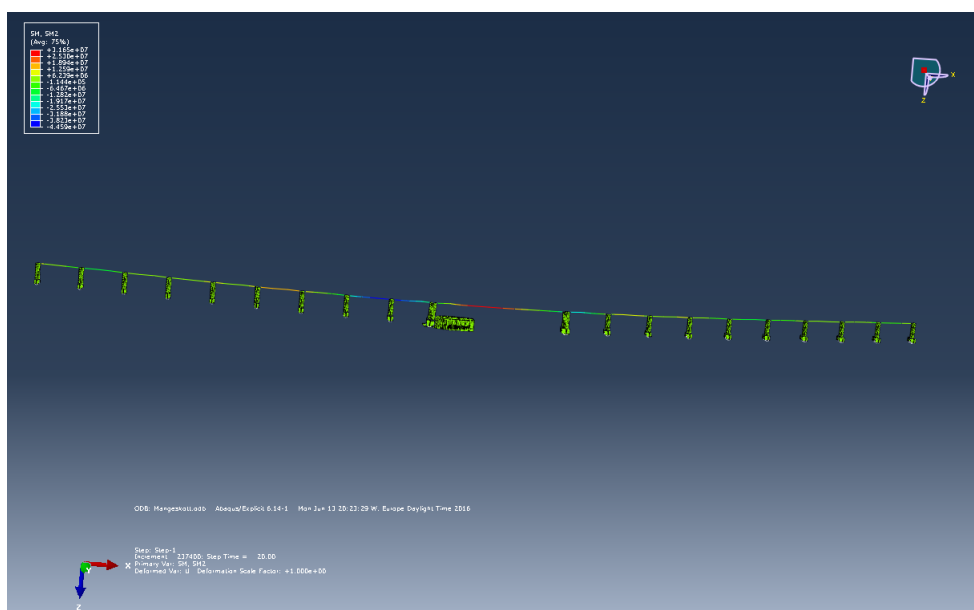
Figure 83: Beam moments at 20 seconds for the model with bulkheads
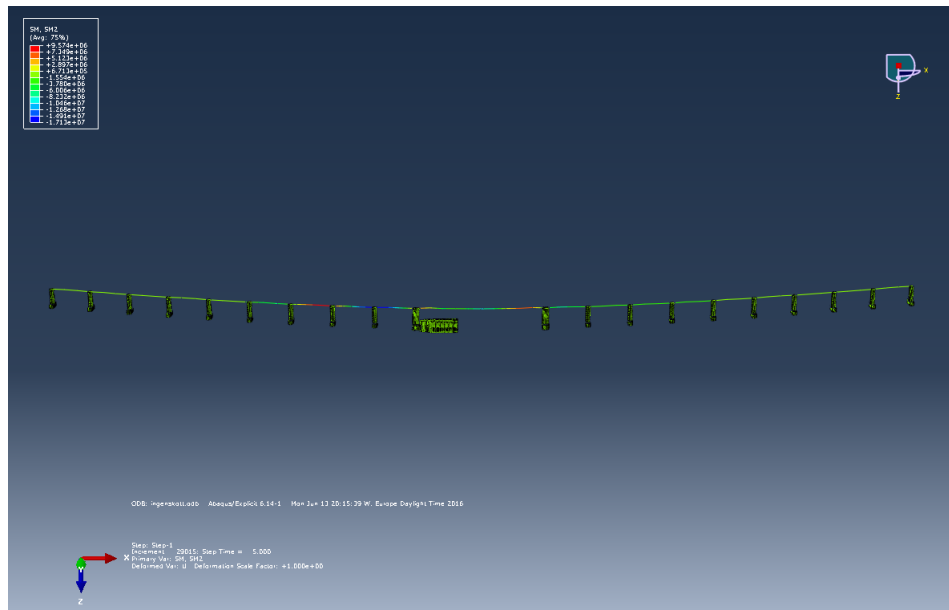
Figure 84: Beam moments at 5 seconds for the model without bulkheads
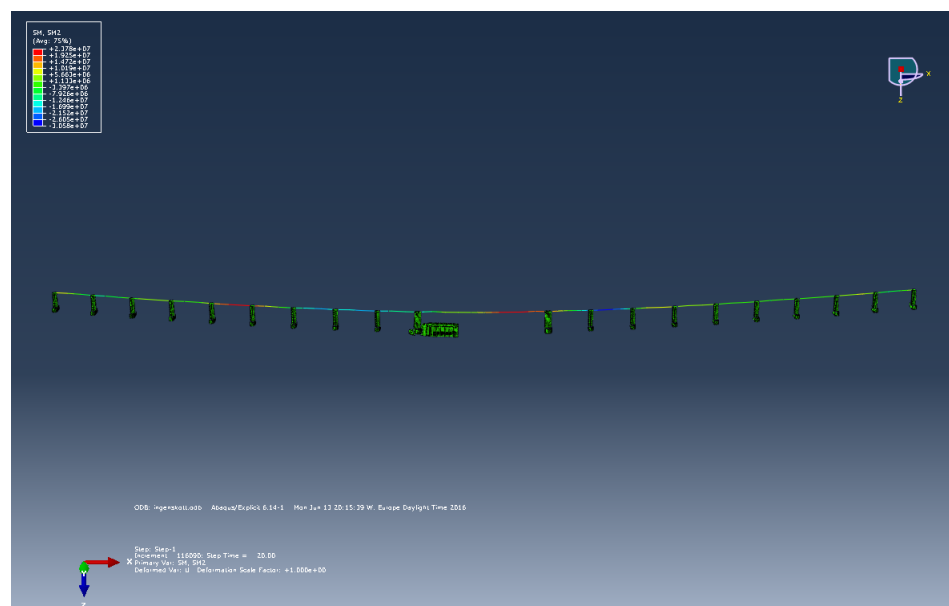
Figure 85: Beam moments at 20 seconds for the modelwithout bulkheads

It can be seen that the moment will distribute itself in the same was as it did in the original analysis. The moment starts at the cylinder where the collision occurs and then goes through the beam. The maximum values that could be found is 31.7 MNm for the model with many bulkheads and 23.8 MNm for the model without bulkheads.

9.8.5   Kinetic energy

The first plot is of the kinetic energy.
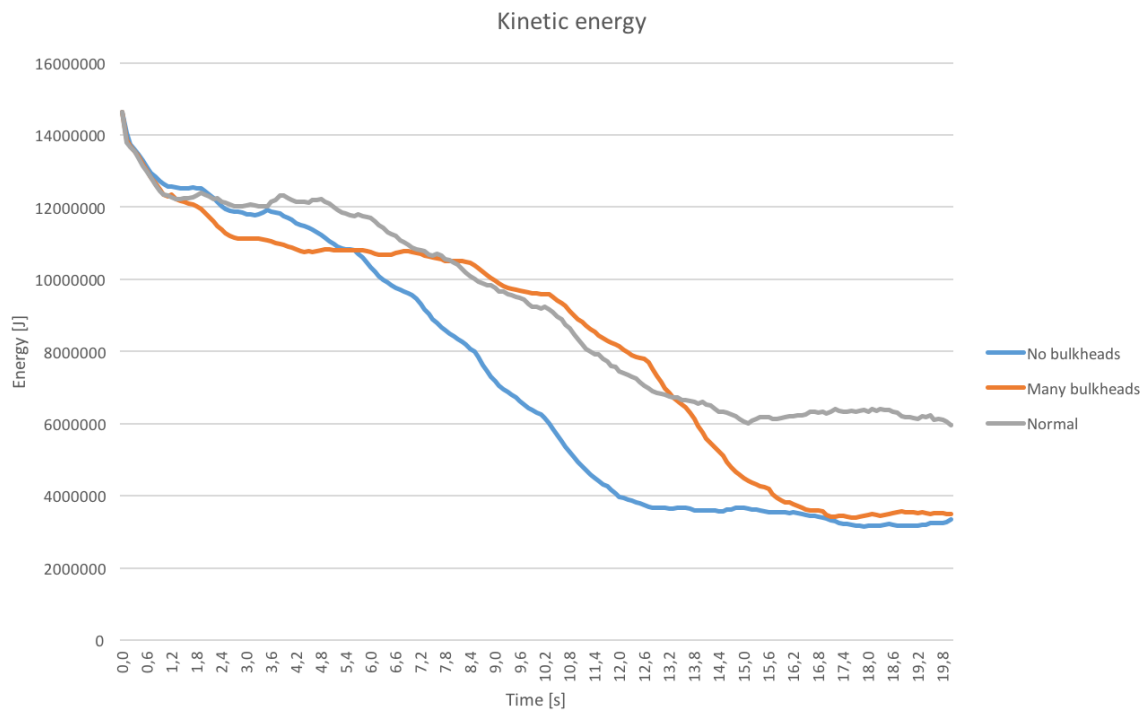
Figure 86: Significance of amount of bulkheads on the kinetic energy

As can be seen from the plot all three alternatives start out similar to each other, but from 1.5 seconds and further, they defer from each other. The alternative with many bulkheads flattens out for a period, before it starts to decrease more rapidly. The analysis without any bulkheads on the other hand would start to decrease earlier, but both of them will end up with about the same amount of kinetic energy in the end. The original analysis on the other hand will end up with a higher level of kinetic energy.

9.8.6 Internal energy

The amount of internal energy is plotted in the figure below.
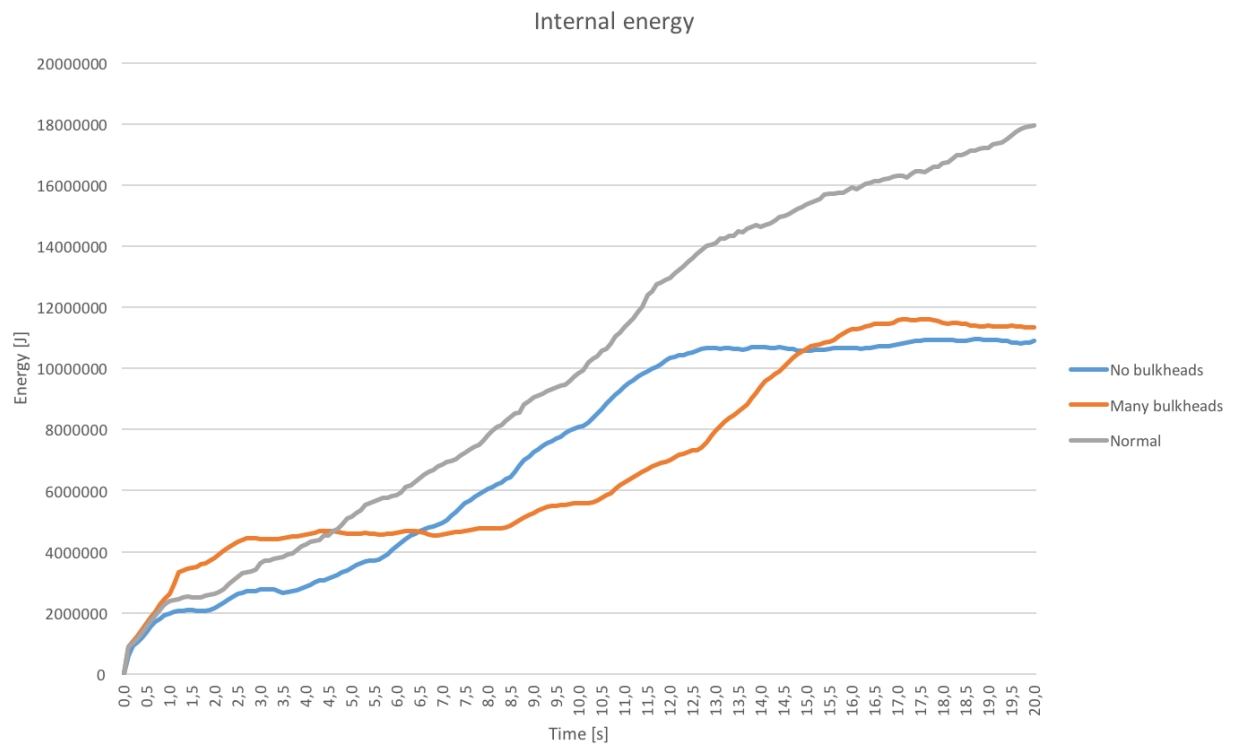
Figure 87: Significance of amount of bulkheads on the internal energy

In the figure we can see that the analyses with none and several bulkheads not will defer a lot from each other, and after 20 seconds end up with almost equal internal energies. The original alternative on the other hand will continue to increase and end up with the largest amount of internal energy.

9.8.7 Strain energy

The strain energy are plotted underneath for comparison of the amount of bulkheads.
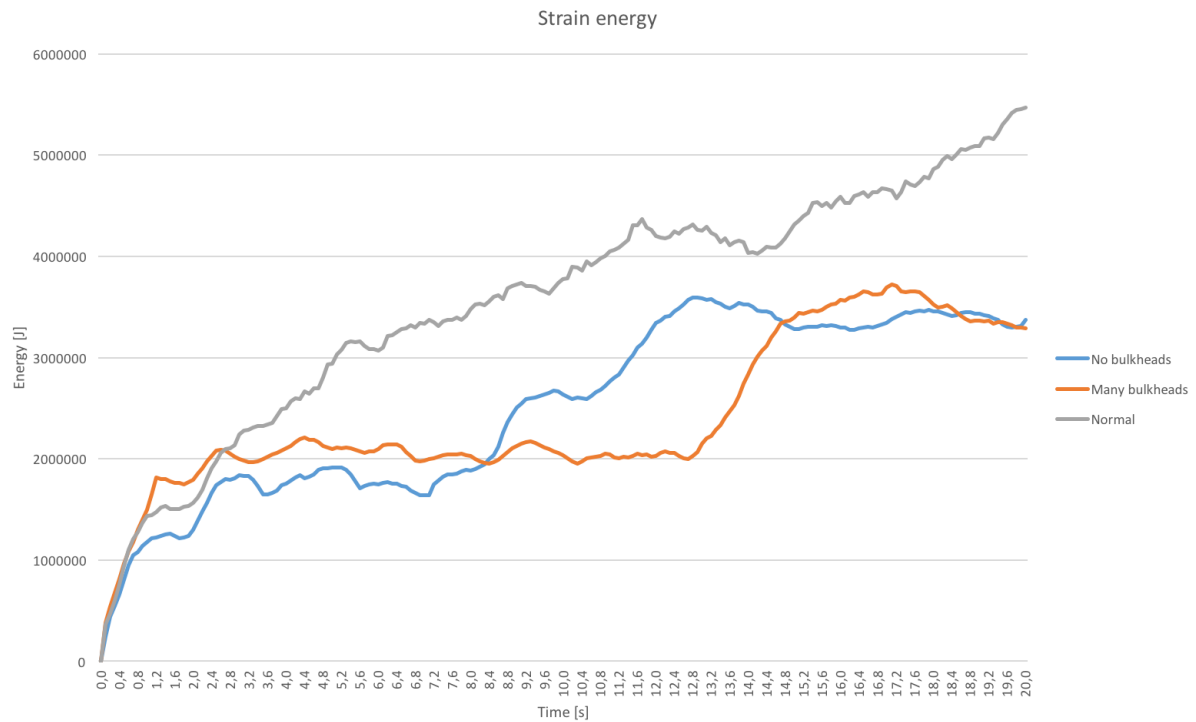
Figure 88: Significance of amount of bulkheads on the strain energy

In the plot for the strain energy it can be seen that This follow the same tendencies as the previous plots has done. The plot for many and none bulkheads follow each other quite closely, and end at almost the same amount of strain energy. The curve for the original run on the other hand will have a larger magnitude.

9.8.8   Artificial energy

The comaprison of the artificial energy is shown in the figure below.
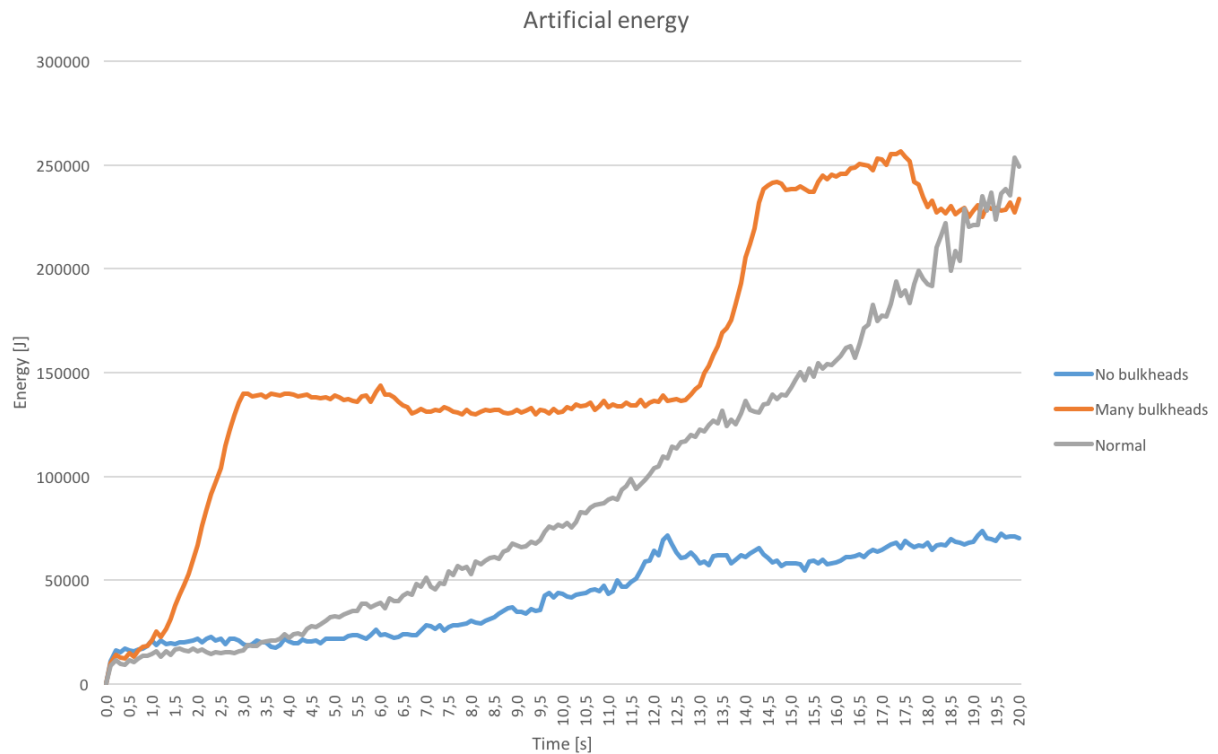
Figure 89: Significance of amount of bulkheads on the artificial energy

In the plot we can see that the artificial energy will have the largest value for the alternative with many bulkheads. The alternative with no bulkheads has the smallest amount of artificial energy in its system. This is probably related to the number of elements the pontoons is divided into. The pontoon with many bulkheads will have a lot more elements after meshing than the one without.

9.8.9 Plastic dissipation

The next plot is of the plastic dissipation in the structures.
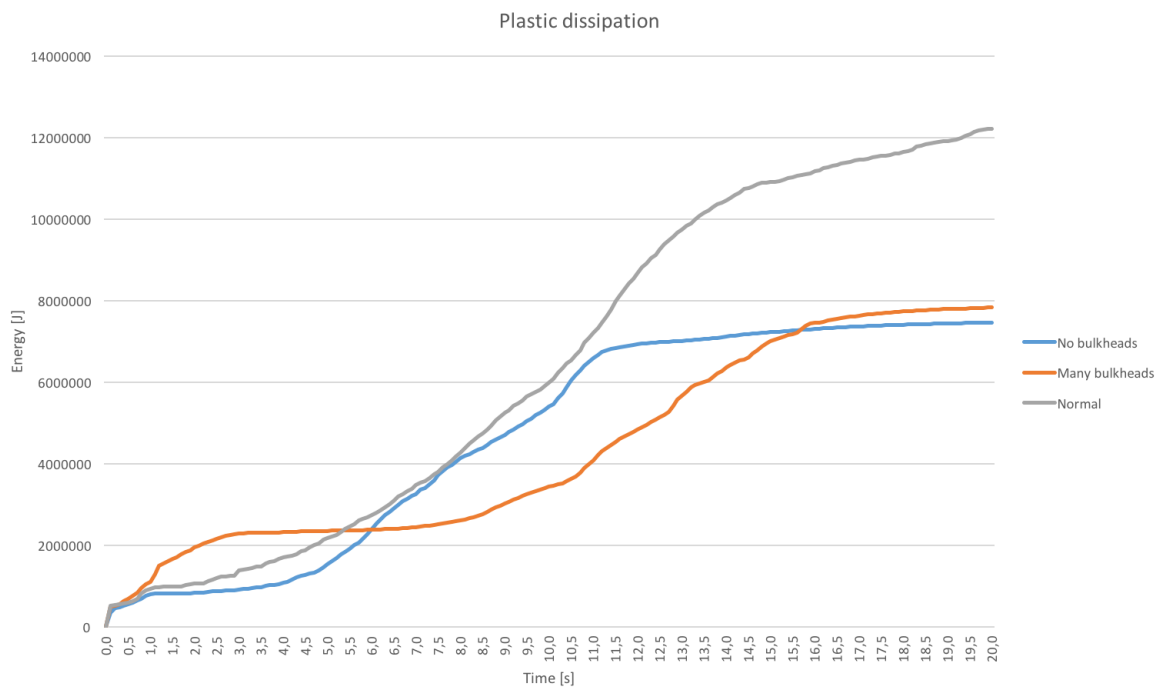
Figure 90: Significance of amount of bulkheads on the plastic dissipation

The trend here is quite equal to what has been observed earlier. The alternatives with many and no bulkheads follow each other relatively good, while the energy for the original run is larger than the two others.

9.8.10   Viscous dissipation

The last energy is that of the viscous dissipation. The results are shown in the figure below.
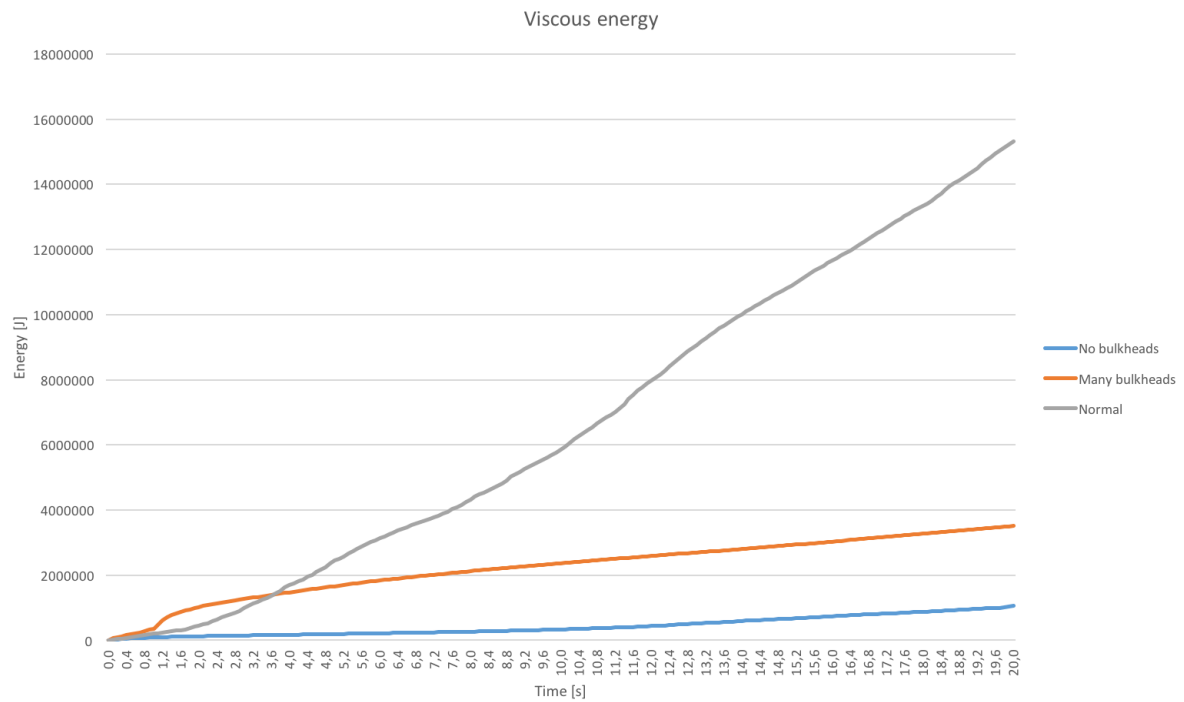
Figure 91: Significance of amount of bulkheads on the viscous dissipation

In the plot it can be seen that the pontoon without any bulkheads also will have the least amount of viscous energy, while the original run, is very much lager than the other two also here. But as the two other curves flattens out, the original one keeps on increasing.

10 Discussion

A floating bridge that crosses a Norwegian fjord without a larger city inside the fjord is not going to have a lot of service ships traveling in it. Since the vessel that pass the bridge mostly will be smaller vessel and passenger ships such as cruise ships, it will probably be of interest to design the bridge with the principles of ductility design. It is more likely that it is possible to evacuate the humans driving on the bridge rapidly before the bridge looses buoyancy and sinks. A cruise ship on the other hand with several hundred passengers may take a lot longer time to rescue, and there is a larger possibility of loosing many human lives. From a socioeconomic view, the largest catastrophe is to lose a human life. It therefore of interest to save as many persons as possible.

The results section consists of values for the stresses both local and global, forces and moments in the road as well as several different energy levels. For the stresses that occur in the original run with a shell thickness of 2 cm for the pontoon, it can be seen that both the pontoon and the vessel will sustain significant damage. The ship is the structure that will feel the largest stresses, but both the structures will clearly be over in the plastic region. For the pontoon it looks as if a couple of bulkheads has been penetrated. If the pontoon will continue to float or sink is dependent on the number of bulkheads that has been flooded. As for the global stresses, there will be some distribution of forces in the bridge. But these forces are not large enough to cause significant damage on the other components of the bridge. As for the moments and forces in the road, these components are responsible for the transmittance of stresses and forces from one pontoon to another. when it comes to the displacements in the collision, these will become very large, which will be a recurring pattern for all of the analyses. they will all have displacements in the range above 1 meter. As for the energies, these do follow the patterns that were expected. The kinetic energy will decrease over time. the kinetic energy is absorbed as internal energy, and mainly as strain energy. The artificial energy is low compared to the internal energy, which is good because it means that the results are not governed by zero-energy modes, and hourglassing has been kept to a low level. The plastic dissipation in a structure will also be of similar shape as the strain and internal energy, but with a smaller magnitude than that of the internal energy. The plastic dissipation is a measurement of how much energy has been dissipated through in-elastic processes, this means that plasticity must have occurred in the model, which also was determined by the

magnitude of the stress in the structures.

As for the mesh refinement study, a very good convergence was not achieved. But the possibility to achieve convergence was limited by the computational power of the computer that was used, together with problems related to the memory on the computer. Although this was not achieved, it could be seen that the results over time would become more and more equal to each other. To be able to run one final analysis would have been preferred to see if convergence could be reached.

For the significance of the shell thickness, it could be observed that this would have a large significance on the results. For the local stresses on the pontoon experiencing the collision, the Von Mises stress was 213 MPa for the thick pontoon, and 305 MPa for the thin pontoon. This is a big difference and it means that the thick pontoon will not have any development of plasticity at all, while the thin pontoon is well into the plastic region, and will have deformed so greatly that the pontoon probably have lost its buoyancy. For the distribution of stresses to the other pontoons, they are relatively small, and is not close to the yield criterion. the other pontoons can therefore in both cases be seen as safe, and not in danger of flooding. For the beam forces, the pontoon with a thick shell will have a larger force in its beam than the model with a thin beam, but both are lower then the beam force in the original run. For the moment, the same relationship can be observed between the thick and thin shell. The thick will have the largest moment value, and the thin the smallest. Here, the original shell thickness will have a value for the moment that lies between the other two. For the energy levels, it is the thick shell that has the highest kinetic energy end value, as well as the highest value for internal energy in the end. That it has the largest value for the internal energy could be expected as it has more material to absorb the kinetic energy as internal energy. This will also prevent the steel from deforming plastically, and limit the damage in the structure. This also holds for the remaining energies.

For the comparison of the model with and without bulkheads it can from the local stress be seen that the alternative with many bulkheads will have a smaller stress value in its pontoon. This is also confirmed by the maximum stress values in the pontoons. For the pontoon without any bulkheads this is 330 MPa, and the largest stress value that occurred so far. For the pontoon with many bulkheads this value is 235 MPa, and just at the yield stress of the applied steel. The stress distribution in the bridge is not significant, as it just leads to small specks of stress concentration in a few of the other pontoons. This value will be larger for the model without any bulkheads, but not large enough to have any significance on the structures integrity.The beam forces will for both these cases be smaller than they have been for the other scenarios. But it can be observed that the force value is just 0.35 MN for the analysis with many bulkheads, and for the other case this value is 3 MN. By taking a view on the moments in the beam, this will be largest for the alternative without any bulkheads with a value of 31.7 MNm. This is smaller than the value from the original analysis, but larger than the result for the model with many bulkheads, which has a maximum value of 23.8 MNm. For the energies, both of the two alternatives will in general take a different path, but will end up around the same energy level after 20 seconds. The original analysis given for most of the energies a larger value than the other, except for the kinetic energy and viscous dissipation. Bulkheads are also very important if a collision does occur. The bulkheads will stop the entire compartment from flooding, and if only a few takes in water it can either slow down the rate that the bridge will sink, or keep it afloat.

11   Conclusion

In this thesis I have looked into the consequences of a vessel colliding into a pontoon of a floating bridge. The aim was to see how the bridge would respond to the impact. From the results for the energies it can be observed that the kinetic energy has not disappeared after 20 seconds, which indicates that both the pontoon and the vessel has gathered a common speed, and has not stopped to move. The kinetic and internal energy mirrors each other, which confirms that all of the kinetic energy that disappear during the impact is dissipated as internal energy, in several smaller components that makes up the total internal energy. It can be found that a thick shell element will not deform plastically, but make the vessel take up most of the forces in the collision. The opposite can be seen for a thin-walled shell. This will deform much more, and take a larger part of the forces in the impact. For the analysis of the models with many or no bulkheads the same patterns can be recognized. The model with many bulkheads will have smaller values for the stresses in the structure, but still it is on the yield stress limit.

Because the bridge should take the largest amount of energy, to let i sink first, it is the original run that comes the closest to this scenario. The structure is a little bit too strong, and the thickness should be smaller than it is in that analysis, but not as small as it is for the thin shell element analysis. Both the analyses for the thick shell elements and many bulkheads will give large stresses in the vessel, and sink it. The analyses for the thin walled shell and the alternative will give a very large damage to the pontoon, and even with bulkheads it would flood quickly and loose its buoyancy.

12   Further work

From the mesh refinement study, it can be seen that one more analysis should have been ran. It is not a very clear convergence in the results. This was unfortunately not possible to perform, because the computer crashed and was not able to conduct the study. Also, the analysis with the finest mesh size that was used here took 5 days to complete. It is difficult to foresee how much longer this analysis would have taken, if it was possible to conduct it. Another solution would have been to design a smaller bridge, with only the middle section, and not the entire bridge. To improve the study, it would therefore have been of interest to run the analysis on a stronger computer.

Design changes could be made to the bridge as well. These would include making a suspension bridge in the middle with towers and tethers. This would make the bridge more realistic. It can also be an alternative to design the entire superstructure of the bridge which would be made up of steel trusswork.

Several other parameter studies could also be of interest to look more into. This could be designing a more accurate bow of the ship with a bulbous bow. This would make the analysis more realistic, but designing a bulbous bow from scratch is a time consuming process, which requires a better knowledge of CAD modeling than I have at the moment. Another could be to run the analysis with several different angles on the collision, or changing the vessel size and, mass and speed.

To optimize the bridge entirely even more runs could have been made with respect to the thickness of the bridge. A optimum steel thickness greatly increases the costs of building it. As steel is not a cheap material, it is desired to design it safe enough with respect to the governing standards, but not make it overly conservative as the affects the building cost.

References

Floating bridges - when is the technology ready? `http://www.vegvesen.no/vegprosjekter/ferjefriE39/Konferanse/teknologidagene2015/_attachment/1023747?_ts=14ff497c800&fast_title=10+Coastal+Highway+Route+E39+-+floating+bridge+-+Bruno+Villoria+NPRA.pdf`. Accessed: 2015-10-15.

The tl timoshenko plane beam element. `http://kis.tu.kielce.pl//mo/COLORADO_NFEM/colorado/NFEM.Ch09.pdf`. Accessed: 2016-04-20.

Alaa Kohja. `(URL:https://acia93.wordpress.com/hookes-law-and-materials-behavior/)`. Accessed: 2016-02-20.

Amdahl, J. (1983). *Energy absorption in ship-platform impacts.* Dr. ing. thesis.

Amdahl, J. (2015). Ship collision - lecture notes in tmr4195 design of offshore structures.

Amdahl, J., Endal, A., Fuglerud, G., Hultgreen, L. R., Minsaas, K., Rasmussen, M., Sillerud, B., Sortland, B., Steen, S., and Valland, H. (2015). *TMR4105 - Marin Teknikk Grunnlag.* Kompendium (Norges teknisk-naturvitenskapelige universitet. Fakultet for marin teknikk). Dept. Marine Technology, Trondheim.

Amdahl, J. and Søreide, T. (1983). Energy absorption in ship-platform impacts.

Chuck Pefley. `http://almostoneaday.blogspot.no/2010/09/sunday-bridge-series-hood-canal-bridge.html`. Accessed: 2016-03-12.

de Jonge, T. and Laukeland, L. (2013). Collision between a spar platform and a tanker.

Ehlers, S. (2013). Lecture notes in tmr4320 simulation based design.

Frandsen, A. G., Olsen, D. F., Lund, H. T., and Bach, P. E. (1991). *Evaluation of minimum bridge span openings applying ship domain theory.*

Furnes, O. and Amdahl, J. (1980). Computer simulation study of offshore collisions and analysis of ship-platform impacts. *Applied Ocean Research*, 2(3):119–127.

Gerard, G. (1957). Handbook of structural stability part v: compressive strength of flat stiffened panels.

Hibbitt, Karlsson, and Sorensen (1992). *ABAQUS: Theory manual.* SIMULIA, 6.7 edition. Accessed: 2015-10-01.

Irgens, F. (2010). Formelsamling mekanikk.

Jansen, K. (2015). *Ship impact with a floating bridge.* Project thesis.

Kelly. Solid mechanics part ii: Engineering solid mechanics. `http://homepages. engineering.auckland.ac.nz/~pkel015/SolidMechanicsBooks/Part_II/`. Accessed: 2015-10-20.

Marsh, K. and Campbell, J. (1963). The effect of strain rate on the post-yield flow of mild steel. *Journal of the Mechanics and Physics of Solids*, 11(1):49–63.

Minorsky, V. (1959). An analysis of ship collisions with reference to protection of nuclear power plants. Report, Sharp (George G.) Inc., New York.

Moan, T. (2000). *Accidental Actions: Background to NORSOK N-003.* Norwegian University of Science and Technology, Trondheim.

Moan, T. (2003). *TMR4190 Finite Element Modelling and analysis of Marine Structures*, volume UK-03-98 of *Kompendium (Norges teknisk-naturvitenskapelige universitet. Fakultet for marin teknikk).* Dept. Marine Technology, Trondheim.

NORSOK (2004). Norsok n-004: Design of steel structures.

NrK. `https://www.nrk.no/hordaland/nordhordslandsbrua-er-20-ar-1.11945221`. Accessed: 2015-10-01.

Pettersen, B. (2004). *TMR4247 Marin Teknikk 3 Hydrodynamikk*, volume UK-2004-75 of *Kompendium (Norges teknisk-naturvitenskapelige universitet. Fakultet for marin teknikk).* Dept. Marine Technology, Trondheim.

Randrup-Thomsen, M., Askeland, S., Ask, T., Skorpa, M., Hillestad, S. J., and Veie, J. (2013). Bridge crossings at sognefjorden - ship collision risk studies.

Recinto Universitaro de Mayaguez. `http://academic.uprm.edu/pcaceres/Courses/ MMII/IMoM-5A.pdf`. Accessed: 2016-03-01.

Saabye Ottosen, N. and Petersson, H. (1992). *Introduction to the finite element method*. Pearson Prentice Hall, Harlow.

Skanska, A.-J. . J. . C. . N. . Sognefjorden mulighetsstudie flytebro. `http://www.vegvesen.no/_attachment/513900/binary/828559?fast_title=Mulighetsstudie+for+kryssing+av+Sognefjorden+-+Flytebru.pdf`. Accessed: 2016-02-10.

Statens Vegvesen. Ferjefri e39. `http://www.vegvesen.no/vegprosjekter/ferjefriE39`. Accessed: 2015-09-15.

Storheim, M. and Amdahl, J. (2014). Design of offshore structures against accidental ship collisions. *Marine Structures*, 37:135 – 172.

Teknisk ukeblad. Bjørnafjordan kan få verdens lengste flyte- eller rørbru. `http://www.tu.no/samferdsel/2015/03/10/bjornafjorden-kan-fa-verdens-lengste-flyte--eller-rorbru`. Accessed: 2015-09-20.

Terndrup Pedersen, P., Valsgård, S., Olsen, D., and Spangenberg, S. (1993). Ship impacts: Bow collisions. *International Journal of Impact Engineering*, 13(2):163–187.

Thaulow, C. and Valberg, H. (2015). *TMM4140 Plastisk deformasjon og brudd*. Kompendium (Norges teknisk-naturvitenskapelige universitet. Fakultet for ingeniørvitenskap og teknologi). Institutt for produktutvikling og materialer, Trondheim.

Veritas, D. N. (2010). Design against accidental loads. *Recommended Practice DNV-RP-C204*.

Watanabe, E. and Utsunomiya, T. (2003). Analysis and design of floating bridges. *Progress in Structural Engineering and Materials*, 5(3):127–144.

Wierzbicki, T. (1983). Crushing behaviour of plate intersections. *Structural crashworthiness*, pages 66–95.

Wikipedia. `https://commons.wikimedia.org/wiki/File:Bridge_types.svg`. Accessed: 2015-09-12.

Wikipedia. `https://no.wikipedia.org/wiki/Bergs\T1\oysundbrua`. Accessed: 2015-10-01.

Wikipedia. `https://en.wikipedia.org/wiki/Lacey_V._Murrow_Memorial_Bridge`. Accessed: 2016-03-12.

Yang, P. and Caldwell, J. (1988). Collision energy absorption of ships' bow structures. *International Journal of Impact Engineering*, 7(2):181–196.

13 Appendix

13.1 MatLab script

```matlab
%Masses
m_pontoon = 536440; %Mass of pontoon
m_pontoontop = 206323; %Mass of pontoon top
m_roadcurved = 387463520; %Mass of the road
m_bigcylinder = 1094970; %Mass of the large cylinder
m_bigcylindertop = 110977; %Mass of the large cylinder top
m_bigpontoon = 1143738; %Mass of the large pontoon
m_bigpontoontop = 393577; %Mass of the large pontoon top
m_cylinder = 729981; %Mass of cylinder
m_cylindertop = 49323; %Mass of the cylinder top

m_shiphull = 7317487; %Mass of modeled shiphull


%Total mass of the installation
m_installation = 18*m_pontoon + 36*m_pontoontop + m_roadcurved +
2*m_bigcylinder + 4*m_bigcylindertop + 2*m_bigpontoon + 4*m_bigpontoontop +
18*m_cylinder + 18*m_cylindertop;


a_shiphull = m_shiphull*0.1; %Added mass for ship hull
a_installation = m_installation*0.1; %Added mass for the installation


v_shiphull = 2; %Velosity of the vessel
v_installation = 0; %Velocity of the bridge


E_kinetic = 0.5*(m_shiphull + a_shiphull)*(v_shiphull^2); %Kinetic energy


%Energy that has to be absorbed as strain energy
E_s = 0.5*(m_shiphull + a_shiphull)*(v_shiphull^2)*((((1-
(v_installation/v_shiphull))^2)/(1+((m_shiphull + a_shiphull)/(m_installation
+ a_installation)))));


%Beta is the facter of kinetic energy that is absorbed to be strain energy
beta = E_s/E_kinetic;
beta2 = 1/(1+(m_shiphull/m_installation));


%Bridge dimensions:

b_largep = 30;
b_smallp = 20;
h_largep = 60;
h_smallp = 50;
r_largep = 15;
r_smallp= 10;
z_largep = 20;
z_smallp = 13;


%Volume of bridge [m^3]:

V_bridge = m_installation/1025;


%Area of waterline total bridge:

A_vl = ((2*((h_largep*b_largep)+(3.14*(r_largep^2)))) +
18*((h_smallp*b_smallp)+(3.14*(r_smallp^2)))));


%Area of waterline small pontoon:
```

```matlab
Avl_smallp = ((h_smallp*b_smallp)+(3.14*(r_smallp^2)));

%Area of waterline large pontoon:

Avl_largep = (((h_largep*b_largep)+(3.14*(r_largep^2))));

%Draft of bridge:

T = (V_bridge/A_vl);

%Area of halfcircles on pontoons:

A_litenp = (3.14*(r_smallp^2))/2; %Small pontoon
A_storp = (3.14*(r_largep^2))/2; %Large pontoon

%Distance from circle are center to pontoon center:

a_liten = (h_smallp/2) + ((4*r_smallp/(3*3.14)));
a_stor = (h_largep/2) + ((4*r_largep/(3*3.14)));

%Finding the moment of inertia for the pontoons in the transverse direction:

Ix_smallp = (((b_smallp*(h_smallp^3))/12) + (2*((((9*(3.14^2)) -
64)*(r_smallp^4))/(72*3.14))) + (2*(a_liten^2)*A_litenp));
Ix_largep = (((b_largep*(h_largep^3))/12) + (2*((((9*(3.14^2)) -
64)*(r_largep^4))/(72*3.14))) + (2*(a_stor^2)*A_storp));

%Finding the moment of inertia for the pontoons in the longitudinal direction:

Iy_smallp = (((h_smallp*(b_smallp^3))/12) + (2*((3.14*(r_smallp)^4)/8)));
Iy_largep = (((h_largep*(b_largep^3))/12) + (2*((3.14*(r_largep)^4)/8)));

%Volume of pontoon:

V_smallp = m_pontoon/1025;
V_largep = m_bigpontoon/1025;

%Finding the BM value in the transverse direction:

BMx_smallp = Ix_smallp/V_smallp;
BMx_largep = Ix_largep/V_largep;

%Finding the BM value in the transverse direction:

BMy_smallp = Iy_smallp/V_smallp;
BMy_largep = Iy_largep/V_largep;

%Finding the distance from the keel to the buoyancy center og the pontoon:

KB_smallp = 0.5*T;
KB_largep = 0.5*T;

%finding the distance from the keel to the gravity center of the pontoon:
```

```matlab
KG_smallp = 0.5*z_smallp;
KG_largep = 0.5*z_largep;

%Finding the value of the spring constant in roll motion:

C44_smallp = 1025*9.81*V_smallp*(KB_smallp + BMx_smallp - KG_smallp);
C44_largep = 1025*9.81*V_largep*(KB_largep + BMx_largep - KG_largep);

%Finding the value of the spring constant in pitch motion:

C55_smallp = 1025*9.81*V_smallp*(KB_smallp + BMy_smallp - KG_smallp);
C55_largep = 1025*9.81*V_largep*(KB_largep + BMy_largep - KG_largep);

%Finding the value of spring constant in heave motion:

C33_largep = 1025*9.81*Avl_largep;
C33_smallp = 1025*9.81*Avl_smallp;
```

13.2   List of Excel sheets that has been attached electronically

Artificialveryfine

Internalveryfine

Kineticveryfine

Plasticdissipveryfine

Strainveryfine

Totalveryfine

Viscousveryfine

Totalkinetic

Totalplasticdissipation

Totalstrain

Internalartificial

Totaltotal

Artifcialbulkhead

Artifcialthinthick

Totalartificail

Totalinternal

Internalkinetic

Internalstrain

Internalthickthin

Kineticthickthin

Plasticthickthin

Strainthickthin

Viscousthinthick

Totalviscous

Internalbulkheads

Kineticbulkheads

Plasticbulkheads

Strainbulkhead

Viscousbulkhead

Internalstrainplastic